Thermoplastic-based pyrotechnic compositions

by

Gerard Potgieter

Thermoplastic-based pyrotechnic compositions

by

Gerard Potgieter

Dissertation submitted in partial fulfilment of the requirements for the degree

of

Master of Engineering (Chemical Engineering)

In the Faculty of Engineering, Built Environment and Information

Technology

University of Pretoria

Pretoria

December 2015

DECLARATION

I, **Gerard Potgieter, student No. 27354394,** do hereby declare that this research is my original work and that to the best of my knowledge and belief, it has not been previously in its entirety or in part been submitted and is not currently being submitted either in whole or in part at any university for a degree or diploma, and that all references are acknowledged.

SIGNED on this ——————————day of ——————————————2015.——————

——————————————

Gerard Potgieter

iii

Thermoplastic-based pyrotechnic compositions

Student: Gerard Potgieter

Supervisor: Prof. Walter W. Focke

Department: Chemical Engineering

University: University of Pretoria

Degree: Master of Engineering (Chemical Engineering)

Synopsis

Conventional pyrotechnic time delays are based on powder mixtures pressed into tubes of precise lengths. Pyrotechnics based on filled polymer systems may offer some advantages. This includes continuous manufacture via extrusion processes.

Thermoplastic-based pyrotechnic compositions can be formulated by filling conventional polymer matrices with oxidants such as potassium nitrate. More interesting are fluoropolymer matrices as these strong oxidants enable the design of non-gassing systems with suitable fuels. The presence of fillers dramatically increases the melt viscosity. The random packed limit for monodisperse spherical particles corresponds to a volume fraction of 0.637 (Krieger, 1959). Pyrotechnic compositions with oxidant filler volume fractions below this critical level are only viable for conventional polymers with very high C:H atomic ratios, e.g. polystyrene.

Pyrotechnic compositions comprising of filled thermoplastics were simulated using EKVI thermodynamic software. This allowed for the calculation of the adiabatic flame temperatures, variation of the product composition and gas evolved with varied filler content. The EKVI thermodynamic simulations showed that polystyrene filled with potassium nitrate or potassium permanganate were unlikely to be viable as global maximum temperatures were not achieved below 78 vol.%. A fully fluorinated polymer filled with aluminium, magnesium, magnalium and calcium carbide were shown to be viable between 20 wt.% and 70 wt.% reducing agent. Co-

polymers of tetrafluoroethylene and vinylidene fluoride filled with aluminium or magnesium showed similar adiabatic temperatures as compositions based on perfluorinated polymers with the same reducing agents. The energy required to decompose the thermoplastic binder would, however, lower the amount of energy available for the pyrotechnic reaction.

Open flame burn test showed that the polystyrene-based compositions did not generate enough energy to decompose the thermoplastic fraction to sustain chemical reaction. Viton B filled with calcium carbide could not sustain burning. Compositions using aluminium and magnalium with Viton B as oxidant sustained burning over the range 20 wt.% to 60 wt.%. The effect of morphology was tested by using two grades of aluminium; atomized aluminium, and flake-like aluminium particles.

Energy measurements of Viton B filled with aluminium and magnalium indicated that the maximum energy output occurred in the range 30 wt.% to 40 wt.% fuel for aluminium-based compositions and between 40 wt.% and 50 wt.% for magnalium-based compositions. A maximum burn rate of 82 mm s^{-1} was achieved using a magnalium/Viton B composition. Friction and impact test showed that the compositions are insensitive.

XRD analysis of the combustion residue of Viton B-based compositions using aluminium as fuel showed that the most abundant products formed were Al_4C_3, AlF_3, carbon and an amorphous phase. An elemental balance indicated that the amorphous phase consisted of carbon, aluminium and fluorine. The XRD spectra of the residues of magnalium-based compositions had unidentified reflections. Quantitative XRD was, therefore, not possible on the reaction products of the magnalium-based compositions. TGA analysis on the combustion residue indicated that the combustion residue contained unreacted reagents.

Scanning electron microscopy of the reaction residue revealed the presence of agglomerated cubic particles. EDX analysis indicated that the cubic particles consisted of aluminium and fluorine.

Acknowledgements

The author would like to thank:

- Prof. Walter Focke for his guidance and support. Your enthusiasm for materials science is infectious.
- Suzette Seymore for taking care of all admin. Without you the small problems would have become much bigger problems.
- Ollie, Shepherd and Yolandi for sharing their knowledge of pyrotechnics.
- Wiebke Grote (XRD), Jeanette Dykstra (XRF), Andre Botha (SEM), Dr. Heidi Rolfes (PSA) and Isbe van der Westhuizen (TGA).
- Cliff Thompson, without whom there would not have been any fluoropolymer materials for this project.
- AEL Mining Services and the personnel at AEL for granting me permission to use this material for the purposes of my degree, as well as for the financial and technical support.
- My family for their support through this project. Your nagging may be the reason why it was actually completed.
- Monique Schmidt for ensuring the possibility of having a fully functioning thesis.

Table of contents

List of tables

List of figures

Abbreviations

AlF$_x$	Aluminium fluorides
FTIR	Fourier transform infrared (spectroscopy)
HF	Hydrogen fluoride
PS	Polystyrene
PTFE	Polytetrafluoroethylene
SEM	Scanning electron microscopy
TFE	Tetrafluoroethylene
TGA	Thermogravimetric analysis
VDF	Vinylidene fluoride
EDX	Energy dispersive X-ray spectroscopy
XPS	X-ray photoelectron spectroscopy
XRD	X-ray diffraction

Symbols

a	activity	
c_p	heat capacity	J kg^{-1} K^{-1}
D_0	pre-exponential diffusion co-efficient	s^{-1}
E_a	activation energy	J mol^{-1}
E_D	apparent activation energy for diffusion	J mol^{-1}
G,g	Gibbs energy	J
ΔH_0	standard heat of reaction	J kg^{-1}
H_m	heat of melting	J kg^{-1}
ΔH_p	heat of polymerisation	J kg^{-1}
k	rate constant	s^{-1}
k_0	pre-exponential rate factor	s^{-1}
n	number of moles	
N	total number of moles	
p	pressure	Pa

P	total pressure	Pa
R	gas constant	8.314 J mol^{-1} K^{-1}
S,s	entropy	J K^{-1}
Tad	adiabatic temperature	K
T_b	boiling temperature	K
T_c	maximum temperature	K
T_0	initial temperature	K
T_{ref}	reference temperature	K
v	burn rate	m s^{-1}
α	thermal diffusivity	m^2 s^{-1}
λ	thermal conductivity	W m^{-1} K^{-1}
ρ	density	kg m^{-3}
μ	chemical potential	J mol^{-1}
η	viscosity	Pa s
ϕ	volume fraction	
$[\eta]$	intrinsic viscosity	

Chapter 1 : Introduction

1.1   Introduction

Chemical time delay elements are used to ensure controlled detonation of charges in blasting operations (Mclain, 1980). They consist of pyrotechnic composition filled in small-diameter tubes of varying length (Conkling, 2011). Conventional pyrotechnics consist of intimate mixtures of two or more powders capable of exothermic redox reactions (Bradley et al., 1979). The reducing agent (metal or metalloid) is coupled with a suitable oxidising agent that is usually in the form of a metal oxide. A constant burn rate is desired to ensure the transmission of an initiation impulse occurs in a precise and adjustable time interval. Thus, delay compositions that burn at a constant, predetermined rate without the formation of gaseous intermediates are preferred (Charsley et al., 1980). The combustion in the column is governed by a number of parameters (Berger, 2005). The thermal diffusivity of the mixture is always important, as combustion wave propagation depends on re-ignition of adjacent layers along the burning path. The time delay incurred is determined by the nature of the reactants, the stoichiometry of the pyrotechnic composition and the dimensions of the column, i.e. its length and diameter, and the material of construction of the tube (Mclain, 1980; Berger, 2005).

Theoretical models for the self-propagating layer-to-layer reactions in the solid phase have been developed (Booth, 1953; Margolis, 1993; Margolis, 1985; Margolis, 1983; Margolis & Williams, 1991; Aldushin & Khaikin, 1974; Khaikin & Merzhanov, 1966; Puszynski, Degreve & Hlavacek, 1987). The models link the rate of progression of the reaction through the mixture of the reactants in the form of a cylinder, with some of the physical properties of the powders, the state of subdivision of the powder, the chemical composition and the reaction kinetics between the constituent (Booth, 1953).

Good mixing and adequate particle-particle contact between reactants (i.e. efficient particle packing) is a prerequisite for stable and reproducible burning. It is, however, difficult to ensure unlike particle contacts predominate. An intriguing possibility is to replace at least one of the particulate reactants with a suitable polymer. One possibility is to use a perfluorinated polymer

1

as oxidant in combination with a metallic fuel. This could allow for manufacture of time delays using polymer converting processes such as extrusion. Poly(tetrafluoroethylene) (PTFE) is used in pyrotechnics, but unfortunately, it is also a refractory material (Nielson, Truitt & Rasmussen, 2005). It is, therefore, used in powder form, and powder processing techniques must be applied. Filled PTFE can only be continuously processed into billets using ram extrusion (Ebnesajjad, 2000). This technique requires a sintering step that raises concerns over the safety of processing such pyrotechnic compositions. However, fluoropolymers exist that can be solution- and/or melt-processed. Examples include copolymers of tetrafluoroethylene (TFE), hexafluoropropylene (HFP) and 1,1-difluoroethylene (VDF). A traditional non-saturated aliphatic or aromatic thermoplastic (containing only carbon and hydrogen), coupled with an appropriate oxidising agent, may offer another possibility. Such a polymer would, however, act as the reducing agent. Suitable oxidants would, therefore, need to be identified.

1.2   Aim and objective

The aim of this preliminary study was to explore the possibility of using polymer-based compositions as pyrotechnic delay elements. The controlled variables were: the nature of the reducing agent; fuel filler morphology and filler loading (stoichiometry). Performance was analysed by measuring the energy output, burn rate, pressure profile generated, mechanical properties and the products formed during reaction. A desired outcome of this study was to set the stage for future investigations that will deal with the manufacture of such elements in a safe and reproducible manner.

1.3   Outline of dissertation

The dissertation is divided into six chapters. The content of each chapter is outlined.

Chapter 1 outlines the problem statement and discusses the limitations of traditional, powder-based pyrotechnics. The objectives of the investigation are discussed.

Chapter 2 reviews literature relevant to the investigation. The review is divided into four sections. The first section gives a general introduction to pyrotechnics. The second section provides information on the manipulation in reaction rate of pyrotechnics. The third section looks at fluoropolymer-type pyrotechnic reactions. The fourth section discusses thermodynamics, with a specific view on pyrotechnics.

Chapter 3 outlines on the methodology followed. This chapter provides information on the parameters used in thermodynamic simulations. Furthermore, the materials and methods used to prepare pyrotechnic films are highlighted. The methods used for the preparation of thermoplastic-based pyrotechnic films are discussed.

Chapter 4 reports the results of EKVI thermodynamic simulations. The adiabatic reaction temperature, the condensed and gaseous products formed, as well as the quantities of gas generated are reported for all the compositions investigated.

Chapter 5 presents the results of the characterisation of the pyrotechnic films. The effects of the controlling parameters are discussed.

Chapter 6 reports the overall conclusions. Some recommendations are also made.

3

Chapter 2 : Literature review

2.1.   Introduction to pyrotechnics

Pyrotechnics are used in the manufacturing of a wide range of modern products. Notable examples include explosive detonators, tracers, airbag inflators, flares, smoke grenades and fireworks.

The study of high energy reactions is subdivided into four main categories, namely: pyrotechnics; propellants, primary explosives and high explosives. Delay elements are required to ensure exact detonation timings. Primary explosives, on the other hand, are used to initiate the bulk high explosive (Conkling, 1985: 88). Delay compositions and primary explosives react at combustion velocities below the speed of sound in a process commonly known as deflagration, while high explosives react at supersonic speeds (Conkling, 1985: 1). Constituents reacting via deflagration are collectively known as pyrotechnics.

Detonator delay elements are split into two main classifications: pyrotechnic and electronic delay elements. Electronic delay elements make use of circuits or semiconductor microchips to achieve the desired time delay. This results in highly accurate timing, but also implies a higher manufacturing cost (Ricco, 2004). Pyrotechnic time delays make use of chemical reactions to achieve time delays. This allows for the inexpensive manufacture of robust delay elements (Ricco, 2004).

A typical detonator is shown schematically in Figure 2-1. The pyrotechnic compositions are pressed into a rigid metallic shell. The starter signal travels to the detonator via a shock tube. Stable delay compositions are ignited using a starter element. However, detonators using readily ignitable delay compositions forgo starter elements. Ignition of pyrotechnic delay elements is followed by constant velocity propagation (Mclain, 1980) . This is essential, as the timing of the initiation pulse must be transferred in a precise and adjustable manner. The specific delay required is adjusted by changing the composition, length, diameter and the housing material of construction of the delay element (Mclain, 1980). One important aspect of traditional detonator

delay compositions is that little to no gas must be generated during the reaction. This ensures a constant combustion velocity at varied ambient pressures (Conkling, 1985: 129).

Once the delay element has fully propagated, a primer charge that is usually composed of lead azide or lead styphnate is ignited. The primer, in turn, sets off the base charge of a high explosive (Conkling, 1985: 127-128).
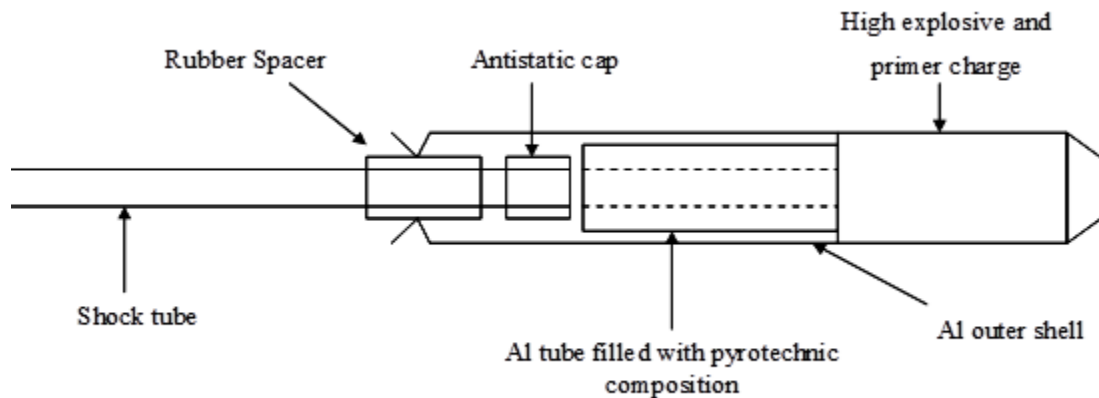
Figure 2-1: Delay element schematic (Ricco, 2004)

A subclass of pyrotechnics, called thermites, is of special interest as they are characterised by the large heats of reaction that often reach adiabatic reaction temperatures in excess of 2 000 °C. In this class of pyrotechnic reaction, a metal reacts with the oxide of another metal. This class of thermite reactions find use not only in the pyrotechnics industry, but also in thermal welding and advanced high temperature synthesis of specialised materials (Munir & Anselmi-Tamburi, 1989)

2.2.   Reaction rate manipulation

Conkling (1985: 97) defines a successful high energy mixture as a mixture that can be ignited by external stimuli, but is stable in the absence of such stimuli. Furthermore, the mixture must be able to sustain ignition throughout the composition. This can be seen as a reaction front propagating throughout the composition as a combustion wave.

5

A simplified formula of a typical pyrotechnic redox reaction is presented in Equation 2-1 (Rogachev & Mukasyan, 2010).

$$M + \frac{y}{x}AO_x \rightarrow MO_y + \frac{y}{x}A$$

2-1

M is the reducing agent and is usually in the form of a metal or metal alloy. AO_x is the oxidizing agent and MO_y the oxidized fuel. A is the reduced metal or non-metal corresponding to the oxidizing agent.

Pyrotechnic formulations are only ignitable if the metal forms a more stable oxide than the oxide with which it reacts (Wang et al., 1993). In other words, the Gibbs free energy change of the reaction must be negative for corresponding thermite formulations to be able to ignite and propagate. Many metals have higher reducing potentials than non-metal constituents (Wang et al., 1993). Their reducing potential, however, decreases with an increase in temperature (Wang et al., 1993).

A schematic of a common pyrotechnic reaction is shown in Figure 2-2. A compacted mixture of reducing agent and an oxidising agent is allowed to react. The reaction is initiated by raising the temperature of one end of the mixture to the ignition temperature. Once ignited, the reaction propagates in the form of a combustion wave. The products MO_y and A remain as combustion residues. A temperature gradient is also shown in Figure 2-2 below the composition. The red and blue colours correspond to the highest and lowest temperatures respectively. The elevated temperature on the reactant side is as a result of heat conduction through the unreacted metal, whereas the elevated temperature on the product side occurs as a result of slow cooling (Wang et al., 1993).
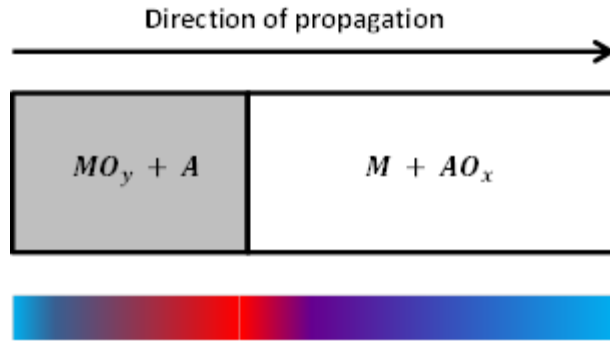
Figure 2-2: Schematic of the high temperature synthesis process for TIC production (adapted from: Munir & Anselmi-Tamburi, 1989)

A series of weight drop experiments by Bowden (1952) experiments showed that the kinetic energy available is capable of raising the temperature by only a few degrees, much less than the required amount for ignition. This suggests that the ignition of pyrotechnic reactions is may be due to the formation and propagation of localised hot spots rather than the effect of overall heating (Balzer et al., 2002). A key aspect of the mode by which hot spots cause combustion propagation in thermites can be seen when analysing the energy balance over a hotspot (Equation 2-2) (Balzer et al., 2002)

$$\Delta E_{Hotspot} = E_{rx} - E_{cond} - E_{conv} - E_{rad} - E_{Endo} \qquad 2\text{-}2$$

The subscripts rx, cond, conv, rad and endo represent the terms reaction, conduction convection, radiation and endothermic respectively. Positive values of $\Delta E_{Hotspot}$ result in self-propagating reactions, whereas negative values will result in quenched combustion (Balzer et al., 2002). It is unlikely that flame propagation can be initiated and sustained by a single hot spot (Osborne , 2006). As a consequence, it is most likely several hotspots in proximity of each other that are responsible for reaction propagation. The above criterion for self-propagation must be compared to the one suggested by Munir & Anselmi-Tamburi (1989), who stated that a thermite reaction can self-propagate if the adiabatic flame temperature is above 2 000 K. This can, however, only be taken as a rough indication on the performance of a thermite mixture.

Prediction of the rate of propagation of the combustion front requires knowledge about the temperature profile of combustion front, as well as the kinetics of the reaction

7

(Munir & Anselmi-Tamburi, 1989). Two limiting cases have been utilised for the prediction of the kinetics of the reaction: Arrhenius kinetics (i.e. the chemical reaction is the rate controlling step) and the diffusion kinetics (mass transport is controlling) (Booth, 1953; Margolis, 1993; Margolis, 1985; Margolis, 1983; Margolis & Williams, 1991; Aldushin & Khaikin, 1974; Khaikin & Merzhanov, 1966; Puszynski et al., 1987).

Khaikin & Merzhanov (1966) developed a model based on chemical kinetics that assumes a thin reaction zone in a gasless reaction. Further assumptions made were that heat transfer occurs only via conduction and that there are no radial heat losses. Lastly, the specific heat and density of the mixture was assumed to be constant. The change in the concentration of species followed n^{th} order kinetics.

$$\frac{\mathrm{d}x}{\mathrm{d}t} = k(1-x)^n \qquad\qquad\text{2-3}$$

where

$$k = k_0 e^{\left(\frac{-E_a}{\mathrm{R}T}\right)} \qquad\qquad\text{2-4}$$

Combination of Equation 2-3 and Equation 2-4 with the boundary conditions set out in the assumptions with rearrangement yielded an expression for the burn rate of solid state reactions. The expression is shown in Equation 2-5.

$$v^2 = \frac{g(n)\alpha k_0 \mathrm{R} T_c^2}{E_a \Delta H_R} e^{\frac{-E_a}{\mathrm{R}T_c}} \qquad\qquad\text{2-5}$$

Here, $g(n)$ = a weak function of the reaction order that varies between 0.5 and 2. Equation 2-5 can be rewritten as

$$\ln \frac{v}{T_c} = 0.5 \left(\ln \frac{\alpha k_0 \mathrm{R}}{E_a \Delta H_R g(n)} - \frac{E_a}{\mathrm{R}T_c} \right) \qquad\qquad\text{2-6}$$

The slope of the linear graph plotted using Equation 2-6 between $\ln\frac{u}{T_c}$ vs $\frac{1}{T_c}$ can, therefore, be used to calculate the activation energy, and the intercept allows for the calculation of k_0.

When reaction effects are dominated by mass and energy transport phenomena, the particle size, mass diffusivity and thermal diffusivity play a large role (Hardt & Phung, 1973). An Arrhenius-type temperature dependence for the mass diffusion coefficient is assumed. This allows for the calculation of the burn rate of randomly packed media, such as thermites, with diffusion based kinetics. The expression derived can be seen in Equation 2-7.

$$v^2 = 6\left(\frac{\alpha D_0}{E_D d^2}\right)\frac{R T_C^2}{(T_c - T_0)}\ e^{\left(\frac{-E_D}{R T_c}\right)}$$

2-7

The implications of the model shown in Equation 2-7 are that compositions that generate high temperatures, coupled with low activation energies, result in the highest burn rates. From a physical standpoint, particle size, as well as the thermal and mass diffusivity, affects the burn rate in this model.

Khaikin & Merzhanov (1966) as well as the model shown in Equation 2-7 represent the limits of the reaction rates of pyrotechnics. Furthermore, both models highlight that the reaction rate of thermite reactions is governed by a small number of variables. The most important are: the enthalpy of reaction; activation energy; adiabatic reaction temperature; packing density; thermal diffusivity and mass diffusivity.

2.2.1. Reactant pairing

Thermite reactions are always redox-type reactions. As a result, the chemical potential of a pyrotechnic composition is controlled by electrochemical potential of the reducing agent/ oxidising agent pairing. Electron acceptors and donors that readily allow electron transfer, whilst remaining stable through transport and storage, make for the best commercial pyrotechnic performance (Conkling, 1985: 20).

9

The activation energy provides a measure of the ease of a specific thermite pairing to be ignited. It can be thought of as the energy required to break the bonds between the original chemical species. Electronegativity, the measure of an atom's ability to attract electrons, is used as an indication of a chemical species ability to accept electrons. Therefore, a mixture of a species with a low electronegativity, in combination with a species with a high electronegativity will, theoretically, result in a thermite mixture with a high heat of reaction. The combination of this effect with a low activation energy is visualised in Figure 2-3.
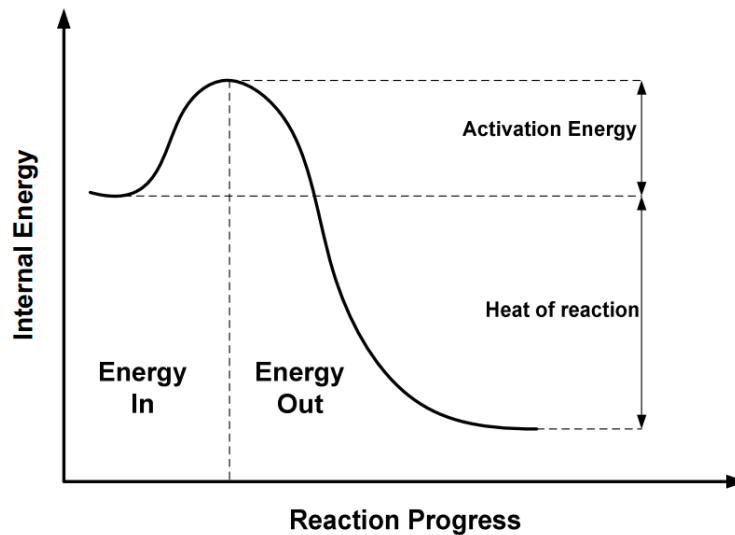
Figure 2-3: Internal energy as a function of reaction completion.

Activation energy has a strong effect on the ignition temperature of a thermite composition. Combination of this effect with the heat of reaction gives an indication on whether a specific thermite composition will be able to sustain the chemical reaction. The reaction is only sustainable if sufficient heat is transferred from the reacting front to the unreacted composition. For this reason, the thermite mixture would not only need to have a low enough activation energy to be initiated, but would have to generate enough heat to be able to sustain the reaction (Conkling, 1985: 98).

An important parameter that indicates the exothermicity of reactions is the adiabatic flame temperature, T_{ad} (Munir & Anselmi-Tamburi, 1989). The high exothermicity of pyrotechnic reactions usually comes at the cost of high activation energies, meaning that the reactions are

often difficult to initiate (Hlavacek & Puszynski, 1996). This is, however, desirable from a safety point of view.

2.2.2. Stoichiometry and the addition of sensitizers/retardants

Optimum energy output of a thermite composition is anticipated close to the stoichiometric point (Conkling, 1985: 113). The easiest way to lower the reaction rate is to change the mass ratio of fuel/oxidiser. Excess metal fuel is, however, ineffective as a retardant because of its ability to react with atmospheric oxygen (Conkling, 1985: 80). Furthermore, addition of slight excess of fuel often results in a faster combustion rate when the reducing agent is a metal (Mclain, 1980). This implies that the thermal diffusivity of the composition may be one of the main mechanisms by which stoichiometry affects the burn rate.

Excess oxidant, on the other hand, usually results in slower reaction rates. This is not only due to the expected lower thermal conductivity, but also due to the dilution that the excess oxidant causes (Wang et al., 1993). Furthermore, it is unlikely that an oxidant will react with atmospheric oxygen, unless it is in the form of a metal oxide that is not completely oxidised, such as manganese (II) oxide.

Addition of inert diluents is an accepted method of lowering the maximum temperatures reached (Manukyan et al., 2011). Addition of material with thermal mass that does not participate in the exothermic chemical reaction also increases the effective distance between reactive particles, decreasing the diffusivity and the thermal conductivity (Manukyan et al., 2011). The effectiveness of the diluent used depends on the physical properties of the diluent (e.g. thermal conductivity and heat capacity) (Wang et al., 1993). When changing mass ratios is undesirable, two different classes of diluents can be added, namely: inert diluents and diluents that undergo endothermic reactions (Conkling, 1985: 80).

The addition of halide salts can increase pyrotechnic reaction rates (Manukyan et al., 2011). Wang et al. (1993) stated that the addition of small amounts of alkali salts, e.g. NaF, KF, NaCl and KCl or alkali earth salts like AlF_3, MgF_2, can increase the burn rate of thermite. Addition of

cryolite ($NaAlF_3$) also showed this effect. Manukyan et al. (2011) showed that addition of NaCl to Mg/MoO_3 thermite increased the reaction rate up to a mole equivalent of 2 (2 mol NaCl for 3 mol Mg). This effect was reversed for higher mass ratios of the salt with a mole equivalent above 5 resulting in no combustion.

The salts containing both aluminium and fluorine showed the greatest burn rate increase in low concentrations, when added to Al/Cr_2O_3 thermite. It is proposed that these salts enhance the reaction rates by lowering the ignition temperatures of the thermite. This is achieved via the disintegration of the fuel oxide layer by chemical reaction (Wang et al., 1993).

2.2.3. Particle size and mixing

Mass diffusion between the metal and oxidant is often the rate determining step when dealing with thermite reactions (Prentice, Pantoya & Clapsaddle, 2005; Riley & Kisi, 2008). Diffusion path length is directly proportional to particle size. As a result, thermite reaction rates increase with a decrease in particle size (Tomasi & Munir, 1999; Prentice et al., 2005; Piercey & Klapötke, 2010). Shimizu, Junji & Hao (1990) analysed the effect of the number of contact points on the reaction rate for a Fe_2O_5/V_2O_5 system. The results confirmed a relation between particle size and reaction rate.

Tomasi & Munir (1999) showed that burn rate was inversely proportional to particle size for diffusion controlled reactions between Al_2O_3, ZrO and Nb. Furthermore, Rugunanan & Brown (1994) showed that burn rates could be changed from 8 mm s^{-1} to 28 mm s^{-1} by reducing the particle size from 14 µm to 2 µm for a system composed of antimony and potassium permanganate. Moore (2005) attributed the enhanced reactivity of thermites composed of smaller particles to better fuel/oxide mixing, effectively allowing the constituents to be in more intimate contact. Makino & Law (1994) did, however, go on to say that the relationship between particle diameter and reaction rate would only be effective up to a certain minimum particle diameter. This is due to the pyrotechnic mixture becoming homogeneous.

12

The advent of the nanotechnology age has spilled through to thermite technologies. This is due to the fact that many fuel and oxidant nano-sized powders (nanopowders) have become commercially available (Rogachev & Mukasyan, 2010). As a result, several laboratories globally are doing extensive research in the field (Gash, Simpson & Satcher, 2002). This class of thermite has been called metastable intermolecular composites (MICs), nanothermite or superthermite.

Aumann (1995) stated that Al/MoO$_3$ nanothermite mixtures react more than 1 000 times faster than the corresponding micron-sized mixtures. The enhanced reactivity of MICs has allowed thermite to become a viable explosive (Moore, 2005). This is further verified by the fact that some nanothermite reactions proceed at burn rates exceeding 2 000 m s^{-1} (Shende et al, 2008; Farley & Pantoya, 2012). Firmansyah et al. (2012) stated that the ignition temperature of thermite based on nano-aluminium has ignition temperatures well below the ignition temperature of the corresponding thermite based on micron sized particles.

The increased reactivity offered by smaller constituent particles is, however, meaningless unless effective mixing can be attained. This is due to non-desired mixing ratios being present through the bulk of the pyrotechnic composition. The effect of mixing on performance is more pronounced when using nano-scale particles due to the agglomerates formed (Wei, Dave & Pfeffer, 2002). Prentice *et al.* (2005) showed that nano-scale compositions prepared via a sol-gel technique resulted in a more complete reaction than those prepared via a traditional solvent-based technique.

2.2.4. The passivation layer

Most metals are thermodynamically unstable when exposed to air (Pourbaix, 1966). This is due to corrosion, which results in the formation of compounds that are similar to the mineral ores from which the metals are derived. Due to a surface oxide layer, the metal fuels used in pyrotechnic reaction are never perfectly pure. This layer acts as a barrier, inhibiting further oxidation. This is especially important in metal nanopowders, as they would be pyrophoric in air without the passivated oxide layer (Pantoya & Granier, 2005). Aluminium particles, for example, are always surrounded by a layer of amorphous alumina (Aumann, 1995). As a result, the fuel is

13

not in contact with the oxidiser until application of external energy causes the failure of the alumina layer when utilising aluminium-based thermites.

The thickness of the oxidised layer on fuel particles depends on the specific metal particle and the method by which it is passivated (Hasani, Panjepour & Shamanian, 2012). Table 2-1 list the passivation shell thickness for aluminium as reported by several groups.

Table 2-1: Passivation layer thickness for nano- aluminium powder

Particle size (nm)	Alumina thickness (nm)	Reference
200	2.9-3.6	Aumann (1995)
96	2	Firmansyah et al. (2012)
80	4	Prentice et al. (2005)
17-202	4-8	Pantoya & Granier (2005)

Piercey & Klapötke (2010) stated that the passivation of the metal must be taken into account when using fuels in the sub-micron scale. This is due to the fact that the oxide layer accounts for a significant mass fraction of the total particle. There is, therefore, less fuel available for the reaction, resulting in non-stoichiometric fuel/oxidiser ratios.

Levitas et al. (2007) modelled the effect of oxide layer thickness on the propagation rate of aluminium combustion. Central to the model is the fact that aluminium has a lower melting temperature than the oxide that encapsulates it. Phase transition of the aluminium from solid to liquid is accompanied by a 6 % increase in specific volume (Gesner, Pantoya & Levitas, 2012). The volume increase causes an internal pressure increase of up to 2 GPa. This, in turn, causes the encapsulating oxide shell to be put under a hoop stress. This process continues until the oxide shell fails, and molten aluminium is dispersed into the reaction zone.

2.2.5. Bulk density

Increases in bulk density of thermite mixtures results in a reduction in the number of voids (Pantoya & Granier, 2005). Decreasing the number of voids increases the number of particle-

14

particle contact points and, therefore, the thermal conductivity. This causes an increase in the combustion rate (Wang et al., 1993).

Pantoya & Granier (2005) showed that the effect of bulk density was different depending on the particle size of the powders used. The micron-sized thermite showed an increased reaction rate with an increase in bulk density, as expected. In contrast, the nanothermite showed the inverse effect. The difference is attributed to the melt-dispersion mechanism whereby the nanothermite reaction process is initiated. Pantoya et al. (2009) stated that the reduced void space does not allow for effective kinetic energy transfer, as described by Levitas et al. (2007). The above nanothermite based mechanism must be compared to solid-solid diffusion process that is attributed to triggering traditional thermite systems (Pantoya et al., 2009)

2.3. Fluoropolymer-based pyrotechnics

Metal powder with halocarbon compound-based compositions are widely used in pyrotechnics (Koch, 2012: 358). This is specifically due to the electronegativity of halogen-based compounds, as it allows them to react with a multitude of metal fuels (Farley & Pantoya, 2012). Furthermore, owing to the high enthalpy of formation of the metal- halogen bond (H-X), this class of thermites features high energy densities (Koch, 2012 : 358).

The metal-fluorine bonds have among the highest enthalpies of formation of all the metal-halogen and metal-oxygen combinations. It enables the formulation of compositions that cannot be outperformed by any other pyrotechnic combination (Koch, 2012). This is evidenced by the fact that the formation of magnesium fluoride produces more heat than the formation of magnesium oxide (Kubota & Serizawa, 1987). As a result, peak pressures and gas production increase when using fluorine compared to oxygen-based oxidising agents (Watson, Pantoya & Levitas, 2008).

15

2.3.1   Types of fluoropolymer-based pyrotechnics

Polytetrafluoroethylene (PTFE) contains 75 wt.% fluorine. Therefore, it is a good source of fluorine for pyrotechnic applications (Osborne, 2006). A common example of PTFE as an oxidising agent is in the magnesium-Teflon-Viton (MTV) reaction, used in aerial countermeasure applications (Steinhauser & Klapötke, 2008). Teflon and magnesium react as shown in Equation 2-8.

$$(C_2F_4)_n + 2n\text{Mg} \rightarrow 2n\text{C} + 2n\text{MgF}_2 \qquad \text{2-8}$$
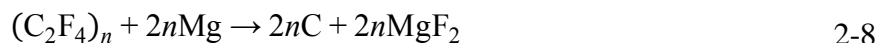
The work done by Ladouceur showed that PTFE decomposes to TFE, which in turn rapidly decomposes to CF_2 (Douda, 1991). This implies that the intermediate step for the reaction between PTFE and magnesium is the reaction between CF_2 and magnesium rather than the reaction between magnesium and F_2. As a result, Equation 2-8 can be rewritten as Equation 2-9.

$$CF_2 + \text{Mg} \rightarrow \text{C} + \text{MgF}_2 \qquad \text{2-9}$$

The stoichiometric point for the magnesium-Teflon reaction occurs at 33 wt.% magnesium. Commercial compositions are usually fuel-rich (Kubota & Serizawa, 1987). This is especially true for counter-measure flare compositions that require the production of much heat and smoke. The possibility of producing of condensed, as well as gaseous products depending in the mix ratio means that MTV can used for many applications, as shown in Figure 2-4.

The reaction between PTFE and aluminium is receiving attention from researchers. This is due to unavailability of bulk quantities of magnesium nanoparticles. As a result, substitution of magnesium with aluminium nanoparticles has been investigated for traditional MTV applications. Although the energy output is lower, it was found that nano-aluminium-substituted MTV had faster burn rates with similar sensitivities.

16
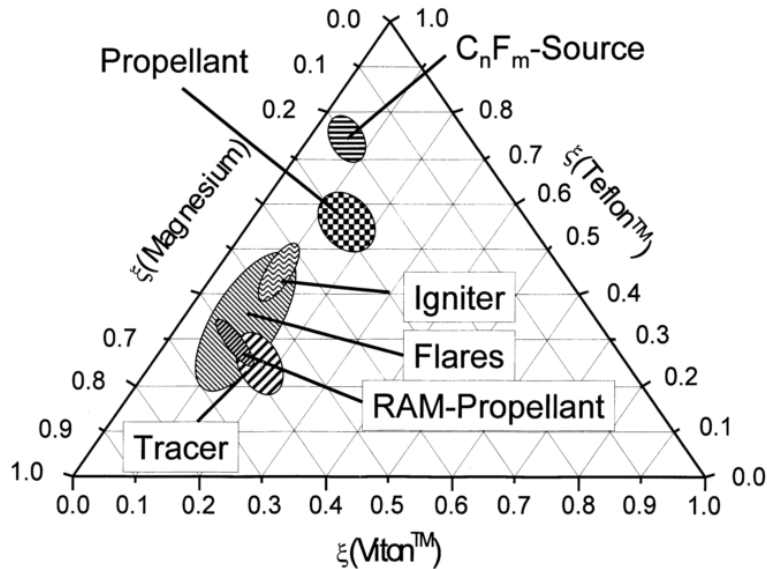
Figure 2-4: MTV application as a function of specific component ratios (Koch, 2002a)

Stacy et al. (2009) determined the effectiveness of Al/Teflon nanothermite for underwater deflagration purposes, citing the possibility of thermite torch manufacture as a possible application. The experiments showed the formation large vapour columns. This lowered the heat transfer between the product gas and the water and was postulated to allow for enhanced cutting potential. Furthermore, hydrophobic properties offered by fluoropolymers enables the manufacture of compositions that find use in a variety of environments, where traditional pyrotechnics cannot be used (Stacy et al., 2009).

A co-polymer of vinylidine fluoride (VDF), tetrafluoroethylene (TFE) and hexafluoropropylene (HFP) is used as a binder in many pyrotechnic formulations. The co-polymer is known by several trade names, with Viton from DuPont being well known. Viton is commercially available in three main grades: Viton A; Viton B and Viton F, with corresponding fluorine content of 66 wt.%, 68 wt.% and 70 wt.% respectively. The high fluorine content enables Viton to react with metal fuels, making it ideal as a binder in pyrotechnic formulations. Furthermore, Viton helps with the processing of pyrotechnic compositions and serves as a barrier to magnesium corrosion (de Yong & Smit, 1991).

17

The MTV and NSI (NASA standard initiator) are two pyrotechnic compositions that make use of Viton as a binder. Hohmann & Tipton (2000) showed that the most important factors affecting the performance of different Viton grades as binder was the glass transition temperature and the polydispersity of the polymer.

2.3.2. Rheology of filled polymers

The viscosity of the polymer melt will almost always increase with the addition of filler particles (Krieger, 1959). The magnitude of this effect depends on the following:

- Particle shape,
- Particle size distribution,
- Particle-particle interactions, and
- The applied shear rate (Barnes, 2003).

The effect is small until the filler approaches a volume fraction (ϕ_f) of 0.3 for monodisperse spherical particles (Barnes, 2003).

The Krieger equation (Equation 2-10) can be used to estimate the viscosity increase of polymer melts, as a function of volume fraction filler.

$$\eta_r = \frac{\eta}{\eta_o} = \left(1 - \frac{\phi}{\phi_m}\right)^{-[\eta]\phi_m} \qquad \text{2-10}$$

The subscripts r, o and m stand for the relative, unfilled and maximum respectively. $[\eta]$ is the intrinsic viscosity and describes the thickening power of filler particles. Spherical particles are assigned an intrinsic viscosity value of 2.5 (Barnes, 2003). This effect is shown in Figure 2-5 for monodisperse spherical particles ($\phi_m = 0.637$) and bidisperse spherical particles ($\phi_m = 0.87$)
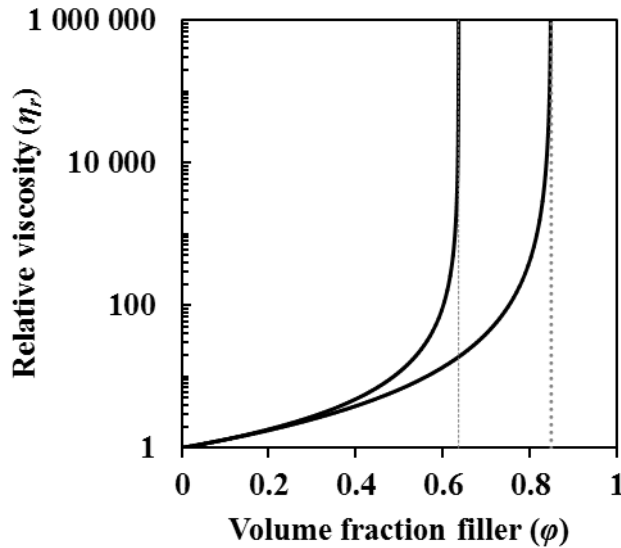
Figure 2-5: Predictions of the Krieger model for the relative viscosity as a function of the volume fraction filler atomised filler particles for ϕ_m values of 0.637 and 0.85

2.3.3. Manufacture of fluoropolymer-based pyrotechnics

Although Teflon is by strict definition a thermoplastic, PTFE based pyrotechnics cannot be manufactured via traditional polymer processing techniques (Nielson et al., 2005; Frick et al., 2013). This is because PTFE does not become fluid below its degradation temperature like traditional polymers owing to its extremely high molar mass (Lee, 2005).

The most common manufacturing technique for commercial MTV products is mixing PTFE and magnesium powders into a 8 wt.% - 20 wt.% Viton solution (Koch, 2012). Hexane is added so that the Viton precipitates on the solid constituents. The composition is dried and granulated, before being pressed. The pressed pellets are sintered and annealed, so that compositions of sufficient strength are made (Nielson et al., 2005). This technique is hazardous, as both the pressing and annealing may result in accidental ignition if care is not taken. Furthermore, the solvents used are flammable.

It is possible to use twin screw extruders for the manufacture of MTV-type compositions if the PTFE and magnesium are wetted with ethanol before being fed into the extruder (Koch, 2012:

19

283). A Viton solution is injected, and all the constituents are thoroughly mixed. A vacuum section is added to the extruder for solvent removal.

2.4. Thermodynamics

One of the main indications of the spontaneity, as well as exothermicity of reactions, is the adiabatic combustion temperature, T_{ad} (Wang et al., 1993). Furthermore, T_{ad} enables the identification of possible intermediates and the phases that may be present in reactions.

Munir & Anselmi-Tamburi (1989) defined T_{ad} as the temperature to which the product is raised due to chemical reaction, under adiabatic conditions. In other words, it is the temperature that a certain reaction would reach if no heat transfer occurred between the products and the surroundings. The total free energy can be calculated using Equation 2-11.

$$G = \sum_i n_i \mu_i \qquad \text{2-11}$$

n_i is the number of moles of species i. μ_i, the chemical potential, and can be calculated using Equation 2-12.

$$\mu_i = \mu_i^0 + RT \ln a_i \qquad \text{2-12}$$

The superscript 0 represents the reference temperature. The activity of gaseous species are approximately equal to partial pressure, assuming that they behave as ideal gasses (Equation 2-13).

$$a_i = \frac{p_i}{P} = \left(\frac{n_i}{N}\right) \qquad \text{2-13}$$

If the all substances are considered to be pure, the chemical potential is described using Equation 2-14.

$$\mu_i = \mu_i^0 = g_i^0 \qquad \text{2-14}$$

Combination of Equation 2-11, 2-12, 2-13 and 2-14 yields:

$$G = \sum_{i=1}^{l} n_i^g \left(g_i^g + RT \ln P + RT \ln\left(n_i^g / N \right) \right) + \sum_{i=1}^{s} n_i^c \cdot g_i^c \qquad \text{2-15}$$

The superscripts g and c represent the gaseous and condensed species, respectively, while l and s are the number of gaseous and condensed species in the system, respectively. g_i is related to the entropy, S, and enthalpy of the system via Equation 2-16.

$$g_i = \Delta h_i - T\Delta S \qquad \text{2-16}$$

Under adiabatic conditions, i.e. with no heat losses to the environment, the heat generated (Q) can be calculated using Equation 2-17.

$$Q = -\sum_i \int_{298}^{T} n_i^0 C_{p_i} \mathrm{d}T + \sum_i \Delta h_i \cdot \Delta n_i \qquad \text{2-17}$$

The superscript 0 denotes the initial amounts, and Δn_i the change in the number of moles in the system. The adiabatic flame temperature can be calculated by solving Equation 2-18 with respect to T_{ad}.

$$Q = \sum_i \int_{T_0}^{T_m} n_i C_{p_i} \mathrm{d}T + \sum_i H_m n_i + \sum_j H_p n_j + \sum_k \int_{T_m}^{T_{ad}} n_k C_{p_{li}} \mathrm{d}T$$
$$+ \sum_l \int_{T_b}^{T_{ad}} n_l C_{p_g} \mathrm{d}T + \sum_l H_b n_l \qquad \text{2-18}$$

Here, it is assumed that the system only contains liquid and gaseous species at T_{ad}.

21

Chapter 3 : Experimental

3.1.   Modelling

Thermodynamic simulations were done using EKVI thermodynamic simulation software. Thermodynamic data was received from EKVIbase Index 2.17. The adiabatic reaction temperature, condensed species concentration and gaseous species concentration were recorded for varied filler loadings. The gas evolved per unit reactant composition as a function of the filler loading was also noted. Simulations were performed at constant pressure of 100 kPa, with the reference temperature set to 25 °C. The adiabatic reaction temperature over the range was taken as an indication of the stoichiometric point.

Polymers were simulated as their respective monomers. This was a valid assumption, as monomers are the main decomposition products of their respective polymers (de Yong & Smit, 1991). This was done for all simulated compositions, except polystyrene. The data for styrene was not available in the thermodynamic database; therefore, ethylbenzene was used as the corresponding monomer. The error incurred is minimal, as the physical properties of both species are similar (Green & Perry, 2007: 2-73). Furthermore, ethylbenzene has a similar chemical structure to styrene, with ethylbenzene containing two more hydrogen atoms. Ethylbenzene would, therefore, offer a conservative approximation for styrene in thermodynamic simulations, as more water would be generated from the chemical reaction with an oxidant.

Addition of the polymer raw materials as monomers in the gaseous phase would, however, have introduced an inaccuracy to the model as the heat of polymerisation (ΔH_p) would have been neglected. This is especially true for the compositions that make use of PTFE as oxidant, as it has the highest polymerisation energy (ΔH_p) of all polymers considered (Koch, 2002b; Roberts, 1950). The polymerisation values listed in Table 3-1 show, that although the PS and Viton have smaller ΔH_p, they cannot be ignored either. Addition of the polymers as monomers would, therefore, result in a higher predicted adiabatic temperature, which would result in prediction of incorrect product spectra.

Table 3-1: Polymerisation energy of the simulated polymers

Polymer	Polymerisation energy (kJ $g_{monomer}^{-1}$)
PS	0.768
Viton	0.342
PTFE	1.72

Corrections for ΔH_p were done by charging helium gas with the reactants. This acted as a thermal sink that did not participate in the reaction. The amount of helium gas required for each composition was calculated by first simulating each composition with the polymer in the monomer form. The amount of helium required to compensate for ΔH_p was calculated by setting the enthalpy of helium at the adiabatic temperature (of the calculations based on the monomers) equal to the polymerisation energy. The enthalpy of helium was calculated using EKVI. The results shown in Figure 3-1 reveal that the enthalpy of helium varies linearly with temperature. This would allow for facile compensation of ΔH_p as variation of the quantities of helium charged would directly vary the energy offset incurred.
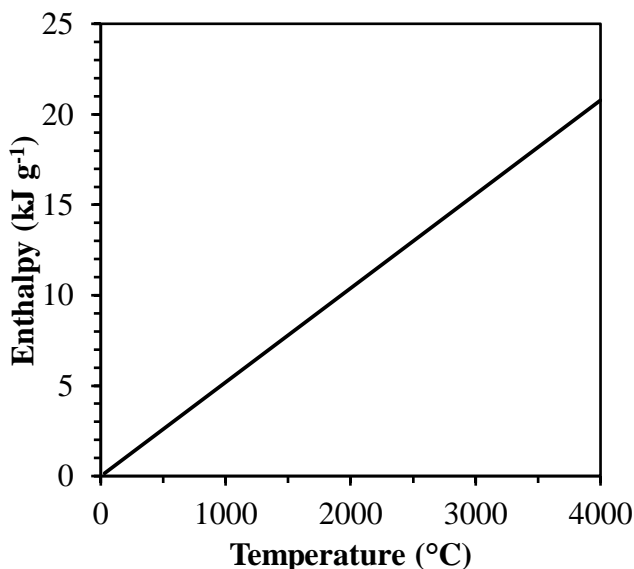

Figure 3-1: Enthalpy of helium at 100 kPa predicted using EKVI.

The thermodynamic simulations will inherently not reflect the real results of experimental tests. This is because of the assumption that equilibrium is attained and the fact that kinetic factors are

23

ignored (de Yong & Smit, 1991). Furthermore, calculations are based on ideal gas equations of state (de Yong & Smit, 1991).

3.2. Outline

The possibility of manufacturing thermoplastic-based pyrotechnic films was tested by making different solid compositions. The compositions tested where:

- Polystyrene with potassium nitrate
- Polystyrene with potassium permanganate
- Viton B with calcium carbide
- Viton B with aluminium
- Viton B with 50/50 wt.% magnalium

Polystyrene was selected as a reducing agent because of its high carbon-to-hydrogen ratio. This would theoretically result in a high energy output as less water is formed during the reaction with an oxidant. Formation of water saps the enthalpy of reaction owing to the phase changes associated with its transformation into steam at elevated temperatures. Potassium nitrate and potassium permanganate were selected as oxidants because of their wide use in the pyrotechnics industry.

Viton B was selected as an oxidising agent, due to its high solubility in ketone-based solvents, coupled with its high fluorine content (68 wt.%). Calcium carbide was selected as a reducing agent because of the low vapour pressure of calcium fluoride. The reaction between calcium carbide and a fluorine-based oxidant will should, therefore, result a gasless formulation. Pure calcium could not be used because it is pyrophoric. Aluminium was selected as a reducing agent because of the considerable amount of research that has been done on aluminium/fluoropolymer-based pyrotechnics. This would, therefore, allow for the comparison of results to known values. Furthermore, there was access to aluminium with different morphologies so that the effect of morphology on pyrotechnic films could be quantified. Magnalium was selected as a reducing agent because of its chemical stability compared to pure magnesium. Furthermore, 50/50 wt.%

24

magnalium has a lower melting point than the constituents of the alloy, and should, therefore result in in a pyrotechnic composition that should ignite at lower temperatures (Shimizu, 1981).

The compositions were simulated using EKVI thermodynamic software. The effect of stoichiometry was investigated. Pyrotechnic films were produced by dissolving the thermoplastic polymer in acetone and adding the solid fuel powder so that the reducing agent volume fraction varied from 20 wt.% to 60 wt.%. Open flame burn tests were performed for initial screening tests. A silicon-bismuth cuprate starter composition was added as an igniter composition to the compositions that did not ignite using a propane flame alone. No further tests were performed on the compositions that did not even ignite when the silicon-bismuth cuprate starter was used.

The energy output and pressure signal of the remaining compositions were tested in a bomb calorimeter in a helium atmosphere at a pressure of 30 bar. The reaction residue was collected and analysed using X-ray diffraction (XRD), thermogravimetric analysis (TGA) and scanning electron microscopy (SEM). XRD was done so that the crystalline phases present could be identified and compared to simulated results. TGA was done to determine the mass loss of each residue. This provided information on the nature of the amorphous phase identified in the XRD analysis. SEM was used to identify the morphology of the reaction residues.

3.3. Materials

Fluoropolymer Viton® B-50 pellets (ex Du Pont), containing 68 % fluorine, were donated by Necsa. It was categorized as FKM Type 2 according to ISO 1629:2013, since it is a copolymer of vinylidene fluoride, hexafluoropropylene and tetrafluoroethylene. FTIR spectroscopy confirmed the sample identity. The FTIR spectrum is shown in Appendix C.

Flake-like aluminium, grade APS 11 micron, was purchased from Alfa Aesar. This grade has a purity of 99.7 % on a metals basis. Atomised aluminium powder (grade A120FB) was supplied by Ginman. Magnalium powder was manufactured and supplied by the CSIR. The latter two powders were ball-milled and passed through a 325 mesh sieve. The lower fractions were retained.

KNO_3, $KMnO_4$ and CaC_2 were sourced from Sigma Aldrich. KNO_3 and $KMnO_4$ was ground using a mortar and pestle. CaC_2 was ball milled for 96 h. The resulting powder was passed through a 325 mesh sieve. The lower fractions were retained.

3.4. Methods

Three different compositions were made using magnalium, aluminium flake and atomised aluminium powder as reducing agents, with Viton B as the oxidant.

Pyrotechnic films were made using the slurry process described in Hohmann & Tipton (2000). A 16.6 wt.% Viton B solution was prepared by adding Viton B to ethyl acetate and stirring for 24 h at room temperature. Predetermined quantities of reducing agents were added to the Viton B solution. Homogeneity of the composition was ensured by mixing with a magnetic stirrer set to its maximum mixing speed of 1 250 rpm. The reducing agents were added, so that the final composition fuel content varied from 20 wt.% to 60 wt.% in 10 wt.% increments. The mixture was dried on flat Teflon-coated trays for 72 h in a refrigerator set to 4 °C. The pyrotechnic films were carefully removed, so that film defects due to handling could be minimised. The films were visually inspected for any imperfections.

Film thickness was determined by placing the pyrotechnic films between two reinforced phenolic plates and measuring the distance that they were displaced using a micrometer.

3.5. Characterisation

A Malvern Mastersizer Hydro 2000MY instrument was used to determine particle size distributions.

XRD analysis was performed on a PANalytical X-pert Pro powder diffractometer. The instrument featured variable divergence and receiving slits and an X'celerator detector using Fe filtered Co Kα radiation (λ = 0.178901 nm). XRD data analysis was done using X'Pert

26

Highscore plus 4.1 software. The ARL Perform'X Sequential XRF and Uniquant software was used for XRF analyses. The samples were prepared as pressed powder briquettes.

A Parr Instruments 6200 calorimeter utilizing 240 mL high pressure oxygen combustion was used for energy measurements. Measurements were made in a helium atmosphere at 30 bar. The pyrotechnic films were prepared for sampling by grinding the films in a blender with liquid nitrogen. The resulting powder was used with sample size kept constant at 25 mg. Compositions were ignited using nichrome wire. The change of pressure (ΔP) with time was measured using a NI piezoelectric pressure transducer. The signal was recorded using a Parr pressure recording system, which used a 2.5 kHz sample rate. 30000 data points were recorded per sample run.

The reaction residue was collected after each run. The reaction residue from the bomb calorimeter was analysed on a Perkin Elmer 4000 TGA. An air atmosphere was used. The reaction residue was placed in a 70 µL alumina crucible. The temperature was raised from 25 °C to 900 °C at a rate of 10 °C min^{-1}, after which the temperature was kept constant for 30 min. The sample was then cooled to 25 °C at 30 °C min^{-1}. The resulting residue was collected for SEM analysis.

Open flame speed tests were performed using a 40 W Synrad Inc. CO_2 laser as ignition source. The samples strip dimensions measured 7.5 mm × 50 mm. All samples were ignited with the ignition source set to 12 W. The reaction was recorded using a Gopro Hero 3 camera, recording at 120 frames per second, at a resolution of 1 280 by 720 pixels (720p). Video data was analysed using Microsoft movie maker set to a 0.125x playback speed.

Tensile properties were tested performed on a LLOYD instruments LRX plus tensometer. A 50 N load cell was used. The gauge length was set to 100 mm. Tests were done at a speed of 100 mm min^{-1}. The elongation at-break was measured for each sample.

A Jeol JSM-5800 scanning electron microscope was used to visualize the morphology of the reaction residue particles. The accelerating voltage was 20 kV. Before viewing, samples were

sputter coated with gold using a Gatan Ion Beam Coater. A Noran EDX was used to conduct energy dispersive X-ray spectroscopy analysis.

Ignition sensitivity tests were performed using BFH-10 bam fall hammer impact sensitivity test apparatus. The aluminium-based compositions were tested using a 10 kg hammer, equating to a maximum energy of 98 J. The magnalium-based composition was tested using a 5 kg weight. Friction sensitivity tests were done using a FSKM 50-20K bam friction sensitivity test apparatus. Weight B9 was used. Sensitivity tests were performed on compositions using 30 wt.% fuel.

Chapter 4 : EKVI thermodynamic simulation results

Thermodynamic simulations were done in order to determine product stream compositions and adiabatic reaction temperature as a function of stoichiometry. All simulations were done at 100 kPa pressure and at adiabatic reaction temperature. The reactants were charged at 25 °C. The reducing agent/oxidant ratio was varied. The adiabatic temperature, condensed species, gaseous species and gas amount were determined.

The maximum temperature was used as an indicator of the exothermicity of each composition. The condensed and gaseous products were reported so that the toxicity of products could be checked. Identification of the gaseous products would also give an indication of the pressure dependence of the pyrotechnic compositions.

4.1. Polystyrene as fuel

Polystyrene was simulated by the addition of ethylbenzene in the gas phase, since the thermodynamic database did not contain styrene. Two oxidising agents were simulated: potassium nitrate (KNO_3) and potassium permanganate ($KMnO_4$). A ratio of 0.225 $g_{He}/g_{ethylbenzene}$ to compensate for the polymerisation energy of polystyrene.

4.1.1. KNO_3 as oxidant

Figure 4-1 shows the simulated results for the reaction between ethylbenzene and potassium nitrate. Adiabatic temperatures increased from 450 °C to a global maximum of 1 300 °C at 90 wt.% KNO_3. Initially, carbon was the most abundant condensed product formed. Increased KNO_3 content, however, led to a decrease in the amount of carbon formed and increased potassium carbonate formation.

Initially, hydrogen and methane are the most abundant gaseous products formed. Carbon monoxide, nitrogen and water vapour content increased with increased KNO_3 content. The maximum carbon monoxide levels occurred at 80 wt.% KNO_3, showing that the reaction is

29

limited by the quantity of oxidant present in that regime. A decrease in gas evolved per unit reactant is observed above 80 wt.% KNO_3. Carbon monoxide levels rapidly decreased above 80 wt.% KNO_3. This is accompanied by an increase in KOH, CO_2 and H_2O levels.

A peak carbon dioxide level was not reached in the range of 0 wt.% – 90 wt.% KNO_3. This indicates that the stoichiometric point for the reaction between ethylbenzene and KNO_3 lies between 90 wt.% – 100 wt.% KNO_3. Polystyrene and KNO_3 have densities of 1 050 kg m^{-3} and 2 110 kg m^{-3}, respectively (Green & Perry, 2007: 2-22). This means that the stoichiometric point would occur above 82 vol.% KNO_3- higher than the limit for randomly packed, monodisperse particles.
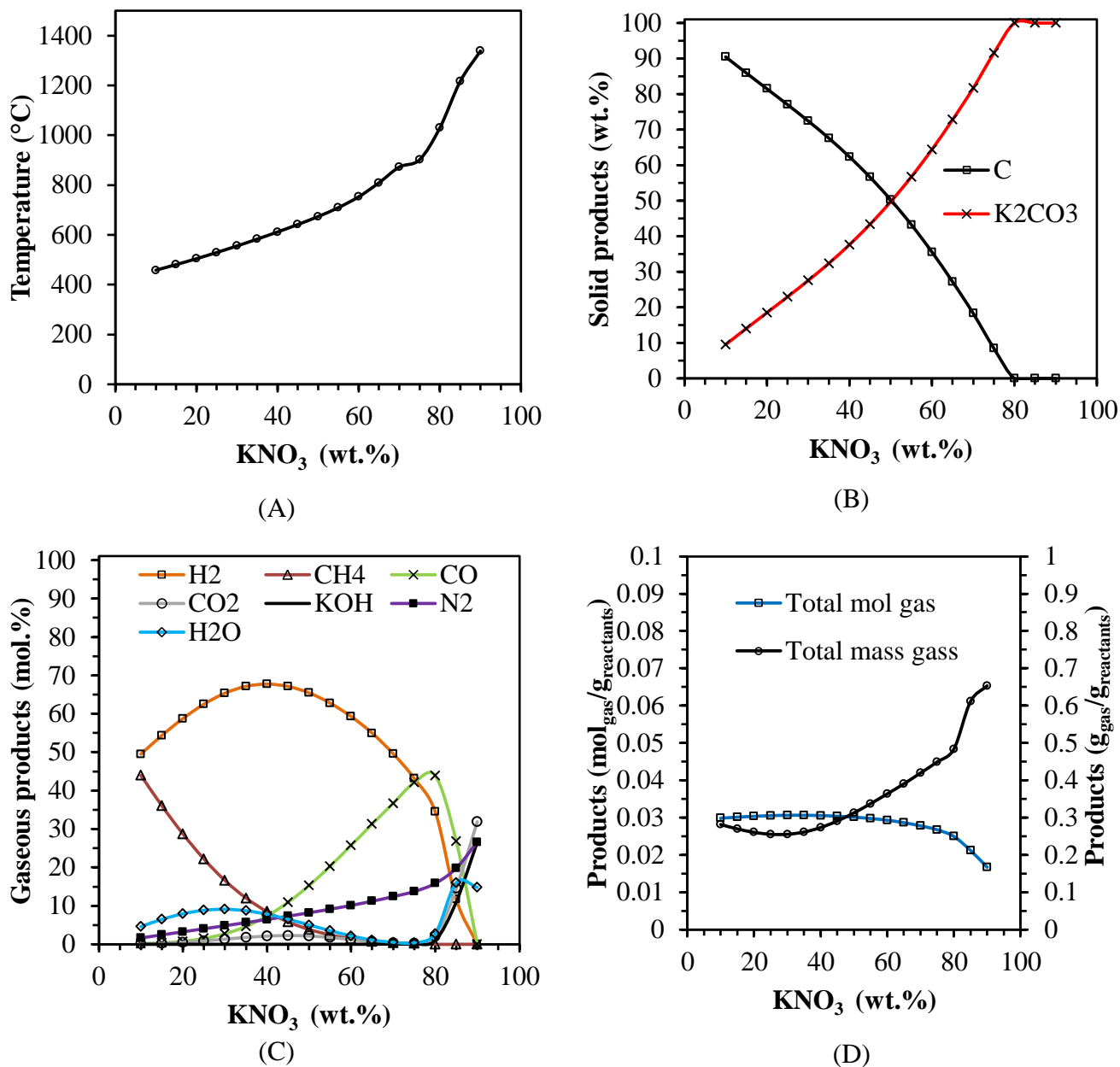
Figure 4-1: Simulation results for the reaction of potassium nitrate with ethylbenzene with varied oxidant dosing. (A) Adiabatic temperature as a function of KNO_3 loading. (B) Species evolved as a function of KNO_3 loading. (C) Gaseous products formed as a function of KNO_3 loading. (D) Gas produced per unit reactant as a function of KNO_3 loading.

31

4.1.2. KMnO$_4$ as oxidant

Figure 4-2 shows the simulated results for the reaction between ethylbenzene and potassium permanganate. Adiabatic temperatures rises in an almost linear manner from 450 °C to the maximum temperature of 1 200°C at 90 wt.% KMnO$_4$. The condensed species is, initially, mainly comprised of carbon. The carbon content, however, decreases in a semi-linear fashion with an increase in oxidant content. Above 85 wt.% KMnO$_4$, all elemental carbon is present as CO, CO$_2$ or K$_2$CO$_3$.

The gas per unit reactant decreased in a linear fashion up to 85 wt.% KMnO$_4$, where after the rate increased. The mass of gas evolved per unit reactant reached a minimum at the point of maximum hydrogen evolution. The maximum mass of gas evolved was observed at 90 wt.% KMnO$_4$.

CH$_4$ and H$_2$ are the most abundant gaseous species at low oxidant levels. CH$_4$ levels, however, decrease over the whole range and is non-existent above 85 wt.% KMnO$_4$.The maximum CO concentration also occurs at 85 wt.% KMnO$_4$. It is, therefore, postulated that the main reactions that occur are the decomposition of ethylbenzene to CH$_4$, carbon and hydrogen. The reaction between carbon and KMnO$_4$ forms K$_2$CO$_3$ and MnO. Further increases in oxidant levels results in the oxidation of hydrogen and carbon to form water vapour, CO and, eventually, CO$_2$. The water and CO$_2$ formations become appreciable above 85 wt.% KMnO$_4$, indicating a more complete oxidation of ethylbenzene. The absence of a maximum temperature peak, as well as carbon dioxide/ water peak indicates that the stoichiometric point does not occur in the range 10 wt.% − 90 wt.% KMNO$_4$. This means that the stoichiometric point would occur at a filler ratio in excess of 78 vol.% KMnO$_4$ (density of KMnO$_4$ = 2 700kg m^{-3}) (Green & Perry, 2007: 2-22). It is, therefore, unlikely that pyrotechnic compositions based on polystyrene with KMnO$_4$ will be melt processable.
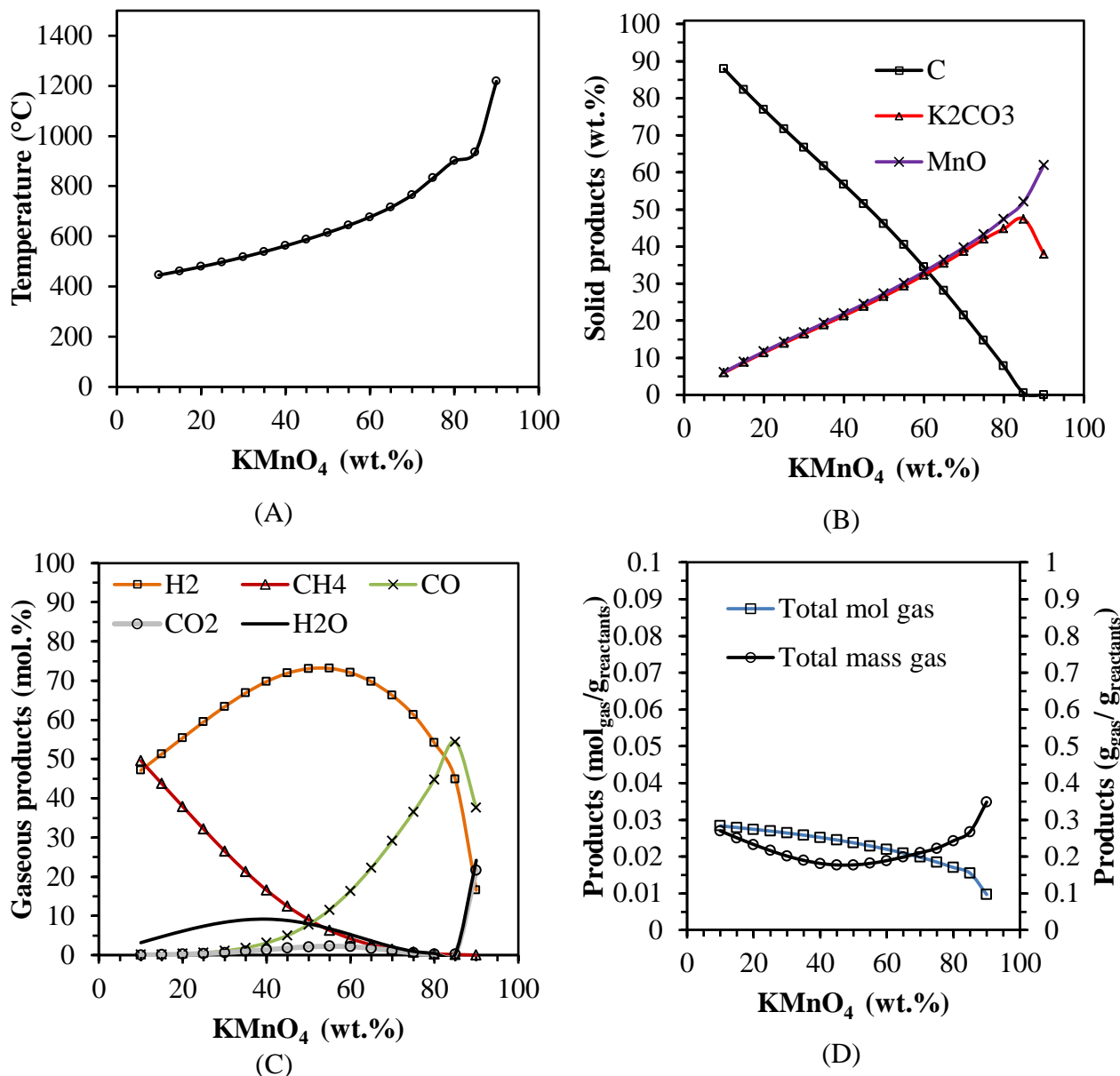
Figure 4-2: Simulation results for the reaction between ethylbenzene and potassium permanganate with varied oxidant volume fractions. (A) Temperature as a function of $KMnO_4$ loading. (B) Condensed species evolved as a function of $KMnO_4$ loading. (C) Gaseous species evolved as a function of $KMnO_4$ loading. (D) Gas produced per gram reactant as a function of $KMnO_4$ loading

33

4.2. Fluoropolymer-based systems

4.2.1. Perfluoronated polymer as oxidant

Reactions of polytetrafluorethylene (PTFE) were simulated by charging the monomer, TFE. The reactions between TFE and different reducing agents were simulated at 100 kPa. A ratio of 0.1 g_{He}/g_{TFE} was used for the simulations using aluminium, magnesium and magnalium. The lower adiabatic temperature predicted for the reaction between TFE and CaC_2 resulted in the addition of 0.18 g_{He}/g_{TFE}.

4.2.1.1. Aluminium as fuel

The simulated results shown in Figure 4-3 reveal the adiabatic temperature increases from 2 200 °C to the maximum value of 3 170 °C at 35 vol. % aluminium. The adiabatic temperature decreases rapidly between 40 wt.% and 50 wt.% aluminium. A steady decrease in the adiabatic temperature is observed in oxidant loadings above 50 wt.%.

Only carbon is present in the condensed product stream up to 50 wt.% aluminium. CF_4 derived from the decomposition of TFE is initially the most abundant gaseous product. Increasing aluminium content, however, results in the consumption of gaseous CF_4 and the development of aluminium fluorides (AlF_x). This indicates that TFE decomposes into CF_4 and C before reacting with the reducing agent.

The production of aluminium carbide (Al_4C_3) rapidly increases above 50 wt.% aluminium, indicating that more aluminium is present than required for the complete conversion to AlF_3. Al_4C_3 content reaches a maximum at 65 wt.% aluminium, where after condensed aluminium content increases, showing that aluminium is in excess. The adiabatic flame decreases due to the dilution caused by the excess aluminium.

34

The maximum gas generation of 0.02 $mol_{gas}/g_{reactant}$ occurred at 50 wt.% aluminium. This point corresponds to the highest specific mass of the gaseous products developed. Since there is only AlF_x present, it must be in the fully fluorinated form- AlF_3.
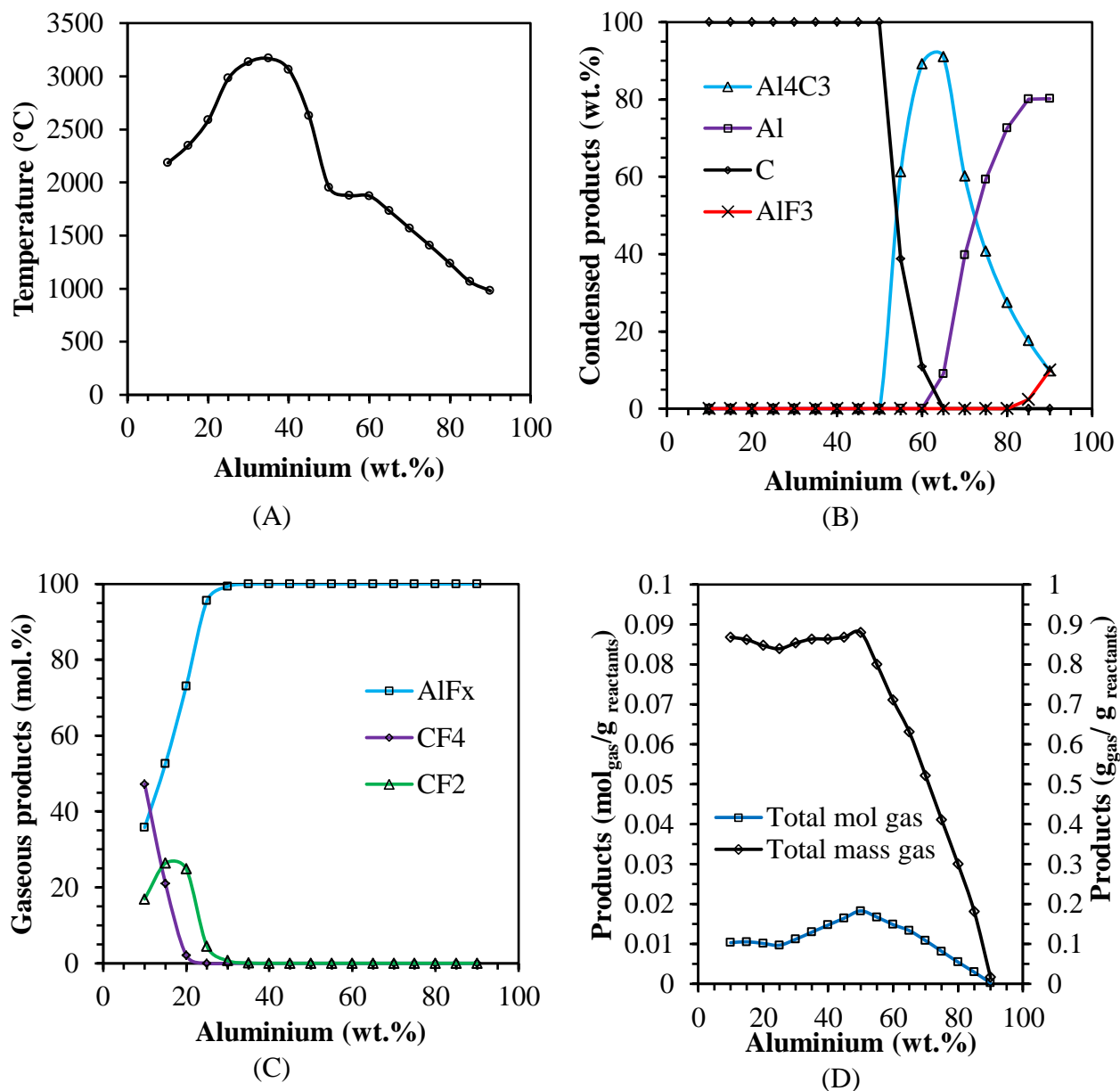

Figure 4-3: Simulation results for the reaction between aluminium and TFE for different reducing agent loadings. (A) Adiabatic temperature as a function of aluminium loading. (B) Condensed species evolution as a function of aluminium loading. (C) Gaseous species evolved as a function of aluminium loading. (D) Gas evolved per gram reactant as a function of aluminium loading.

35

4.2.1.2. Magnesium as fuel

The simulated results, shown in Figure 4-4, reveal that the adiabatic temperature increases from 2 000 °C to the maximum temperature of 3 000 °C between 10 wt.% and 35 wt.% magnesium. Carbon is the only condensed species present below 45 wt.% magnesium. Gaseous CF_4 and CF_2 derived from the decomposition of PTFE are initially present. Both are, however, fully consumed above 35 wt.% magnesium. This shows that the stoichiometric point for the reaction that produces magnesium fluoride (MgF_2) occurs at 35 wt.% magnesium.

After the maximum temperature is reached, adiabatic temperature rapidly decreases with increasing magnesium content. MgF_2 overtakes carbon as the most abundant condensed species. Gas phase MgF_2 condenses with the decrease in temperature. Gas evolved increases to a maximum at 70 wt.% magnesium. This is due to the adiabatic temperature being higher than the boiling point of magnesium (Green & Perry, 2007: 2-27).

Adiabatic temperature remains constant before decreasing at 90 wt.% magnesium. The product streams contain mostly magnesium with decreasing quantities of carbon and MgF_2. Magnesium is the most abundant gaseous product at high magnesium content. The amount of gas evolved at high magnesium loadings was, however, negligible.

4.2.1.3. Magnalium as fuel

Figure 4-5 shows the simulated results for the reaction between 50/50 wt.% magnalium and TFE for different magnalium loadings. Adiabatic temperature increases with increasing magnalium loading to a maximum value of 3 100 °C at 35 wt.% magnalium. Carbon is the main condensed product formed below 50 wt.% magnalium. The gaseous products contain TFE decomposition products, as well as magnesium fluoride and aluminium fluorides. All gaseous TFE decomposition products are consumed above magnalium loadings of 30 wt.%.
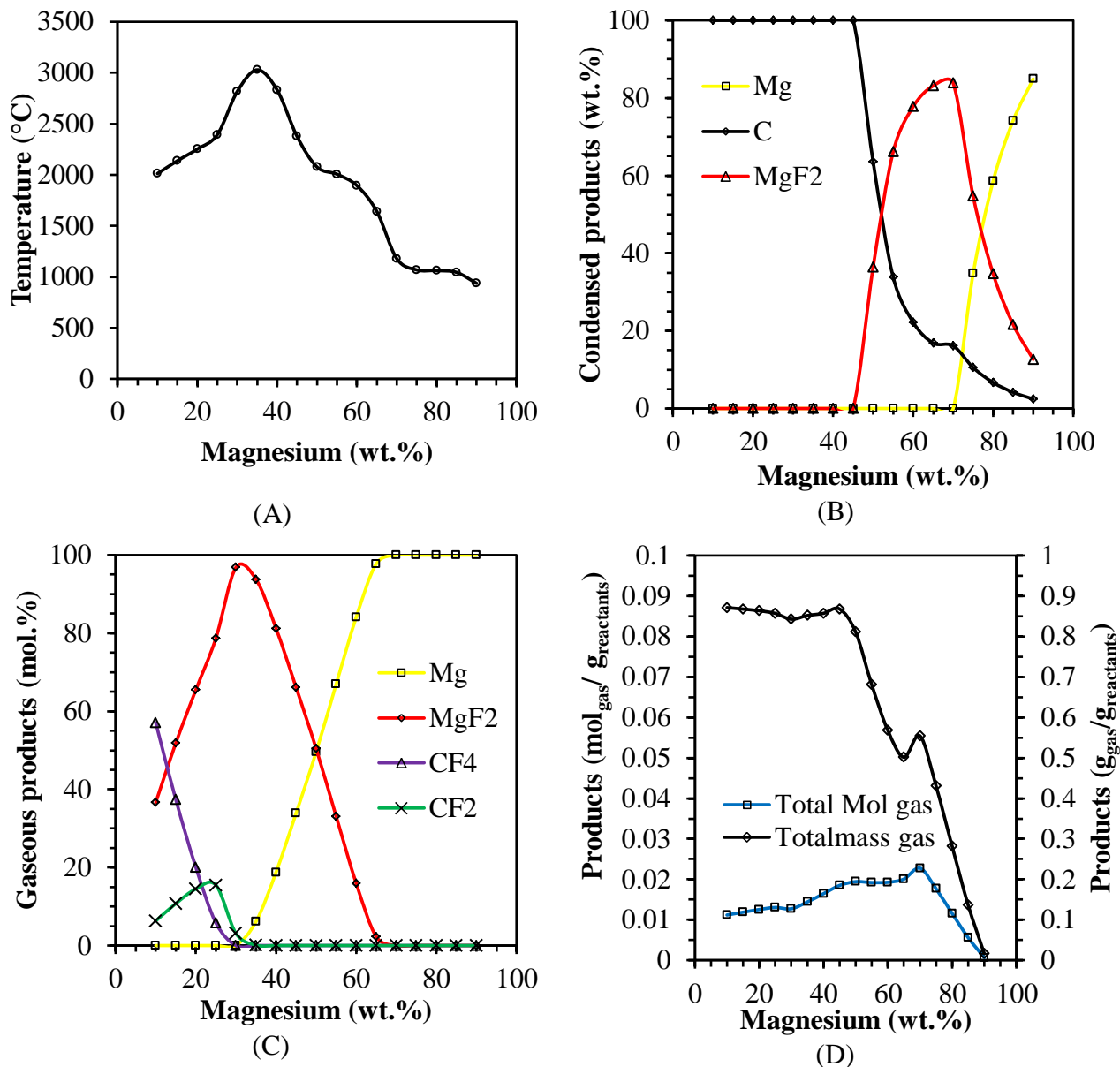
36

Figure 4-4: Simulation results for the reaction between magnesium and TFE. (A) Adiabatic temperature as a function of magnesium loading. (B) Condensed species as a function of magnesium loading. (C) Gaseous species as a function of magnesium loading. (D) Gas evolved per gram reactant as a function of magnesium loading.

Gaseous MgF_2 reaches a peak concentration at 30 wt.% magnalium. Increased magnalium content causes an increase in MgF_2 content in the condensed stream. This indicates that the adiabatic temperature moved below the boiling point of MgF_2. The adiabatic temperature decreases above 35 wt.% magnalium. The maximum gas generation occurs at 55 wt.%

37

magnalium. Carbon and MgF_2 content decreases in the condensed product stream above 50 wt.% magnalium.

Condensed elemental aluminium is present in the form of aluminium carbide above 55 wt.% magnalium. This indicates that the formation of MgF_2 is favoured above the formation of aluminium fluorides. Unreacted aluminium and magnesium are present in the condensed phase at 70 wt.% and 80 wt.% respectively, further showing that the formation of MgF_2 is favoured.

The concept of a stoichiometric point may not hold true for this reaction, or rather, there is more than one stoichiometric point. The first stoichiometric point occurs at 35 wt.% magnalium and corresponds to the maximum MgF_2 and AlF_3 content. The second stoichiometric point occurs at 70 wt.% magnalium. This point is associated with the maximum Al_4C_3 content.

4.2.1.4. Calcium carbide as fuel

The simulated results shown in Figure 4-6 reveal that the adiabatic temperature increases from 10 wt.% to 55 wt.% CaC_2. The maximum temperature of 2 200 °C is achieved at the concentration where all TFE decomposition products are consumed. This leads to the maximum concentration of CaF_2 in the gaseous phase.

Increasing CaC_2 loading above 55 wt.% results in a decrease in adiabatic temperatures. This is as a result of dilution, as evidenced by the presence of unreacted CaC_2 above 60 wt.%. Gas evolution remains relatively constant up to 55 wt.% CaC_2, where after it decreases to zero at 85 wt.% CaC_2.
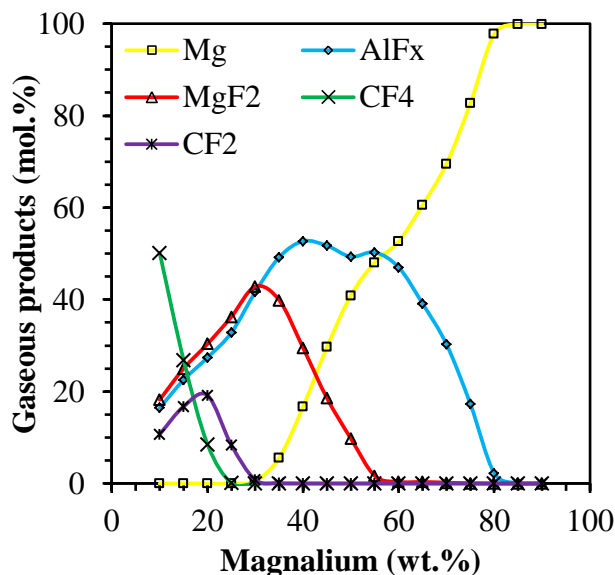
Carbon in the condensed phase is derived from the decomposition of TFE as well as the reaction between CF_4 with CaC_2. The density of CaC_2 is 2 200 kg m^{-3} (Anon, *sa*). This means that the stoichiometric point occurs at 40 vol.% CaC_2, much lower than the limit imposed for randomly packed media using spherical, monodisperse particles.
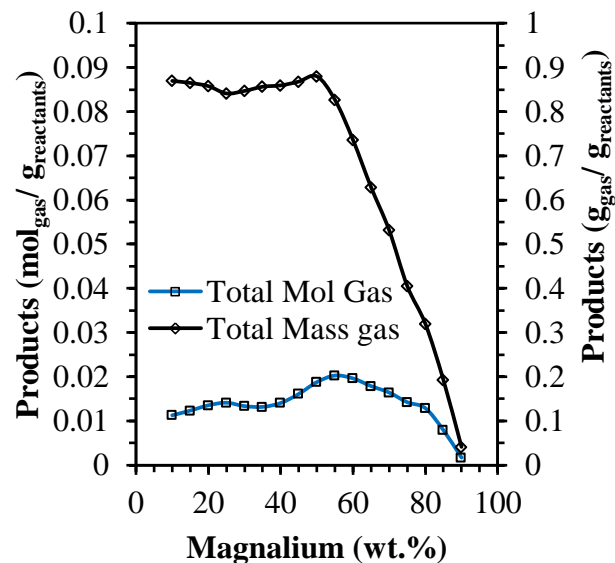
38
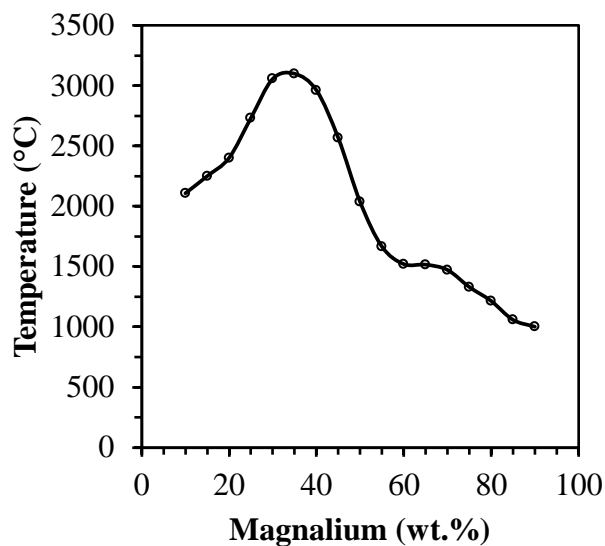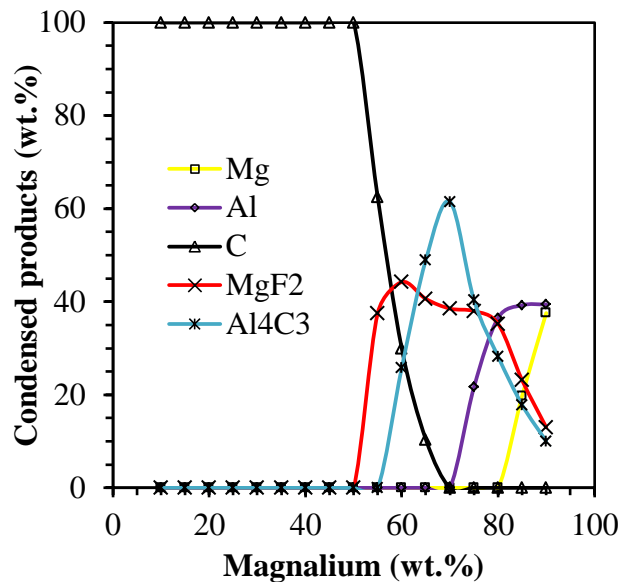
Figure 4-5: Simulation results for the reaction between 50/50 wt.% magnalium and TFE. (A) Adiabatic temperature as a function of magnalium dosing. (B) Condensed species evolved as a function of magnalium dosing. (C) Gaseous species evolved as a function of magnalium loading. (D) Gas evolved per gram reactant as a function of magnalium loading.

39

Figure 4-6: Simulation results for the reaction between CaC_2 and TFE. (A) Adiabatic flame temperature as a function of CaC_2 loading. (B) Condensed species evolved as a function of CaC_2 loading. (C) Gaseous species evolved as a function of CaC_2 loading. (D) Gas evolved per gram reactant as a function of CaC_2 loading.

40

4.2.1.5. Discussion of perfluorinated simulations

The highest adiabatic temperature was seen in the composition that used aluminium as fuel. The system based on magnalium had a maximum temperature that was between that of aluminium and magnesium. The loading at maximum temperature was also at the same loading as that of either aluminium or magnesium.

Compositions based on CaC_2 showed the lowest average adiabatic temperatures of all the compositions. It is postulated that this is due to the high stability of CaC_2 (Wang et al., 1993). Furthermore, the large amount of carbon generated in the reaction products would undergo secondary atmospheric oxidation and would, possibly, offer greater performance than thermodynamic simulations indicate.

The volume fraction filler for all the stoichiometric compositions was well below the limit of 0.637, meaning that traditional polymer processing techniques would be possible if fully fluorinated polymer other than PTFE is used.

4.2.2. Vinylidene fluoride co-polymers

Due to a lack of thermodynamic data, FKM-type fluoropolymers were simulated by charging TFE and vinylidene fluoride (VDF) as two different species. The chemical composition would, therefore, be the same as a co-polymer of the two species. The ratio of TFE to VDF was changed so that the effect of fluorine and hydrogen content could be quantified. The calculations showed that a mixture of 50 mol.% TFE with 50 mol.% 1,1-difluoroethene (VDF) resulted in a polymer with fluorine content of 69.5 wt.%. Combining 30 mol.% TFE and 70 mol.% 1,1-difluoroethene resulted in a polymer with fluorine content of 66 wt.%. Corrections for the polymerisation energy were done by adding 0.03 g_{He}/ $g_{VDF \, co\text{-}polymer}$.

4.2.2.1.　　50/50 VDF/ TFE with aluminium

The simulated results for the reaction between aluminium and a 50/50 (mol basis) mixture of VDF and TFE is shown in Figure 4-7. Adiabatic temperature increases with increasing aluminium content to the maximum value at 25 wt.% aluminium. Carbon is the only condensed species formed at aluminium loading below 45 wt.%. Gaseous products contain the fluoro-elastomer decomposition products, as well as hydrogen fluoride (HF) and aluminium fluorides (AlF_x). The maximum AlF_3 concentration occurs at 15 wt.% aluminium, whereas the maximum AlF_2 concentration occurs at 25 wt.% aluminium. This indicates that the formation of AlF_2 is associated with the generation of higher temperatures.

Adiabatic temperature decreases with increased aluminium content after the stoichiometric point. Al_4C_3 formation becomes appreciable at 45 wt.% aluminium and the gaseous product composition shifts from HF formation to the formation of aluminium fluorides. The maximum gas evolution occurs at 50 wt.% aluminium, with aluminium fluorides being the most abundant gaseous products at that point (specifically AlF).

The adiabatic temperature decreases at a faster rate above 60 wt.% aluminium, where the maximum Al_4C_3 content is reached. Hydrogen is the most abundant species in the gaseous products at higher aluminium loadings.

4.2.2.2.　50/50 VDF /TFE with magnalium as fuel

The simulation results for the reaction between a 50/50 mol.% mixture of TFE and VDF and magnalium is shown in Figure 4-8. Adiabatic temperature increases to the maximum temperature of 3 030 °C at 25 wt.% magnalium. Carbon is initially the only condensed product. The gaseous products comprise of HF and the decomposition products of the fluoro- elastomer. There are also aluminium fluorides and magnesium fluorides present.

42

Adiabatic temperature decreases from 3 030 °C to 1 500 °C at 55 wt.% magnalium. This decrease in temperature is accompanied by the condensation of MgF_2 and, therefore, an increase in the concentration of condensed MgF_2.
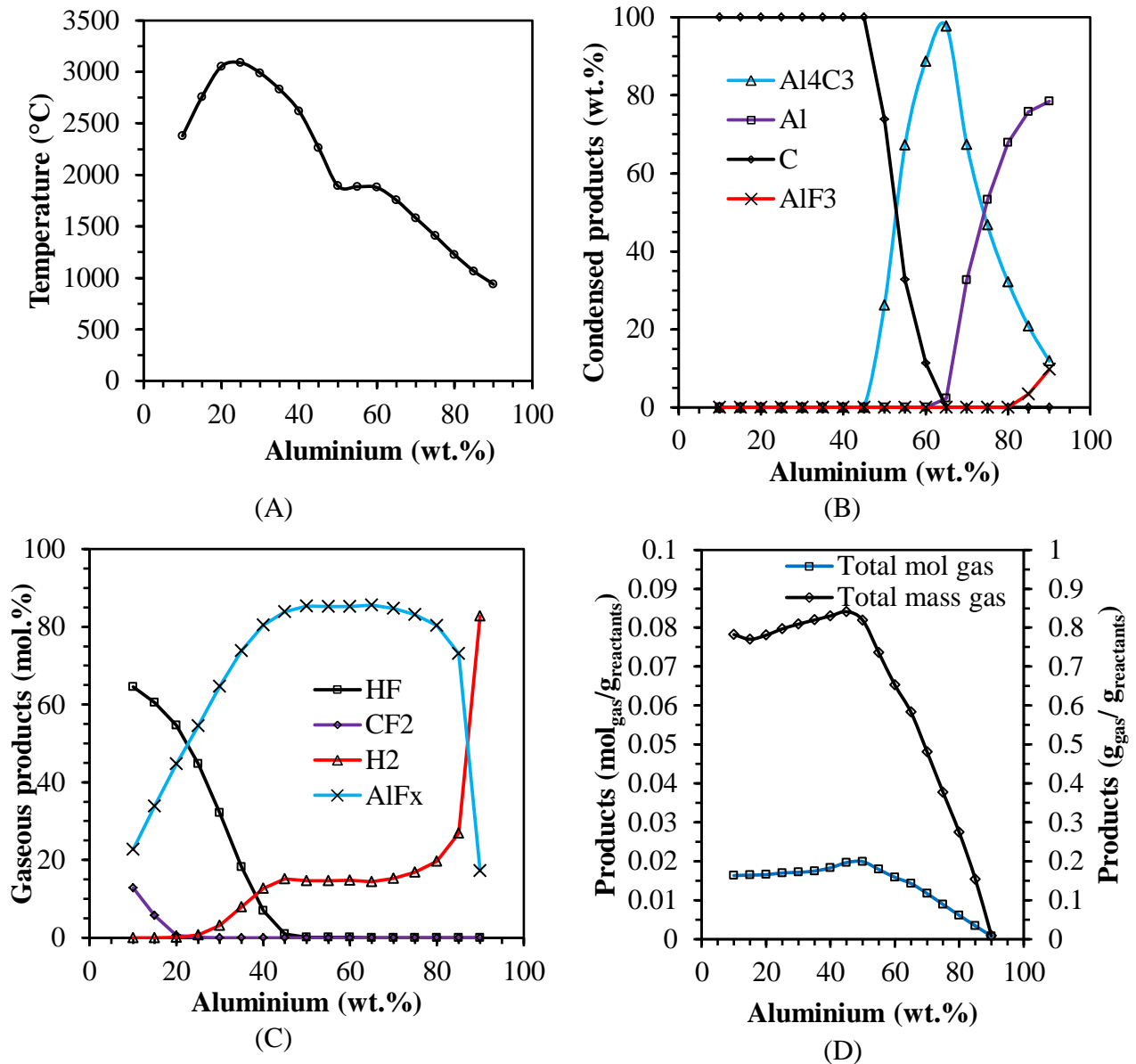

Figure 4-7: Simulation results for the reaction between FKM Type 2 fluoro elastomer and aluminium at 100 kPa. (A) Adiabatic temperature as a function of aluminium loading. (B) Condensed species formed as a function of aluminium loading. (C) Gaseous species formed as a function of aluminium loading. (D) Gas evolved per gram reactant as a function of aluminium loading.

43

HF content decreases to zero at 50 wt.% magnalium. This is accompanied by an increase in H_2 content. AlF_x continues to increase with increased magnalium content to a maximum at 55 wt.% magnalium.
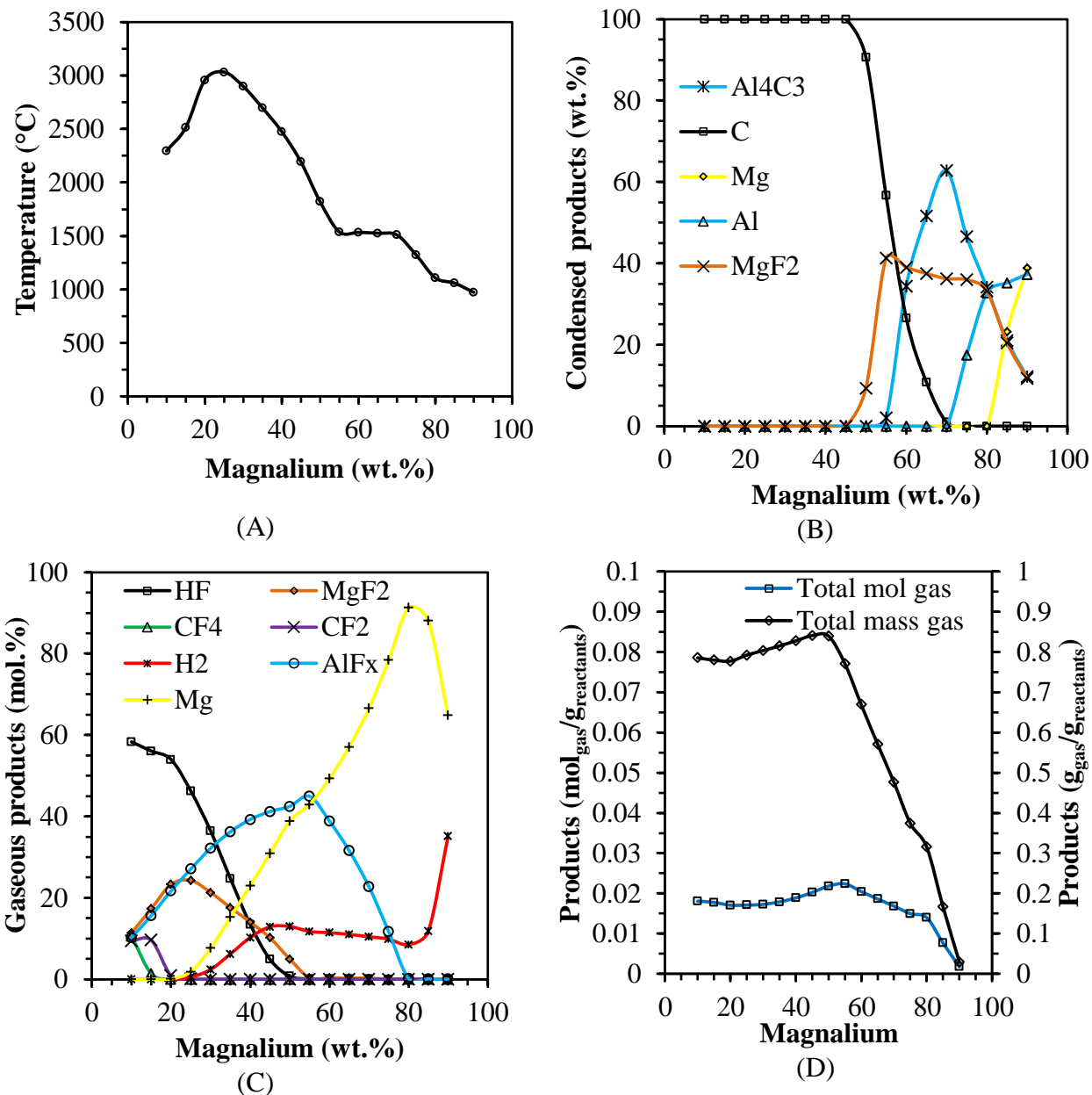

Figure 4-8: Simulation results for the reaction between FKM Type 2 fluoro-elastomer and 50/50 wt.% magnalium. (A) Adiabatic temperature as a function of magnalium loading. (B) Condensed species evolved as a function of magnalium loading. (C) Gaseous species evolved as a function of magnalium loading. (D) Gas evolved per gram reactant as a function of magnalium loading.

44

The gas evolved per unit reactant composition remains relatively constant up to 55 wt.% magnalium. Unreacted condensed aluminium is present above 70 wt.%; whereas, unreacted magnesium is present above 80 wt.%. This is due to the formation of Al_4C_3 instead of AlF_x, as well as the differences in the boiling points of magnesium and aluminium.

4.2.2.3.   70:30 VDF: TFE with aluminium

The simulation results of the reaction between aluminium and a 70/30 mol.% mixture of VDF/TFE are shown in Figure 4-9. Adiabatic temperature increases to a maximum of 2 860 °C at 15 wt.% aluminium. Carbon is the only condensed component up to 45 wt.% aluminium. This coincides with the maximum gas evolved per unit reactant. HF formation ceases above 45 wt.% aluminium. This corresponds to the filler loading where formation ofAl_4C_3 becomes appreciable. AlF_x content reaches a maximum around 65 wt.% aluminium.

Adiabatic temperature decreases to approximately 1 800 °C at 50 wt.% aluminium. This is accompanied by a high concentration of hydrogen in the gaseous stream. Unreacted aluminium appears in the condensed product stream after the maximum Al_4C_3 content is reached. AlF_x vapour content decreases as the adiabatic temperature comes close to the AlF_3 dew point.

4.2.2.4.   70:30 VDF: TFE with magnalium

The simulation results for the reaction between 50/50 wt.% magnalium and 70/30 mol.% mixture of VDF/TFE is shown in Figure 4-10. The maximum temperature of 2 800 °C is reached at 15 wt.% magnalium. Carbon is, initially, the only condensed product. Gaseous products are dominated by the decomposition products of the fluoro-elastomer as well as HF at low magnalium content. AlF_x and MgF_2 are also present.
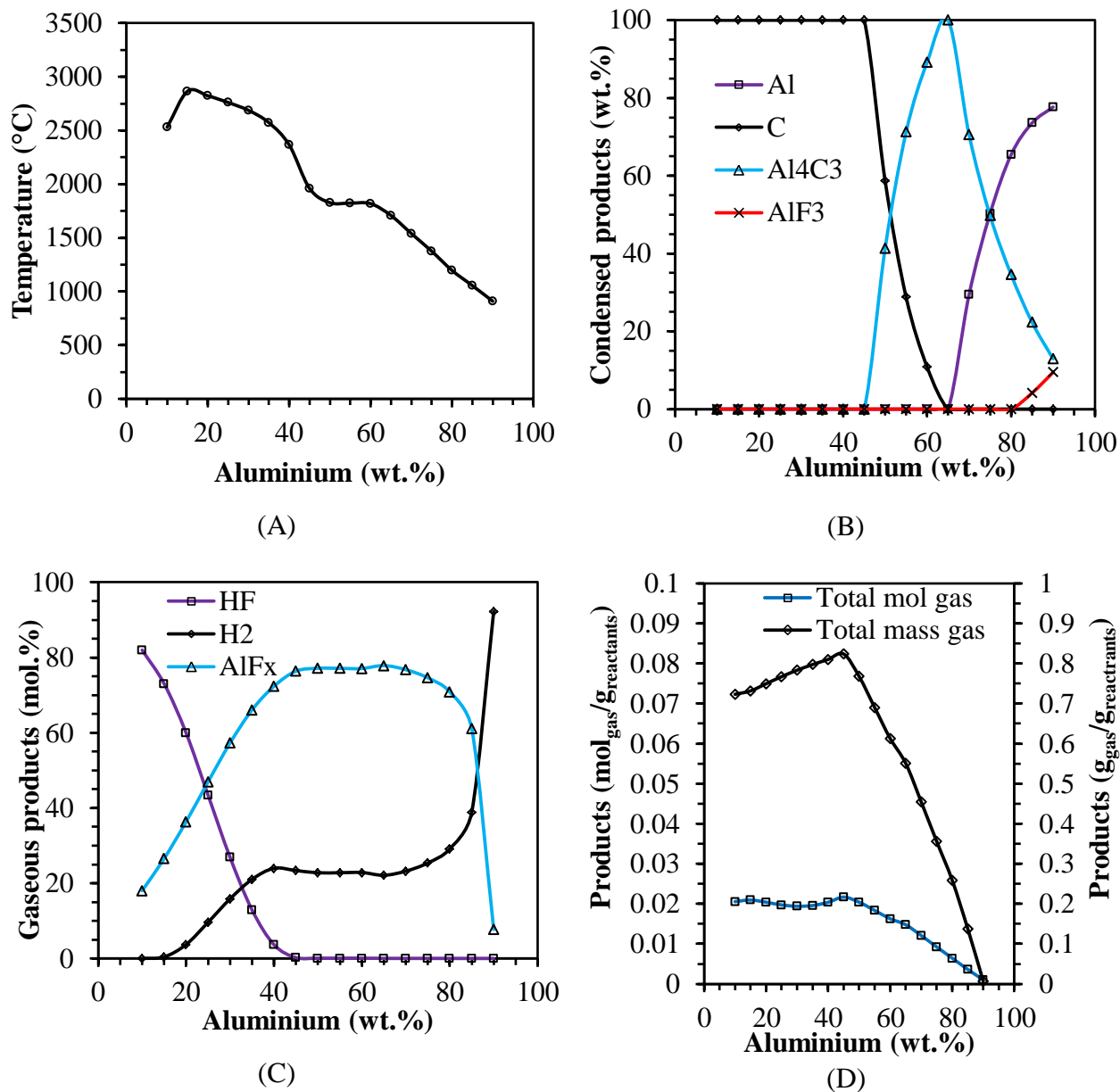
Figure 4-9: Simulation results for the reaction between aluminium and FKM Type 1 fluoro-elastomer. (A) Adiabatic temperature as a function of aluminium loading. (B) Condensed species evolved as a function of aluminium loading. (C) Gaseous species as a function of aluminium loading. (D) Gas evolved per gram reactant as a function of aluminium loading.

46

Adiabatic temperature decreases from 2 800 °C to 1 500 °C at 55 wt.% magnalium. This decrease is accompanied by the appearance of MgF_2 in the condensed phase as the adiabatic temperature approaches the dew point of MgF_2. The gaseous stream is dominated by AlF_x and H_2.

Adiabatic temperature further decreases with increased aluminium content. Unreacted magnesium and aluminium is present in the condensed product stream. H_2 content increases over the whole range. Magnesium vapour and hydrogen are the only species in the gaseous stream above 80 wt.% magnalium.

4.2.2.5.   Discussion of VDF co-polymer simulations

The VDF/HFP co-polymer-based systems showed similar adiabatic temperatures to the fully fluorinated compositions. The filler loading at maximum temperature was, however, lower for each corresponding composition based on the same reducing agents.

The compositions based on 50/50 mol.% VDF/TFE had higher predicted adiabatic temperatures than the compositions based on 70/30 mol.% based compositions. The 50/50 mol.% VDF-based compositions had adiabatic temperatures at 25 wt.% reducing agent. The 70/30 mol.% VDF co-polymer-based compositions had maximum temperatures at 15 wt.% reducing agent. This corresponds to 21 vol.% reducing agent and 13 vol.% reducing agent, respectively. The use of traditional polymer processing techniques would, therefore, be possible using pyrotechnics based on VDF co-polymers.

The use of VDF/HFP co-polymer led to the generation of hydrogen fluoride at low filler loadings, as well as hydrogen at higher filler loadings. This may limit the commercial viability, as the occupational safety and health administration permissible exposure limit is 2.5 mg m^{-3} for HF. Furthermore, hydrogen poses a significant explosion hazard as a H_2/Air mixture can support deflagration in the range 4 % − 75 % (Carcassi & Fineschi, 2005). As a result, FKM-based systems are only viable at filler loading between 45 wt.% and 55 wt.% reducing agent.
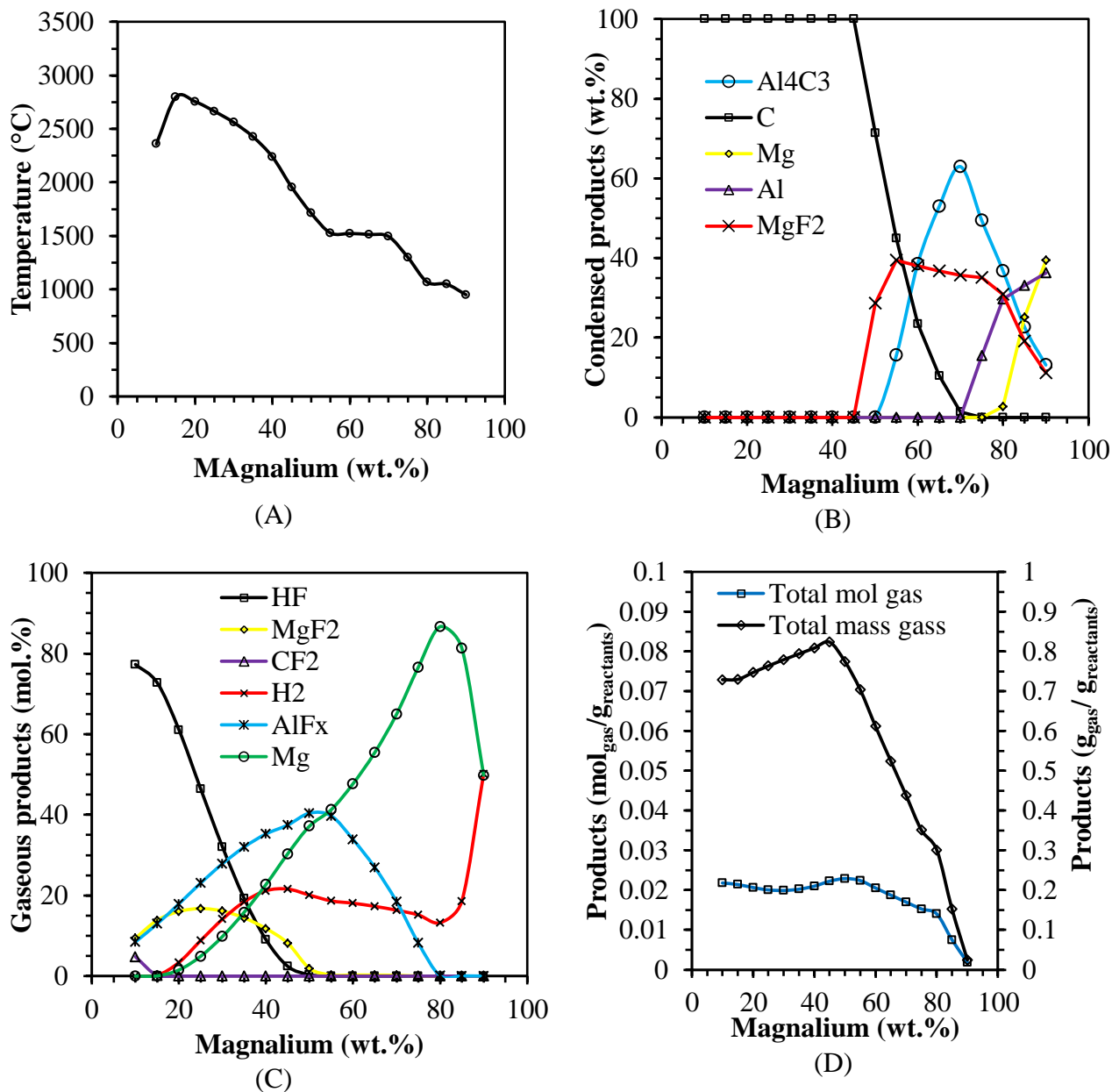
Figure 4-10: Simulation results for the reaction between 50/50 wt.% magnalium and FKM Type 1 fluoro-elastomer. (A) Adiabatic temperature as a function of magnalium loading. (B) Condensed species evolved as a function of magnalium loading. (C) Gaseous species evolved as a function of magnalium loading. (D) Gas evolved per gram reactant as a function of magnalium loading.

Chapter 5 : Experimental results

5.1.   Initial screening

The results of the open-flame burn tests are shown in Table 5-1. The compositions based on polystyrene (PS) did not ignite without the presence of a starter. The addition of a starter, however, only resulted in the ignition of the composition with $KMnO_4$ for filler loadings of 30 wt.% and 40 wt.%. Burning was, however, not sustained, showing that the reaction was kinetically limited. Alternatively, the reaction between PS and the oxidants used did not generate sufficient energy to overcome the depolymerisation energy of PS. The composition based on Viton B with CaC_2 as reducing agent could not be ignited. Addition of a bismuth cuprate starter did not result in a successful ignition for any CaC_2 loading. It is postulated that this occurred because of the thermal stability of CaC_2.

When exposed to a propane burner, the compositions based on Viton B with aluminium and magnalium (Mg/Al) as reducing agents underwent sustained combustion for all filler loadings. No further analysis was performed on compositions that did not successfully ignite in the open flame burn test. As a result, all subsequent tests were only performed on compositions using Viton B as oxidant with aluminium and magnalium as reducing agents.

Table 5-1: Open flame burn test results. X = misfire, O = successful ignition.

Composition	Filler loading (wt.%)				
	20	30	40	50	60
PS + KNO_3	X	X	X	X	X
PS + KNO_3 + starter	X	X	X	X	X
PS + $KMnO_4$	X	X	X	X	X
PS + $KMnO_4$ + starter	X	O	O	X	X
Viton B + CaC_2	X	X	X	X	X
Viton B + CaC_2 + starter	X	X	X	X	X
Viton B + Al (atomised)	O	O	O	O	O
Viton B + Al flake	O	O	O	O	O
Viton B + Mg/Al	O	O	O	O	O

5.2.   Raw material characterisation

The d_{10}, d_{50} and d_{90} particle size of the as-received magnalium powder and the aluminium flake, atomised aluminium and sieved magnalium are reported in Table 5-2. The flake aluminium powder featured a distinct bimodal particles size distribution. Figure 5-1 shows the particle size distributions and Figure 5-2 shows SEM micrographs of the fuel powders. X-ray fluorescence indicated that the magnalium contained 57 wt.% aluminium and 43 wt.% magnesium on a metals basis. XRD confirmed the purity of the aluminium powders. The atomised aluminium, however, contained an amorphous phase as shown in in Figure B-1. This may indicate presence of an alumina layer.

Table 5-2: Fuel particle sizes

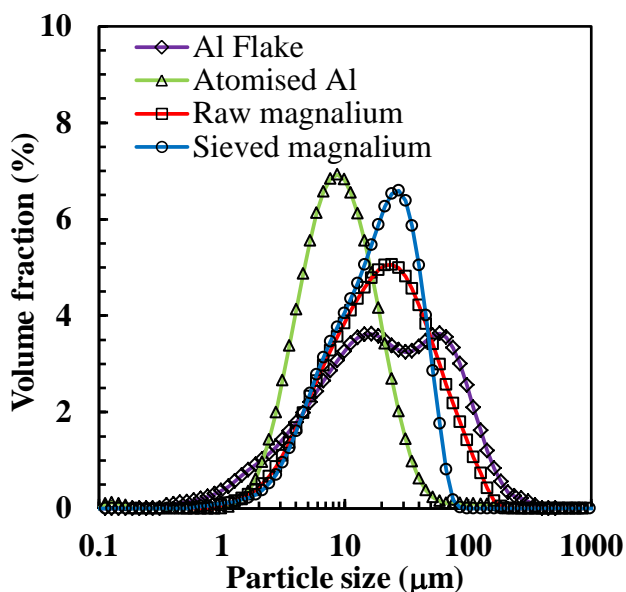| Size, μm	Al flake	Atomised Al	Raw magnalium	Sieved magnalium
d_{10}	3.0	3.8	4.8	5.6
d_{50}	16.0	9.3	20.4	19.6
d_{90}	88.8	23.6	59.9	45.2

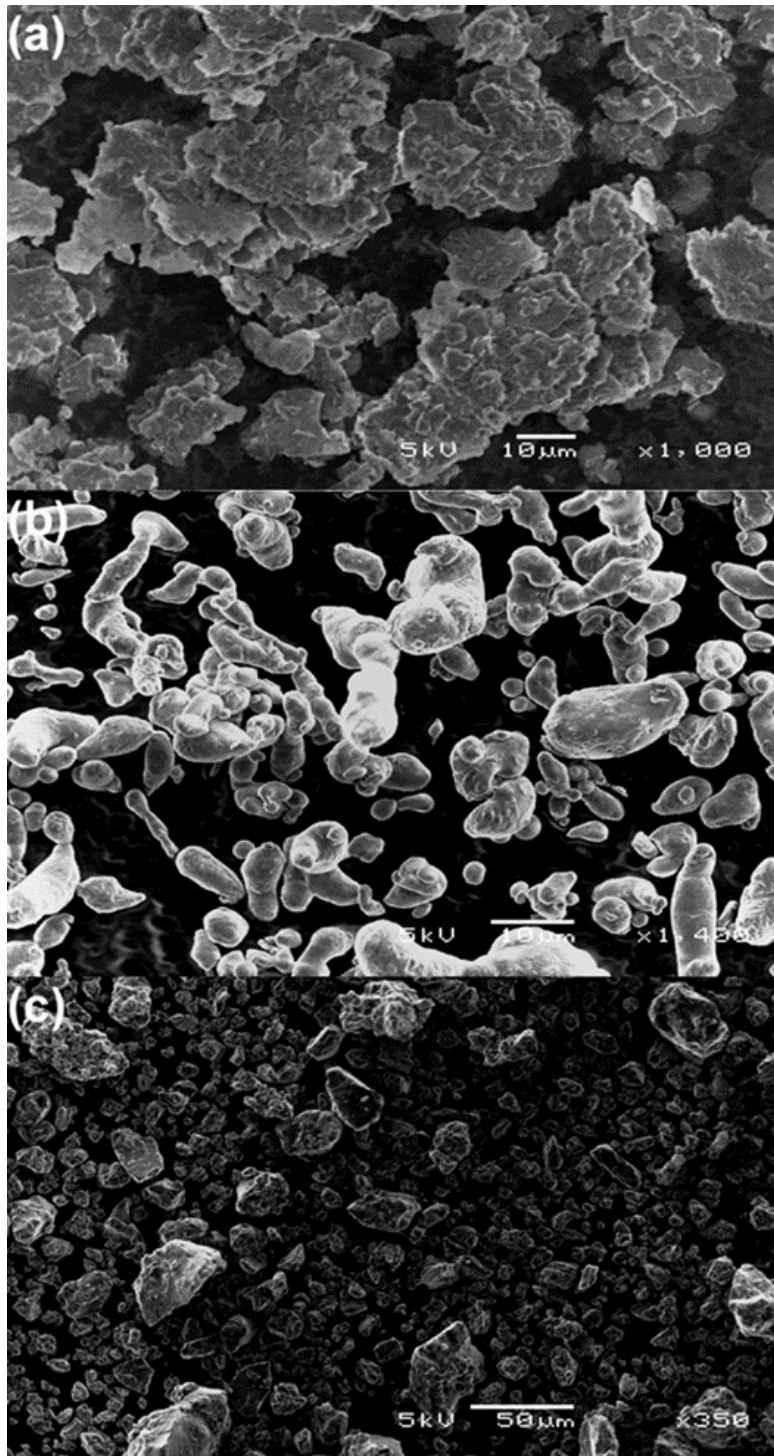Figure 5-1: Particle size distributions of the fuel powders.

50

Figure 5-2: Scanning electron micrographs of the fuel powders. (A) Aluminium flake; (B) sieved, atomised aluminium and (C) sieved magnalium powder.

5.3. Pyrotechnic film characterisation

5.3.1. Mechanical test

The measured mechanical and dimensional properties properties of pyrotechnic films filled with different particle morphologies are shown in Table 5-3. The presence of fillers caused an increase in the film thickness. The morphology, however, had no influence on film thickness. Tensile tests using films filled with flake-like particles were only possible to a maximum filler loading of 20 wt.% ($\phi = 0.14$), as it was not possible to prepare films without imperfections at higher loadings. This limit was present at 50 wt.% loading for films filled with atomised aluminium particles. The presence of the fillers dramatically decreased the elongation to break. This decrease was more pronounced when using flake-like filler particles (Pritchard, 2005: 42). The reduction in tensile strength is predicted to be accompanied by a reduction in impact strength (Pritchard, 2005: 42). The reduction in tensile properties was less pronounced in films made using atomized particles. Spherical particles, therefore, offer better mechanical properties, especially when higher fuel filler ratios are required.

Table 5-3: Physical properties as a function of filler loading.

Particle type	Thickness (μm)	wt.%	Elongation to break (%)	Standard deviation (%)
No Filler	25	Baseline	453	33
Flake-like	26	10	140	19
Flake-like	30	20	69	10
Atomised	26	10	187	24
Atomised	30	20	160	11
Atomised	32.5	30	128	22
Atomised	35	40	86	21
Atomised	37.5	50	71	24

5.3.2. Sensitivity test

Impact and friction tests were done in order to determine the safety limits of the formulations. The results shown in Table 5-4 conform to the requirements set out in STANAG 4487 and EN 13631-4:2002 for impact sensitivity. The possibility of accidental ignition of the aluminium-

52

based compositions was, therefore, very low (Piercey & Klapötke, 2010). The magnalium-based composition on the other hand, was moderately sensitive to impact (Piercey & Klapötke, 2010). Friction tests showed that all compositions were insensitive (>360 N) to friction.

Table 5-4: Impact test results of compositions containing magnalium, flake-like aluminium particles and atomised aluminium powder.

	Magnalium	Flake-like aluminium	Atomised aluminium
Mass (kg)	5	10	10
H_{min} (cm)	55	94	88
E_{min} (J)	27	92	86

5.4. Combustion analysis

5.4.1. Calorimetric results

The energy output of magnalium/Viton B with a fuel content range from 20 wt.% to 60 wt.% was measured in 10 wt.% increments. The pyrotechnic films were cooled with liquid nitrogen and ground in a blender. The mass of composition was measured to three significant figures. The crucible was inserted into the high pressure bomb. The bomb was pressurised to 30 bar using helium. The bomb was submerged in water in a temperature controlled jacket set to 25 °C. The pyrotechnic films were ignited using a nichrome wire. The energy output of the pyrotechnic reaction was inferred from the change in temperature of the water in the temperature controlled jacket.

The results are shown in Figure 5-3. Also shown in Figure 5-3 are the simulated energy outputs from EKVI. The measured energy outputs followed a similar curve to the simulated results, with minimal variation in measurements. The results were, however, shifted to the right, with the maximum energy output occurring between 40 wt.% and 50 wt.% magnalium, whereas the maximum simulation energy output occurred at 25 wt.% magnalium. The maximum measured energy output was 8.3 kJ g^{-1}, whereas the maximum simulated energy output was 8.25 kJ g^{-1}.
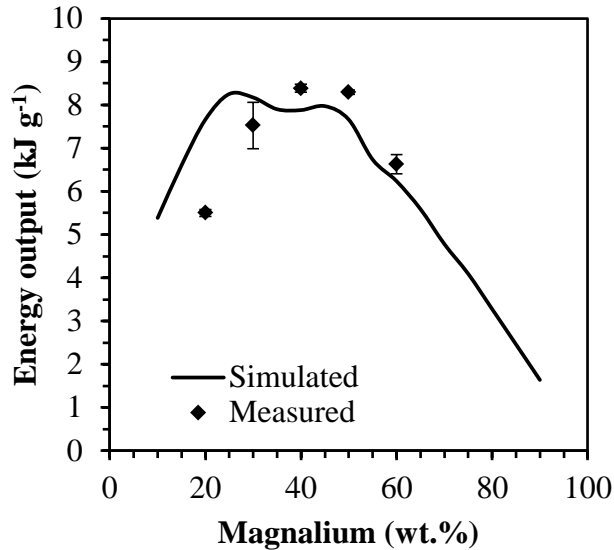
53

Figure 5-3: Comparison of energy outputs obtained from the bomb calorimeter measurements and EKVI simulations for the magnalium-Viton B system

The energy output of compositions using aluminium as fuel as predicted by EKVI simulations is shown in Figure 5-4. The EKVI thermodynamic simulation predicted an approximate linear increase in energy output up to the global maximum at 25 wt.% aluminium, corresponding to an energy output of 8.29 kJ g^{-1}. A continuous decrease in energy output was predicted thereafter. The measured energy outputs of compositions using flake-like aluminium particles and atomised aluminium powder with varied fuel content are also shown in Figure 5-4. The maximum energy output was measured at 30 wt.% aluminium for both compositions. There was an unexpected difference in the measured energy output of the two compositions between 30 wt.% aluminium and 50 wt.% aluminium. This anomaly is attributed to the incomplete combustion of the flake–like particle composition. This was confirmed by inspecting the combustion residue. The measured values of both compositions, however, follow a similar trend to the simulated results.

The shift to the right that is observed for both the aluminium and magnalium-based compositions can be explained by the energy required for the depolymerisation of the Viton B. The compositions containing higher fuel fractions have less Viton B that has to be decomposed. Therefore, the highest measured energy output is measured in compositions that contain more than the stoichiometric amount of metal fuel.
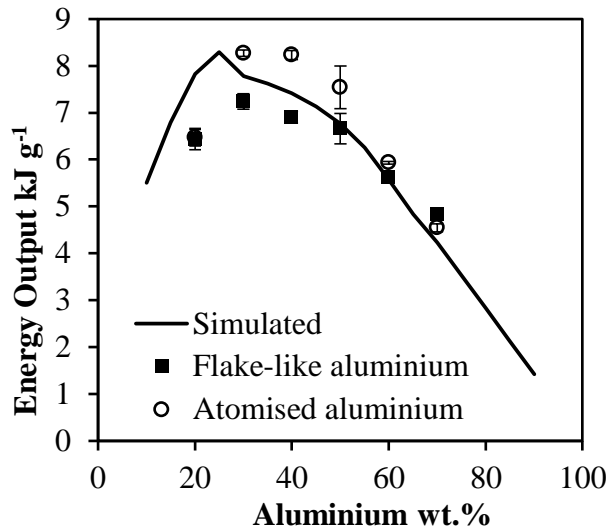
54

Figure 5-4: Energy output comparison of compositions using flake-like aluminium particles and atomised aluminium powder.

5.4.2. Differential pressure (ΔP) analysis

The pressure change due to reaction was measured for 20 wt.% to 60 wt.% fuel for each composition. A 30 bar starting pressure was used. Three runs were performed per filler loading. The time scale is arbitrary, as the figures were shifted so that the relative shapes of each could be seen. The figures were shifted so that the start of each sequential result stated one second apart. The data was filtered and splined. The differential pressure profiles of the compositions based on flake-like aluminium particles, atomised aluminium powder and magnalium are shown in Figure 5-5, Figure 5-6 and Figure 5-7 respectively.

The results reveal a maximum peak value for 30 wt.% magnalium and 30 wt.% atomised aluminium powder, decreasing with increasing reducing agent content. ΔP analysis of the atomised particle aluminium-based composition, however, shows a higher pressure increase for 50 wt.% than 40 wt.%, possibly indicating the effect of enhanced conductivity with higher aluminium loading. The compositions based on the flake-like particles show a maximum ΔP at 50 wt.% aluminium. The absence of residual pressure indicates that the pressure increase was caused, in the main, by the heating of the helium gas used as inert atmosphere, rather than gas

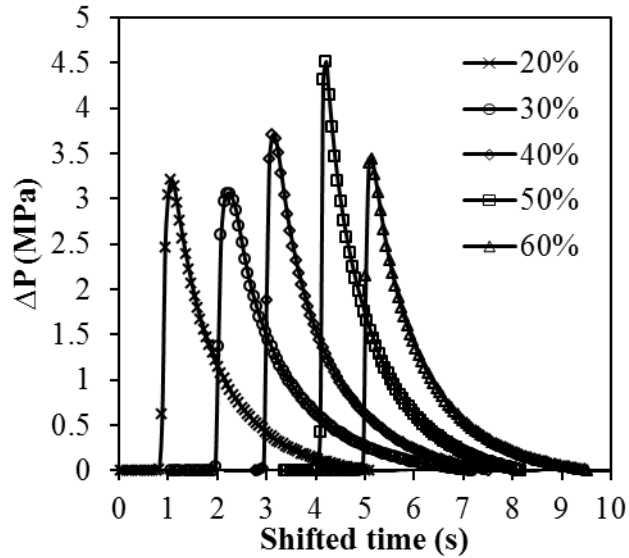generated by the reactions. Alternatively, the gas formed may have condensed after the vessel cooled.

Figure 5-5: Bomb calorimeter ΔP profiles for flake-like aluminium-based compositions

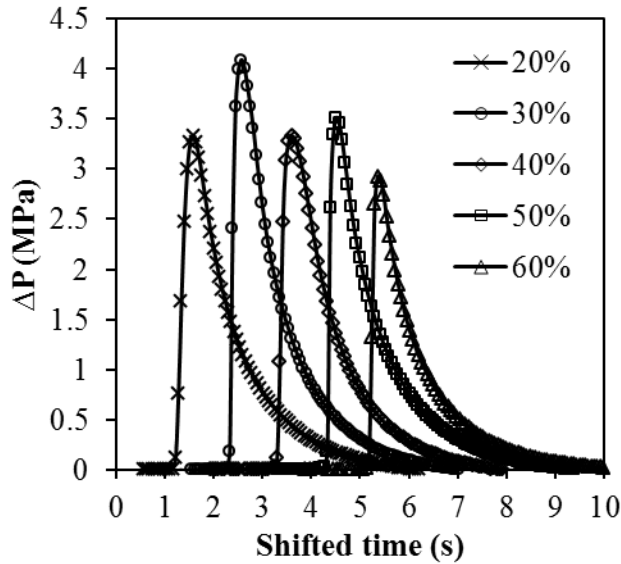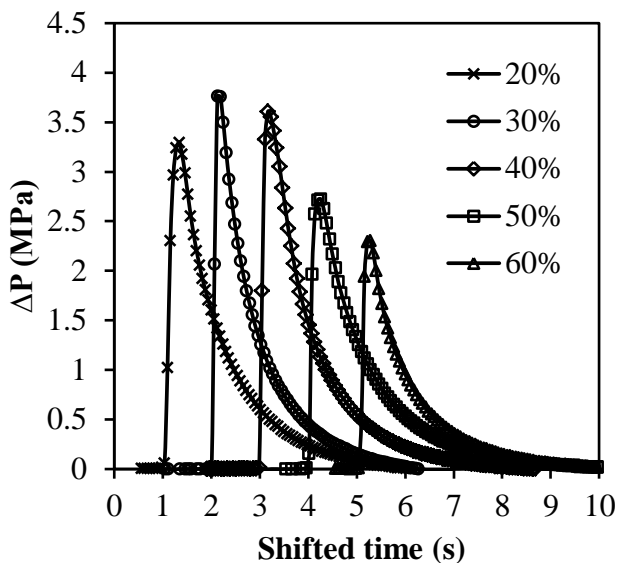Figure 5-6: Bomb calorimeter ΔP profiles for atomised aluminium-based compositions

Figure 5-7: Bomb calorimeter ΔP profiles for magnalium compositions

The instantaneous derivative for each run was determined, and the results are summarised in Table 5-5. Measured heat output was added for comparison.

Table 5-5: Bomb calorimeter pressure data for the Viton B composition

	wt.%	vol.%	ΔP_{max} (Mpa)	Time to ΔP_{max} (s)	$d(\Delta P)/dt_{max}$	Enthalpy (kJ g^{-1})
Magnalium	20	17	3.23	0.27	21.89	5.50
	30	26	3.76	0.24	39.54	7.52
	40	35	3.61	0.185	34.12	8.38
	50	45	2.73	0.18	24.73	8.29
	60	55	2.32	0.185	19.402	6.62
Aluminium flake	20	14	3.21	0.24-0.35	24.32	6.42
	30	22	2.96	0.23	26.12	6.57
	40	31	3.72	0.21	35.2	6.67
	50	40	4.51	0.13	33.46	6.66
	60	50	3.39	0.18	29.34	5.61
Atomised aluminium	20	14	3.26	0.35	15.20	6.47
	30	22	4.00	0.35	29.75	8.26
	40	31	3.54	0.23	23.05	8.23
	50	40	3.61	0.18	32.3	7.54
	60	50	2.92	0.20	32.3	5.93

57

The largest gradient was measured for the 30 wt.% magnalium composition, indicating the greatest instantaneous rate of temperature change. The flake-like aluminium composition, however, had the lowest average time to maximum over the range, indicating the highest average reaction rate. The enhanced reaction rate of the flake-like aluminium-based composition compared to the atomised aluminium based composition is tentatively attributed to a thicker oxide layer covering the latter powder particles.

5.4.3. Burn rate

The sequence of burn rate measurement is shown in Figure 5-8, where lines are superimposed so that the start and end points are clear. The time elapsed for the reaction to proceed between the two points was measured.
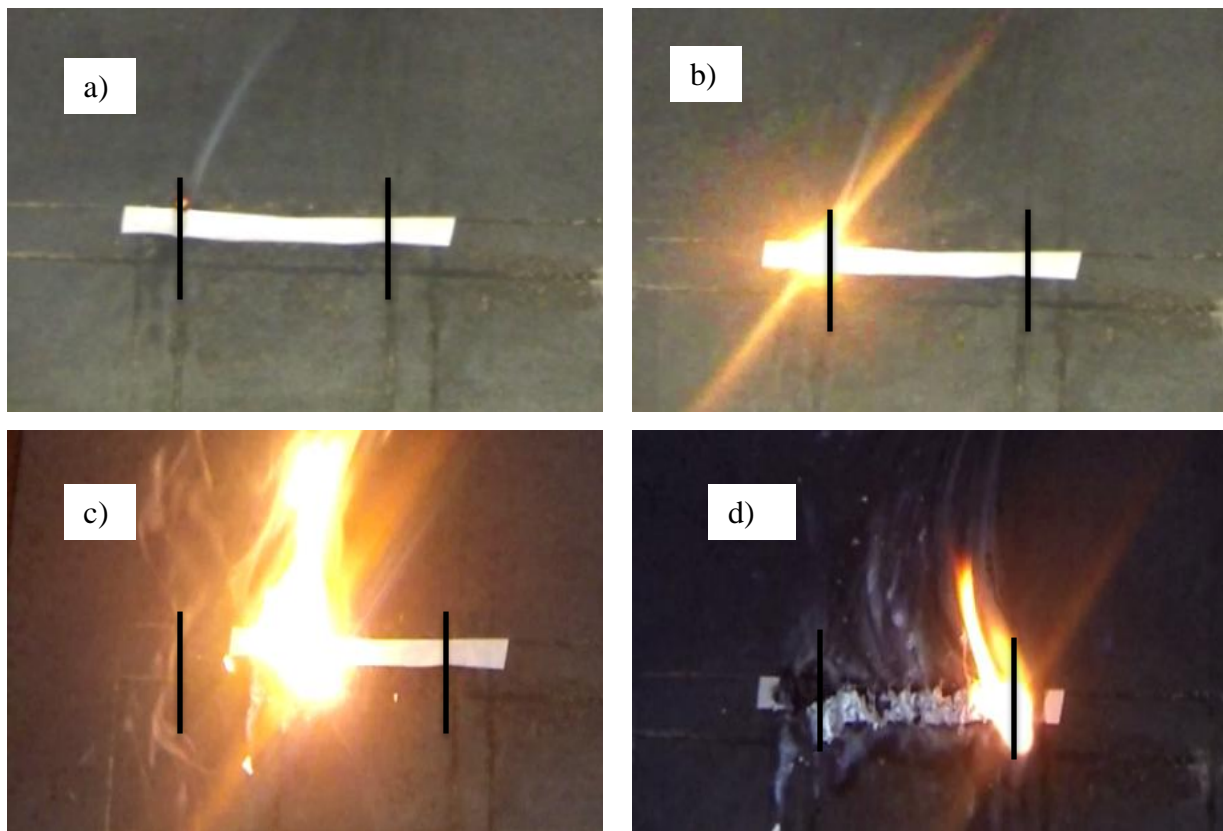
Figure 5-8: Sequence of measurement of the burn rate. a) before ignition. b) at t = 0. c) at an intermediate time. d) time at completion.

Figure 5-9 shows the effect of stoichiometry on the burn rate. Sustained burning at 20 wt.% fuel was only possible using the composition based on Al flake powders. The burn rate of all

compositions increased with increased fuel content. The 40 wt.% and 60 wt.% magnalium compositions where the only exceptions. The fastest burn rate was measured using the magnalium composition with stoichiometric ratios between 50 wt.% and 60 wt.%. The amount of light generated, however, saturated the recording device, limiting the accuracy of the measurements, and leaving uncertainty to the exact maximum burn rate. The slowest sustained burn rate of 12.4 mm s^{-1} was achieved using 30 wt.% atomised aluminium powder.
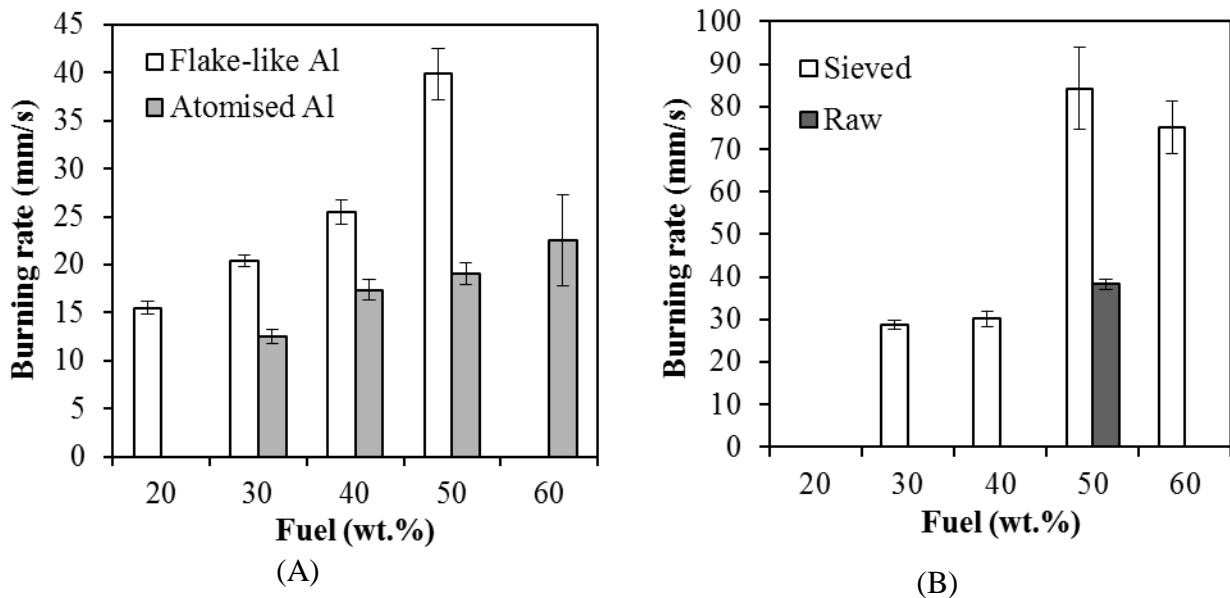
Figure 5-9: Burn rate as a function of stoichiometry. (A) Aluminium as fuel, and (B) magnalium as fuel.

The effect of particle size on burn rate was tested by filling Viton B with raw, unsieved magnalium to 50 wt.%. The burn rate was compared to that of Viton B filled with sieved magnalium to 50 wt.%. The results shown in Figure 5-9 B reveal that the sieved powder had a burn rate that was double that of the unsieved composition.

5.4.4. Summary of combustion analysis

The speed tests showed that the magnalium compositions had a significantly higher burn rate than the aluminium-based compositions for filler volume fraction above 50 wt.%. This trend

59

was, however, not observed in the differential pressure analysis where the highest rate of pressure increase was observed with the 30. wt.% magnalium composition.

The aluminium compositions had a significantly lower burn rate than that measured values reported by Watson, Pantoya & Levitas (2008). The large difference is, however, attributed to the use of PTFE as oxidant as well as smaller aluminium particles (3 µm). The measured burn rate for the magnalium composition was, however, higher than those reported elsewhere (Koch, 2012: 99). The reported values were, based on compositions using PTFE as oxidant with magnalium particles that measured 75 µm to 105 µm.

Compositions based on flake-like aluminium particles consistently showed higher burn rates when compared to compositions based on atomised aluminium. This trend was also observed when comparing the burn rate of flake-like aluminium-based compositions to that of the magnalium-based compositions for filler loadings below 50 wt.%. The ability to sustain burning at 20 wt.% shows that the flake like morphology gives an advantage if low fuel formulations are required. On the other hand, magnalium-based compositions offers an advantage if fast burn rates are required.

The magnalium-based compositions and the aluminium-based compositions had similar energy output results, although the filler fraction at maximum energy output was 50 wt.% for the magnalium composition and 30 wt.% for the aluminium-based compositions.

The reactions are most likely described by a combination of the two reaction rate models developed by Armstrong (1990) and Khaikin & Merzhanov (1966). The main factors determining the burn rate are the activation energy, flame temperature, energy output, thermal conductivity, particle size and diffusion.

Increased filler loading results in an increased thermal conductivity, due to the increase amount of contact points between the metal particles. Magnalium and aluminium have similar thermal conductivities at elevated temperatures, (Green & Perry, 2007: 2-334). The differences in burn rate can, therefore, not be attributed to thermal conductivity.

60

Energy output results, as well as the thermodynamic simulations showed that the aluminium and magnalium formulations had similar energy outputs as well as adiabatic flame temperatures. Particle size analysis showed that all the metal fuel particles used were in the same order of magnitude in size. The differences in burn rate can, therefore, only be attributed to the differences in diffusivity and/or activation energy.

The diffusion rate is proportional to the temperature and inversely proportional to the size of the diffusing species. Again, EKVI simulations showed that the expected flame temperatures were similar. Furthermore, the atomic radii of aluminium and magnesium are comparable in size. The diffusion rates of the reducing agents in the gaseous phase should, therefore, be the same order of magnitude. Thus, the differences in burn rate are attributed to kinetic effects.

Plotted values of burn rate and the thermodynamic simulated adiabatic reaction temperatures, as described in Equation 2-6 is shown in Figure 5-10. A trend line is fitted so that the slope could be calculated. The composition using magnalium as fuel had a marginally lower activation energy than the composition based on flake-like aluminium (124 kJ mol^{-1} vs. 128 kJ mol^{-1}). This, coupled with a lower value for the pre-exponential exponent and a higher heat of reaction at a higher filler loading, may explain the burn rates achieved using magnalium at higher filler loadings.

(A)   (B)
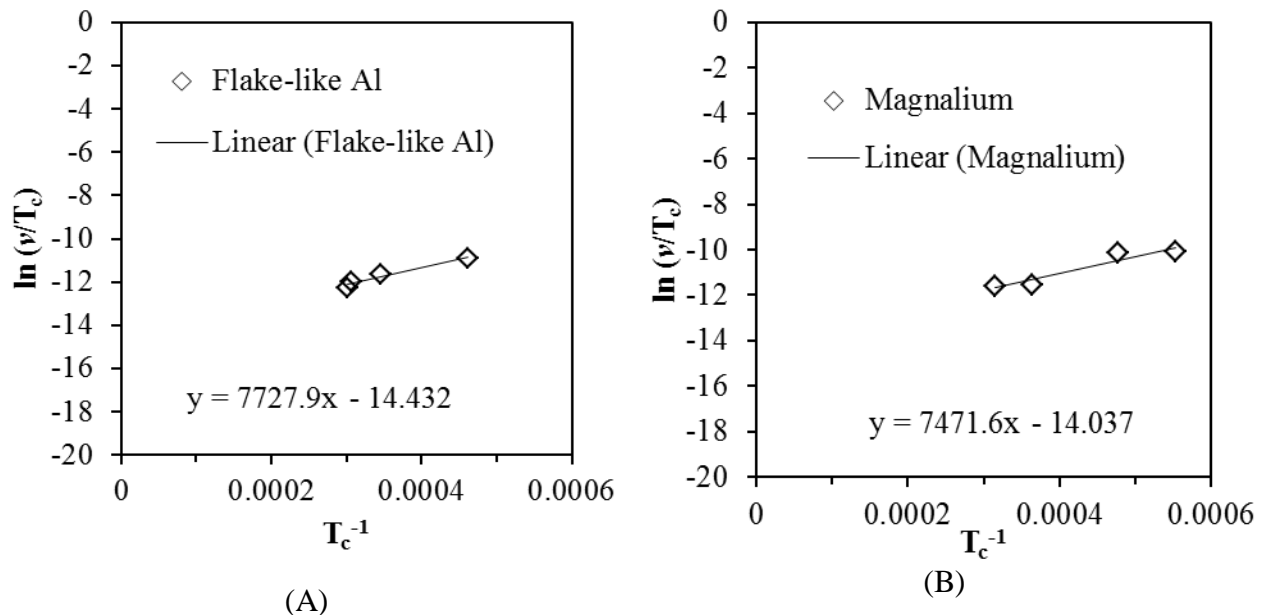
Figure 5-10: Arrhenius plots. (A) Aluminium flake. (B) Magnalium.

61

5.5. Combustion residue characterisation

5.5.1. X-ray diffraction/fluorescence

Quantitative XRD analysis was performed on the reaction products recovered from the bomb calorimeter tests. Quantitate analysis of the reaction products obtained with magnalium as fuel was not possible, as there were unidentified reflections in the corresponding XRD spectra shown in Appendix C. However, the main reaction products identified were graphite, aluminium fluoride, aluminium fluoride and magnesium oxide. The major products found with aluminium as fuel were aluminium carbide, aluminium fluoride, graphite and unreacted aluminium. Small amounts of aluminium fluoride hydroxide ($AlF_x(OH)_{3-x}$) were also detected. Its formation was attributed to the presence of adventitious moisture. A large amorphous fraction was also present, constituting up to a third of the total condensed products.

Table 5-6 summarises the quantitative analyses done on compositions based on flake-like aluminium particles and atomised aluminium powder respectively. The product spectra predicted by EKVI thermodynamic software are also listed in Table 5-6.

Table 5-6: Quantitative XRD analysis of the reaction products of compositions using Viton B

Fuel type:	Flake			Atomised			EKVI Predictions		
Formula	20%	40%	60%	20%	40%	60%	20%	40%	60%
Al_4C_3	1.16	9.23	31.8	0	10.46	19.19	0	27.04	45.06
AlF_3	63.56	50.44	27.82	65.05	50.67	20.47	73.12	61.55	41.95
Al	1.22	5.21	11.22	0.77	5.28	15	0	0	12.97
Graphite	4.82	2.16	1.32	3.96	1.8	1.2	26.87	11.40	0
$AlF_x(OH)_{3-x}$	2.76	0.25	0	1.98	0	0	-	-	-
Amorphous	26.48	31.87	27.83	28.25	31.79	34.14	-	-	-

The XRD results showed lower aluminium carbide and aluminium fluoride formation than predicted for both compositions. This is coupled with lower than predicted aluminium conversion. The large difference between the measured and predicted graphite content is

62

attributed to the formation of amorphous carbon (disordered graphite) due to the presence of hydrogen in the reaction (Ferrari & Robertson, 2000). Perhaps, the match only appears poor owing to the uncertain composition of the amorphous phases.

An elemental mass balance was carried out in an attempt to uncover the nature of the amorphous phase. Matter in the form of $AlF_x(OH)_{3-x}$ was taken as $AlF(OH)_2$ (i.e. x was taken as 1). The results listed in Table 5-7 show that both the flake and atomised aluminium-based compositions at 20 wt.% loading had more elemental aluminium in the products stream than theoretically possible. This indicates that the reaction generated gas phase products. The gaseous products would likely be a mixture of hydrogen and hydrogen fluoride, since fluorine is the limiting element.

Alternatively the large measured amorphous phase could indicate an incomplete reaction. The amorphous phase would then consist of a mixture of Viton B and carbon. A combination of gas formation, as well as non-complete combustion is the most likely scenario.

Table 5-7: Elemental reaction products of the reaction between Viton B and aluminium

Fuel type:	Flake			Atomised			Calculated		
Element	20	40	60	20	40	60	20	40	60
Al	23.45	28.35	44.01	22.03	29.411	39.18	20.0	40.0	60.0
C	5.11	4.45	9.27	3.96	4.41	6.00	24.0	18.0	12.0
F	43.76	34.20	18.87	43.93	34.38	20.67	54.4	40.8	27.2
H	0.07	0.00	0.00	0.05	0.00	0.00	1.6	1.2	0.8

5.5.2. Thermogravimetric analysis

The results of heating the residue of the reacted Viton B filled with aluminium flake, atomised aluminium and magnalium are shown in Figure 5-11, Figure 5-12 and Figure 5-13 respectively. All data show a characteristic slow linear mass loss up to a temperature of 600 °C, an accelerated mass loss that occurs between 600 °C and 750 °C, a linear mass loss between 750 °C and 900 °C

and a further mass loss at the isothermal hold at 900 °C. The mass loss regimes are summarised in Table 5-8.

The linear regime below 600 °C is attributed to the loss of volatiles or perhaps to slow oxidation of carbon present in the residue. The rapid mass loss between 600 °C and 750 °C was, generally, more pronounced in the residue of the formulations containing lower amounts of fuel particles. The mass loss in this regime is also attributed to the oxidation of carbon.

The linear regime between 750 °C and 900 °C shows relatively small mass losses when compared to the other regimes. The mass loss for compositions using flake-like aluminium particles, however, had a smaller mass loss than the other compositions. A smaller mass loss at the isothermal hold at 900 °C was generally measured for compositions containing higher fuel levels. A mass gain was observed for 60 wt.% magnalium composition. This effect is attributed to the oxidation of unreacted aluminium and magnesium in the residue.

Table 5-8: TGA data for the reaction residue of Viton B compositions

	Fuel (wt.%)	Mass loss below 600 °C	Mass loss 600 °C - 750 °C	Mass loss 750 °C - 900 °C	Mass loss at 900 °C	Total
Flake-like aluminium	20	16.9	17.9	1.5	7.7	44
	30	11.9	21.5	2.4	7.4	43.2
	40	7.8	15.8	1.5	3.3	28.4
	50	1.6	11.8	0.6	1.1	15.1
	60	5.0	5.6	0.1	1.8	12.5
Atomised aluminium	20	12.5	25.2	6.5	10.1	44.3
	30	2.5	19.2	2.4	5.4	29.5
	40	6.6	15.1	1.0	1.0	23.7
	50	6.1	9.8	1.3	1.9	19.1
	60	10.5	3.1	0.5	2.2	16.3
Magnalium	20	7.7	29.7	5.7	7.5	50.6
	30	3.2	24.2	4.9	7.4	39.7
	40	4.6	14.4	3.9	4.3	27.2
	50	1.5	14.9	6.6	5.0	28
	60	6.7	3.2	-2.0	-0.8	7.1

5.5.3. Scanning electron microscopy

Figure D-2, Figure D-3 and Figure D-4 in Appendix D show SEM images of the reaction residue of Viton B with flake-like aluminium particles, atomised aluminium powder and magnalium respectively. All aluminium-based residues show the presence of crystals with a cubic habit. EDX revealed that the particles consisted of aluminium and fluorine. The SEM images show that, in general, the size and occurrence of the cubic particles decreased with an increase in the reducing agent content.

Similar cubic particles could only be found in the reaction residue of the 20 wt.% magnalium system and only in what looks like the centre of a disordered residue agglomerates.

SEM images of the reaction residue that had been put through TGA analysis are shown in Figure D-5. The residue of aluminium-based residue is dominated by cubic particles. The amount of disordered residue present in the samples after TGA analysis was also minimal. This is attributed to the burn-off of amorphous carbon residues. Large needle-like particles were observed in the aluminium-based residue. EDX showed that the needle-like particles comprised aluminium and fluorine. The magnalium-based residue was shown to be spherical in shape. The particles were, however, agglomerated.
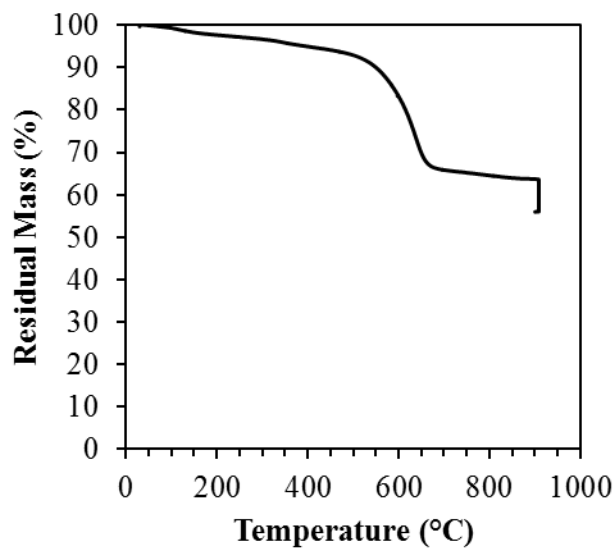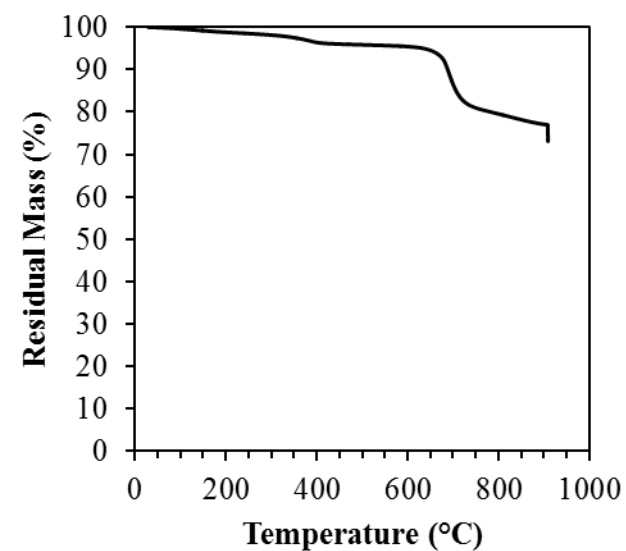
(A)
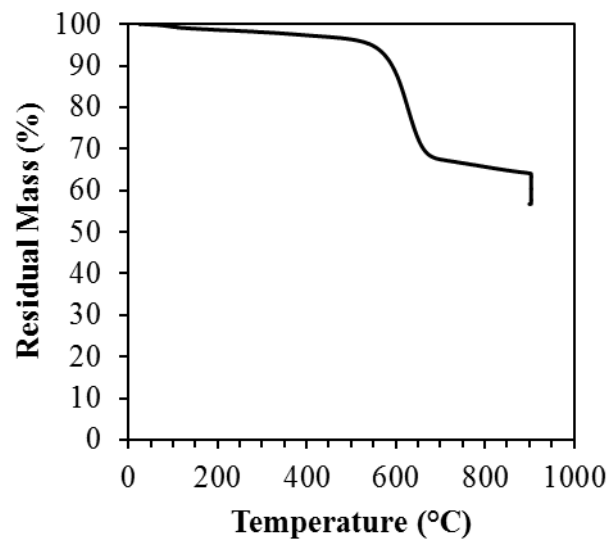
(B)
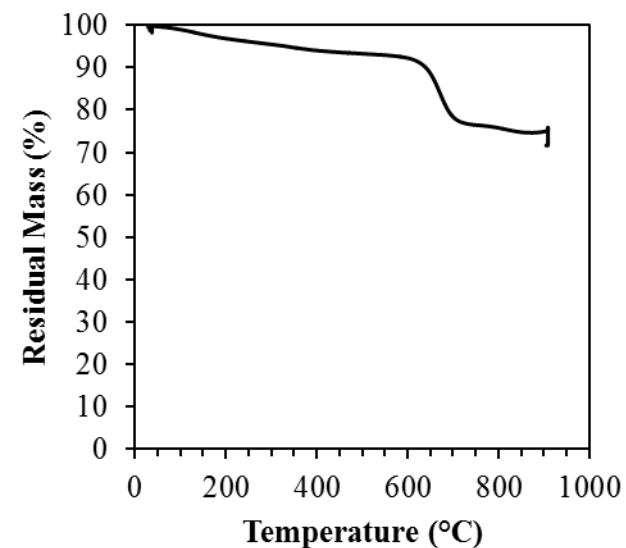
(C)
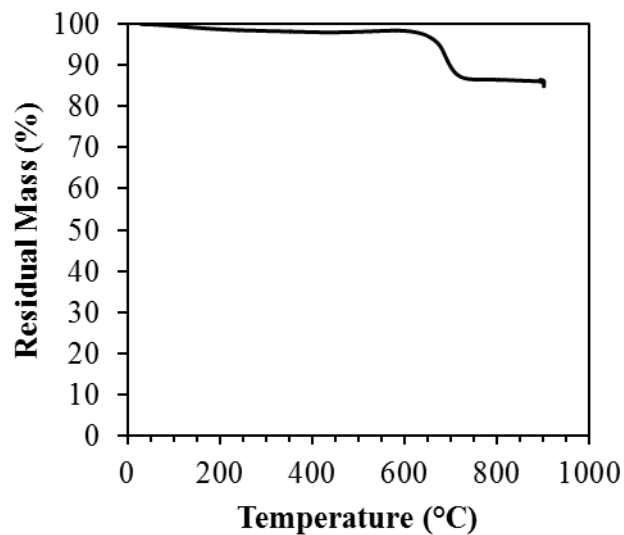
(D)
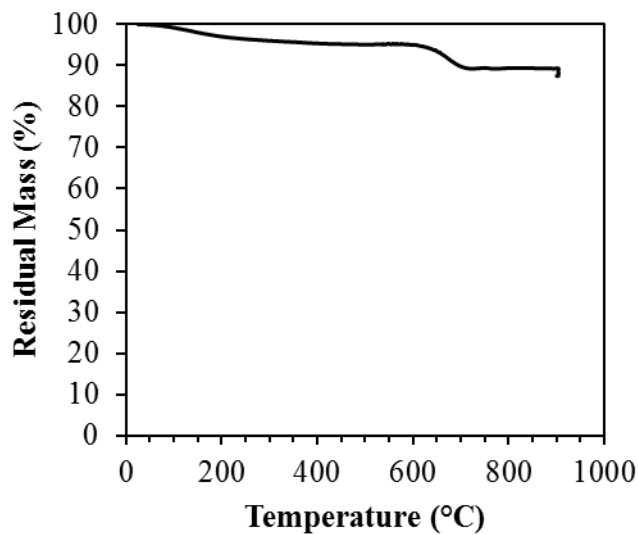
(E)

Figure 5-11: TGA results for residue from the flake-like composition. (A) 20 wt % (B) 30 wt.% (C) 40 wt.% (D) 50 wt.% (E) 60 wt.%

66
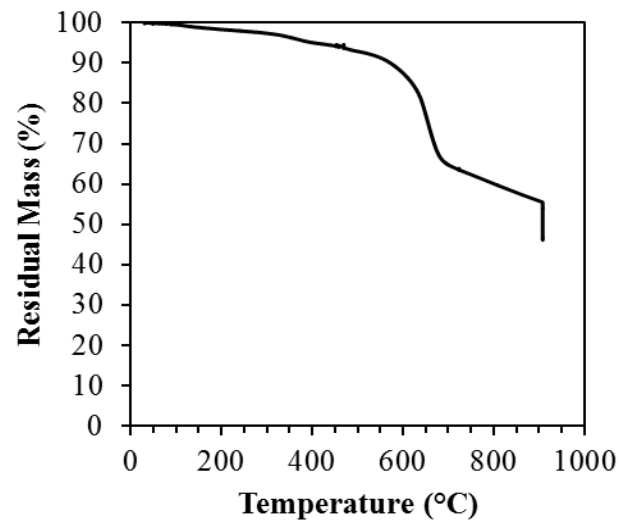
(A)
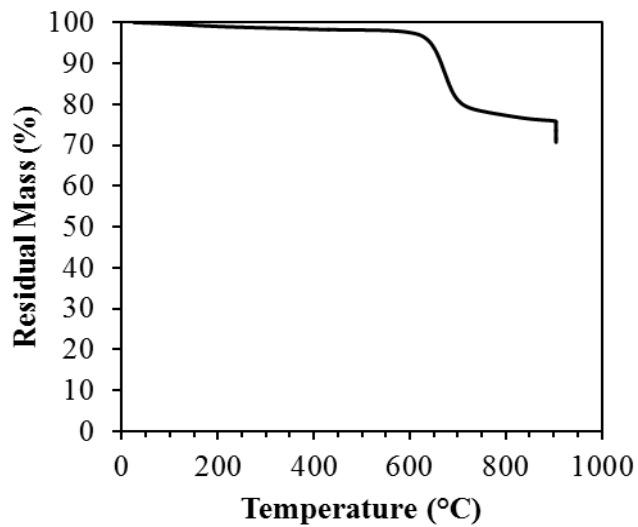
(B)
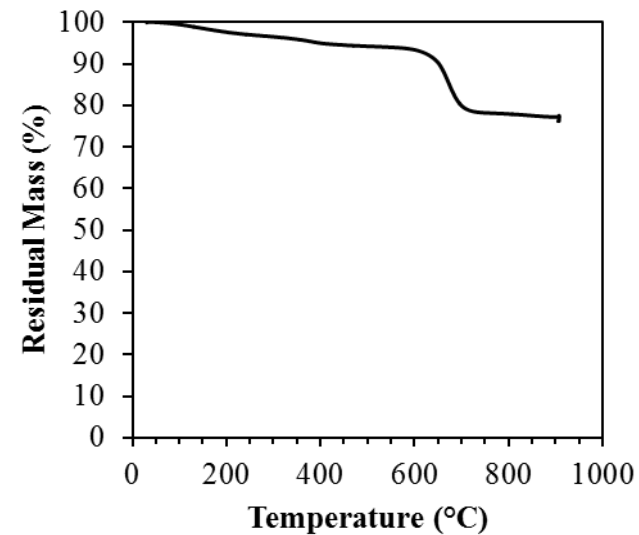
(C)
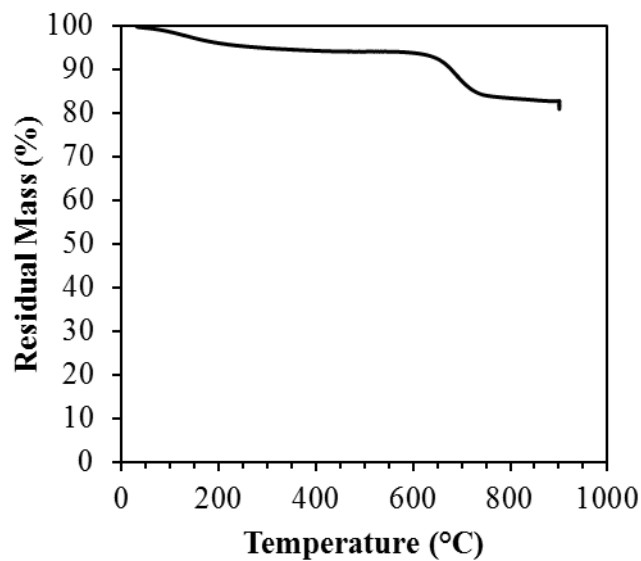
(D)
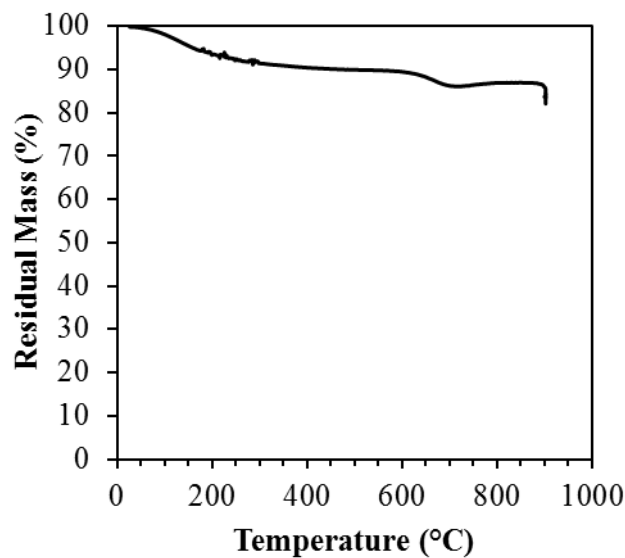
(E)

Figure 5-12: TGA results for residue from the atomised Al composition. (A) 20 wt % (B) 30 wt.% (C) 40 wt.% (D) 50 wt.% (E) 60 wt.%

67
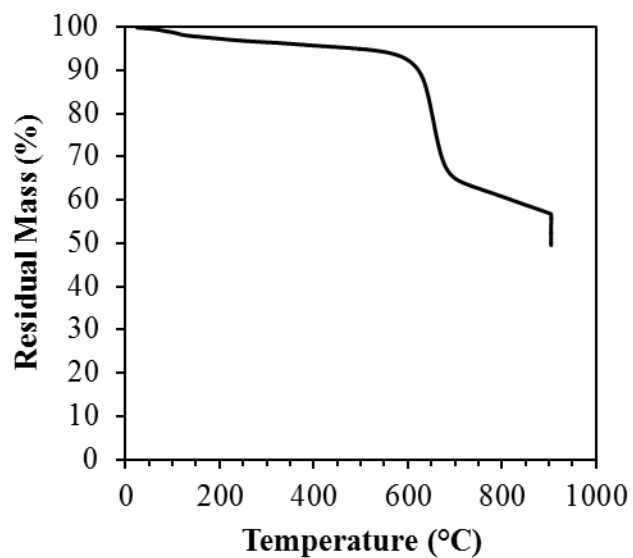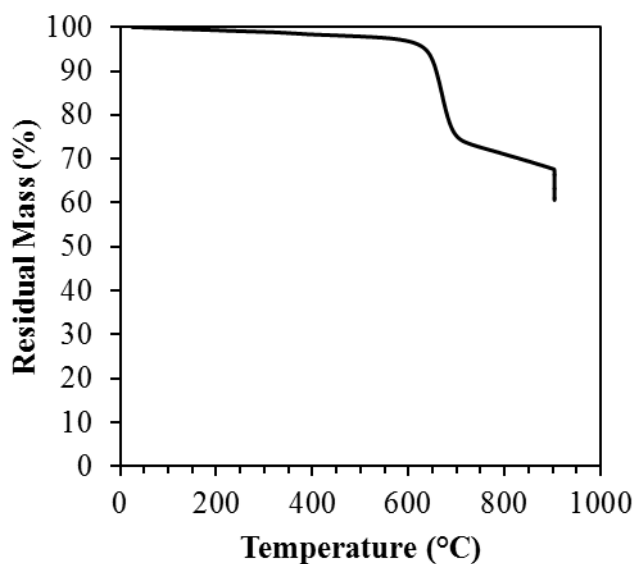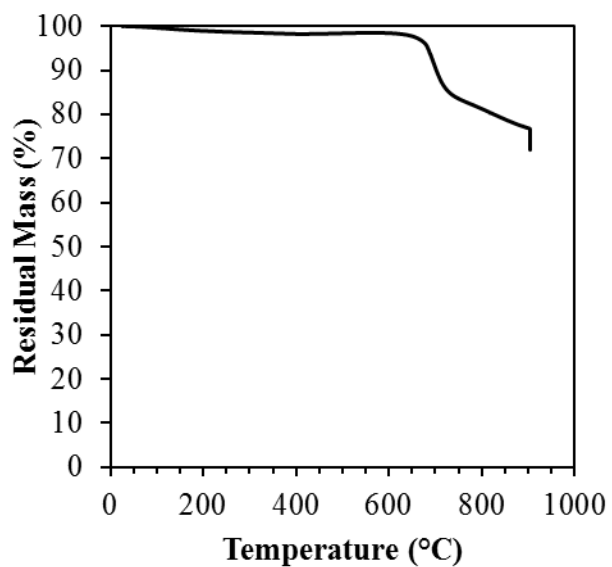
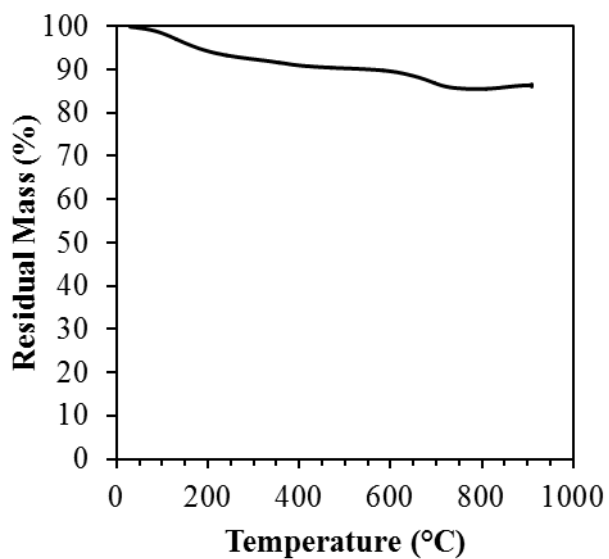Figure 5-13: TGA results for residue from the magnalium composition. (A) 20 wt % (B) 30 wt.% (C) 40 wt.% (D) 50 wt.% (E) 60 wt.%

68

5.5.4. Summary of combustion residue characterisation

Quantitative XRD data showed a significant amount of an unidentified amorphous phase. An elemental mass balance showed the amorphous phase consisted of carbon, aluminium and fluorine. The crystalline products identified where: AlF_3, Al_4C_3, aluminium, graphite and AlF_x $(OH)_{3-x}$.

The TGA tests resulted in higher mass losses than anticipated. Mass loss could only have occurred through evaporation, decomposition or by the formation of volatile species via the reaction with oxygen. Of the phases identified in XRD, aluminium has the lowest boiling point of 2 056 °C (Green & Perry, 2007: 2-7). AlF_3 and Al_4C_3 decompose instead of evaporating, but only at elevated temperatures. Therefore, none of the identified phases were expected to contribute towards the evaporation or decomposition mass loss measured. On the other hand, carbon and Al_4C_3 react with oxygen to form carbon dioxide. The latter, however, also forms Al_2O_3, and would result in a net mass gain (Bearne, Dupuis & Tarcy, 2013).

A possible explanation for the higher-than-anticipated mass loss may be the presence of unreacted components in the combustion residue. This would also explain the lower than expected energy output for the atomised aluminium compositions.

Generation of gaseous products may limit the commercial viability of Viton B-based compositions. Specifically, the generation HF or H_2 raises safety concerns. Compositions using filler ratios above 40 wt.% had a lower propensity to form HF and H_2.

Chapter 6 : Conclusions and recommendations

Thermodynamic simulations showed that polymer consisting of only carbon and hydrogen filled with oxidants were unlikely to be sustain reaction unless filler loadings above 75 vol.% was used. This was above the filler limit described for randomly packed monodisperse particles. EKVI simulations of all fluoropolymer-based systems indicated that the maximum adiabatic temperatures occurred below the filler volume fraction limit described.

Open flame burn tests, however, showed that only Viton B-based compositions could sustain combustion. The non-sustained reaction of the PS-based compositions was attributed to the energy required for the decomposition of the PS. It is postulated that compositions based on Viton B filled with calcium carbide failed to ignite due to the excessive energy required to decompose the reducing agent. Free calcium was, therefore, not available for the reaction.

Energy output, bomb calorimeter pressure profiles and burn rate tests showed that Viton B-based formulations were viable below a filler volume fraction of 60 %. The highest energy output and burn rate was achieved using compositions based on magnalium at 50 wt.%. Flake-like particles were shown to offer faster burn rates at lower filler loadings. This, however, resulted in significantly reduced mechanical properties. Due to a lack of information of the amorphous phase in the atomised aluminium, the lower combustion rate could also be attributed to higher alumina content. Ignition sensitivity tests showed that the aluminium-based formulations are insensitive.

The parameters that could provide optimum performance are: (a) fully fluorinated fluoropolymer with a low melt viscosity to avoid gas formation; (b) mixtures of spherical and flake-like fuel particles to control rheology and (c) fuel with high magnesium content for faster burn rates.

The commercial viability of Viton B will be limited by the generation of HF. It is recommended that the addition of a HF scavengers, e.g. $CaSi_2$, be considered as it may offer a solution (Caflin & Anderson, 2014).

References

Aldushin, AP and Khaikin, BI (1974) "Combustion of mixtures forming condensed reaction products" *Combustion, Explosion and Shock Waves*, *10*, 273–280.

Anon (sa) "Calcium carbide",
http://www.sigmaaldrich.com/catalog/product/aldrich/21039?lang=en&region=ZA&gclid=COnj4qyW8MkCFdVAGwodykIFmA [2015, December 15].

Armstrong, R (1990) "Models for Gasless Combustion in Layered Materials and Random Media" *Combustion Science and Technology*, *71*, 155–174.

Aumann, CE (1995) "Oxidation behavior of aluminum nanopowders" *Journal of Vacuum Science & Technology B: Microelectronics and Nanometer Structures*, *13*(3), 1178.

Balzer, J, Field, J, Gifford, M, Proud, W and Walley, S (2002) "High-speed photographic study of the drop-weight impact response of ultrafine and conventional PETN and RDX" *Combustion and Flame*, *130*(4), 298–306.

Barnes, HA (2003) "A review of the rheology of filled viscoelastic" *Rheology Reviews*, 1–36.

Bearne, G, Dupuis, M and Tarcy, G (2013) *Essential Readings in Light Metals, Aluminum Reduction Technology*, Wiley and Sons, New Jersey.

Booth, F (1953) "The theory of self-propagating exothermic reactions in solid systems" *Transactions of the Faraday Society*, *49*, 272–281.

Bowden, FP (1952) "Initiation and growth of explosion in liquids and solids" *American Journal of Physics*, *20*, 250.

Caflin, KC and Anderson, PE (2014) "In-situ remediation of hydrogen fluoride during a detonation event" *Propellants, Explosives, Pyrotechnics*, *39*(6), 904–908.

Carcassi, MN and Fineschi, F (2005) "Deflagrations of H_2–air and CH_4–air lean mixtures in a vented multi-compartment environment" *Energy*, *30*, 1439–1451.

Conkling, JA (1985) *Chemistry of Pyrotechnics*, Marcel Dekker, New York.

Douda, BE (1991) "Survey of Military Pyrotechnics," Crane.

Ebnesajjad, S (2000) *Fluoroplastics Volume 1: Non-Melt Processable Fluoroplastics*, William Andrew Inc., New York.

Farley, CW and Pantoya, ML (2012) "Reaction kinetics of nano-energetics with halogen containing oxides", Report, Department of Mechanical Engineering, Texas Tech University, Texas.

Ferrari, A and Robertson, J (2000) "Interpretation of Raman spectra of disordered and amorphous carbon" *Physical Review B*, *61*(20), 14095–14107.

Firmansyah, DA, Sullivan, K, Lee, K-S, Kim, YH, Zahaf, R, Zachariah, MR and Lee, D (2012) "Microstructural behavior of the alumina shell and aluminum core before and after melting of aluminum nanoparticles" *The Journal of Physical Chemistry C*, *116*(1), 404–411.

Frick, A, Sich, D, Heinrich, G, Stern, C, Gössi, M and Tervoort, TA (2013) "Relationship between structure and mechanical properties of melt processable PTFE: Influence of molecular weight and co-monomer content" *Macromolecular Materials and Engineering*, *298*(9), 954–966.

Gash, AE, Simpson, RL and Satcher, JH (2002) "Energetic nanocomposites with sol-gel chemistry : synthesis, safety, and characterization," in 2nd International Pyrotechnic Seminar, Westminister.

Gesner, J, Pantoya, ML and Levitas, VI (2012) "Effect of oxide shell growth on nano-aluminium thermite propagation rates" *Combustion and Flame*, *159*, 3448–3453.

Green, DW and Perry, RH (2007) *Perry's Chemical Engineers' Handbook*, 8th edition, McGraw-Hill, New York.

Hardt, A. and Phung, PV (1973) "Propagation of gasless reactions in solids. I. Analytical study of exothermic intermetallic reaction rates" *Combustion and Flame*, *21*, 77–89.

Hasani, S, Panjepour, M and Shamanian, M (2012) "Oxidation and kinetic analysis of pure aluminum powder under non-isothermal conditions" *Open Access Scientific Reports*, *1*(8), 1–7.

Hlavacek, V and Puszynski, JA (1996) "Chemical Engineering aspects of advanced ceramic materials" *Industrial & Engineering Chemistry Research*, *35*(2), 349–377.

Hohmann, C and Tipton, B (2000) "Viton's impact on NASA standard initiator propellant properties," Report, NASA, Houston.

Khaikin, BI and Merzhanov, AG (1966) "Theory of thermal propagation of a chemical reaction front" *Combustion, Explosion and Shock Waves*, *2*, 22–27.

Koch, E (2012) *Metal-Fluorocarban Based Energetic Materials*, Wiley, Weinheim.

Koch, EC (2002a) "Metal-fluorocarbon-pyrolants: III. Development and application of magnesium/Teflon/Viton (MTV)" *Propellants, Explosives, Pyrotechnics*, *27*(5), 262–266.

Koch, EC (2002b) "Metal-fluorocarbon-pyrolants. IV: Thermochemical and combustion behaviour of magnesium/Teflon/Viton (MTV)" *Propellants, Explosives, Pyrotechnics*, *27*(6).

73

Krieger, IM (1959) "A mechanism for non-Newtonian flow in suspensions of rigid spheres" *Journal of Rheology*, *3*, 137.

Kubota, N and Serizawa, C (1987) "Combustion process of Mg/TF pyrotechnics" *Propellants, Explosives, Pyrotechnics*, *148*(12), 145–148.

Lee, JS (2005) "Thermal decomposition of fluoropolymers and firing characteristics of priming compositions with fluoropolymers" *Journal of Applied Polymer Science*, *97*(5), 2054–2059.

Levitas, VI, Asay, BW, Son, SF and Pantoya, M (2007) "Mechanochemical mechanism for fast reaction of metastable intermolecular composites based on dispersion of liquid metal" *Journal of Applied Physics*, *101*(8).

Makino, A and Law, CK (1994) "SHS Combustion Characteristics" *American Ceramic Society*, *77*(3), 778–786.

Manukyan, KV., Kirakosyan, KG, Grigoryan, YG, Niazyan, OM, Yeghishyan, AV, Kirakosyan, AG and Kharatyan, SL (2011) "Mechanism of molten-salt-controlled thermite reactions" *Industrial & Engineering Chemistry Research*, *50*(19).

Margolis, SB (1993) "A model for condensed combustion synthesis of nonstoichiometric homogeneous solids" *Combustion and Flame*, *93*, 1–18.

Margolis, SB (1985) "Asymptotic theory of heterogeneous condensed combustion" *Combustion Science and Technology*, *43*, 197–215.

Margolis, SB (1983) "Asymptotic theory of condensed two-phase flame propagation" *SIAM Journal of Applied Mathematics*, *43*, 351–369.

Margolis, SB and Williams, FA (1991) "Flame propagation in solids and high-density fluids with Arrhenius reactant diffusion" *Combustion and Flame*, *83*, 39–398.

Mclain, JH (1980) *Pyrotechnics from the Viewpoint of Solid State Chemistry*, Franklin Institute Press, Philadelphia.

Moore, K (2005) "Combustion behaviours of bimodal aluminium size distributions in thermites," Report, Department of Mechanical Engineering, Texas Tech University, Texas.

Munir, ZA and Anselmi-Tamburi, U (1989) "Self-propagating exothermic reactions : the synthesis of high-temperature materials by combustion" *Materials Science Reports*, *3*, 277–365.

Nielson, DB, Truitt, RM and Rasmussen, N (2005) "Low temperature, extrudable, high density reactive materials", *US Patent 6,962,634*, assigned to Alliant Techsystems Inc., US.

Osborne, DT (2006) "The effects of fuel particle size on the reaction of Al/Teflon mixtures", Report, Department of Mechanical Engineering, Texas Tech University, Texas.

Pantoya, ML and Granier, JJ (2005) "Combustion behavior of highly energetic thermites: nano versus micron composites" *Propellants, Explosives, Pyrotechnics*, *30*(1), 53–62.

Pantoya, ML, Levitas, VI, Granier, JJ and Henderson, JB (2009) "Effect of bulk density on reaction propagation in nanothermites and micron thermites" *Propulsion and Power*, *25*(2).

Piercey, DG and Klapötke, TM (2010) "Nanoscale aluminum - metal oxide (thermite) reactions for application in energetic materials" *Central European Journal of Energetic Materials*, *7*(2), 115–129.

Pourbaix, M (1966) *Atlas of Electrochemical Equilibria in Aqueous Solutions*, Pergamon Press, Ney York.

Prentice, D, Pantoya, ML and Clapsaddle, BJ (2005) "Effect of nanocomposite synthesis on the combustion performance of a ternary thermite." *The Journal of Physical Chemistry B*, *109*(43).

Pritchard, G (2005) "Plastic Additives," Report, Rapra Technology Ltd., Shrewsbury.

Puszynski, J, Degreve, J and Hlavacek, V (1987) "Modelling of exothermic solid-solid noncatalytic reactions" *Industrial & Engineering Chemistry*, *26*, 1424–1434.

Ricco, IMM (2004) "Alternative oxidants and processing procedures for pyrotechnic time delays," Masters Thesis, Department of Chemical Engineering, University of Pretoria. Pretoria.

Riley, DP and Kisi, EH (2008) "A new solid state synthesis methodology for ternary and higher order compounds" *Materials Forum*, *32*, 1–8.

Roberts, BDE (1950) "Heats of polymerization. A summary of published values and their relation to structure" *Part of the Journal of Research of the National Bureau of Standards*, *44*(March), 221–232.

Rogachev, AS and Mukasyan, AS (2010) "Combustion of heterogeneous nanostructural systems (review)" *Combustion, Explosion, and Shock Waves*, 46(3), 1–25.

Rugunanan, RA and Brown, ME (1994) "Combustion of binary and ternary silicon/oxidant pyrotechnic systems. Part IV: kinetic aspects" *Combustion Science and Technology*, *95*, 117–138.

Shende, R, Subramanian, S, Hasan, S, Apperson, S, Thiruvengadathan, R, Gangopadhyay, K, Gangopadhyay, S, Redner, P, Kapoor, D, Nicolich, S and Balas, W (2008) "Nanoenergetic composites of CuO nanorods, nanowires, and Al-nanoparticles" *Propellants, Explosives, Pyrotechnics*, *2*(2), 122–130.

Shimizu, A, Junji, S and Hao, YJ (1990) "Effect of contact points between particles on the reaction rate in Fe_2O_3-V_2O_5 system" *Solid State Ionics*, *38*, 261–269.

Shimizu, T (1981) *Fireworks- the Art, Science and Technique*, 3rd edition, Pyrotechnica Publications, Texas.

Stacy, SC, Pantoya, ML, Prentice, DJ, Steffler, ED and Daniels, MA (2009) "Nanocomposites for underwater deflagration" *Advanced Materials and Processes*, (October), 33–35.

Steinhauser, G and Klapötke, TM (2008) "'Green' pyrotechnics : a chemists' challenge" *Angewandte Chemie International Edition*, 47, 3330–3347.

Tomasi, R and Munir, ZA (1999) "Combustion synthesis of Al_2O_3–ZrO_2–Nb composites" *Journal of the American Ceramic Society*, *82*(8), 1985–1992.

Wang, LL, Munir, ZA and Maximov, YM (1993) "Review thermite reactions: their utilization in the synthesis and processing of materials" *Journal of Materials Science*, *28*, 3693–3708.

Watson, KW, Pantoya, ML and Levitas, VI (2008) "Fast reactions with nano and micrometre aluminium: a study on oxidation versus fluorination" *Combustion and Flame*, *155*, 619–634.

De Yong, LV and Smit, KJ (1991) "A theoretical study of the combustion of magnesium\Teflon\Viton pyrotechnic compositions", Technical Report, Materials Research Laboratory, Victoria, Australia.

77

Appendices

Appendix A   X-ray fluorescence of the magnalium used

Table A-1: XRF results for the magnalium raw material used

Species	wt.%
MgO	52.86
Al2O3	46.13
BaO	0.30
Fe2O3	0.20
Cs2O	0.17
I	0.09
SiO2	0.08
Cr2O3	0.03
MnO	0.03
MoO3	0.02
Bi2O3	0.02
CuO	0.02
Total	**99.95**

Appendix B : XRD spectra
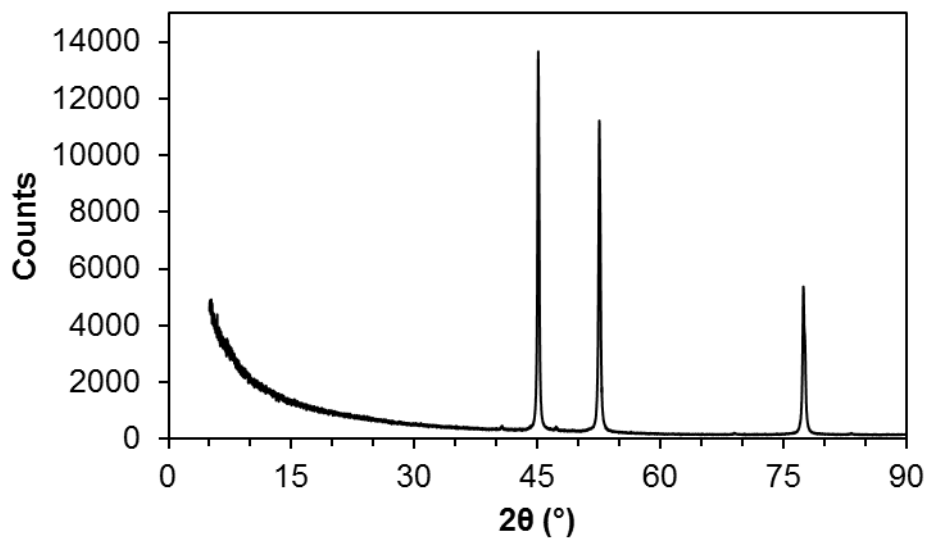
Figure B-1: XRD spectrum for the aluminium used in the compositions
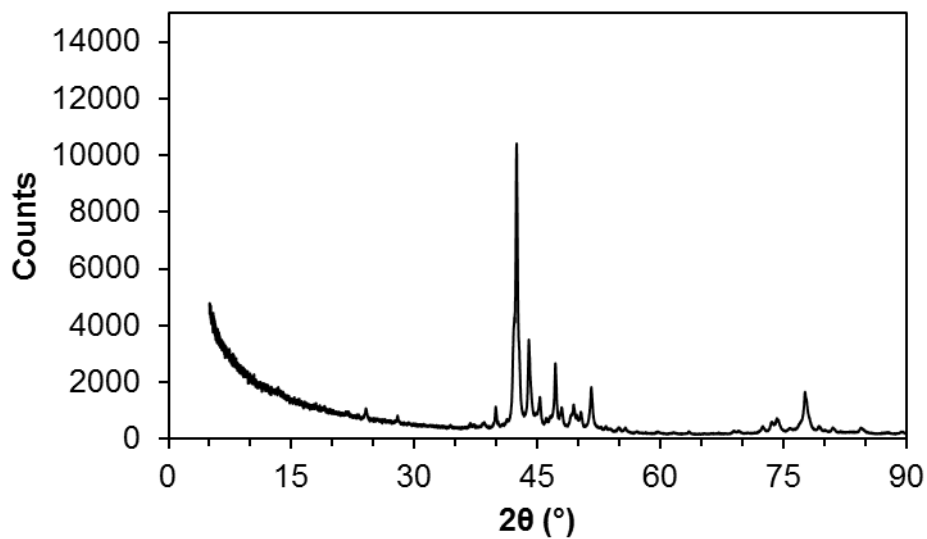
Figure B-2: XRD spectrum for the magnalium used in the compositions
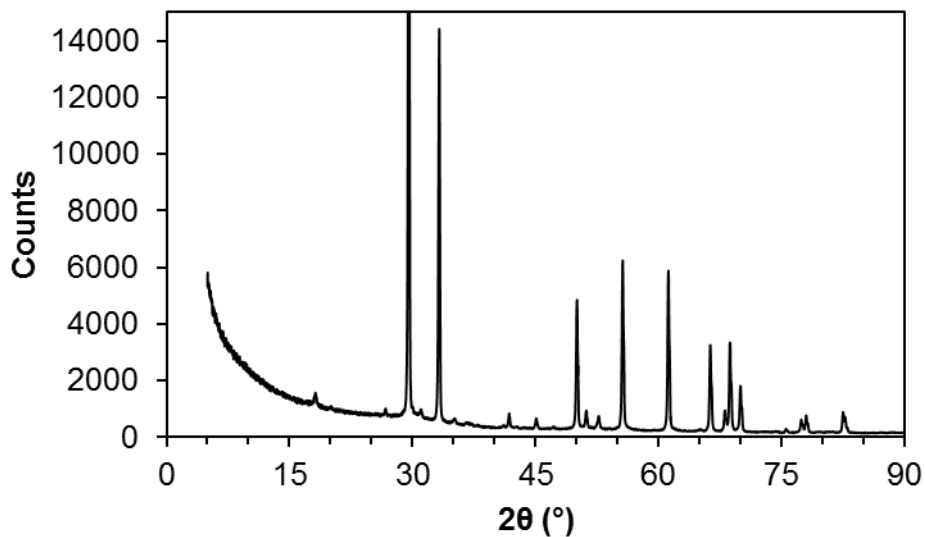
Figure B-3: XRD spectrum of the reaction residue of the 20 wt.% aluminium flake-based composition.
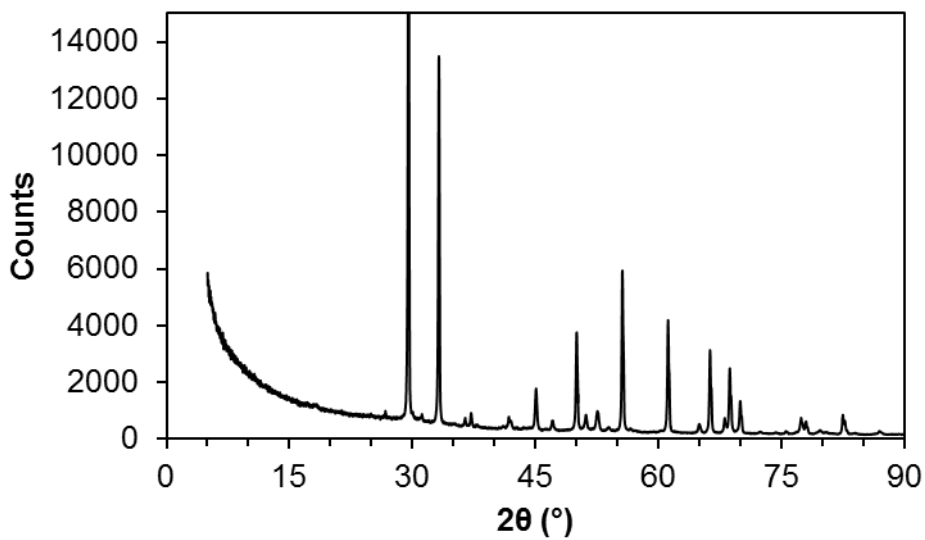
Figure B-4: XRD spectrum of the reaction residue of the 40 wt.% aluminium flake-based composition.

80
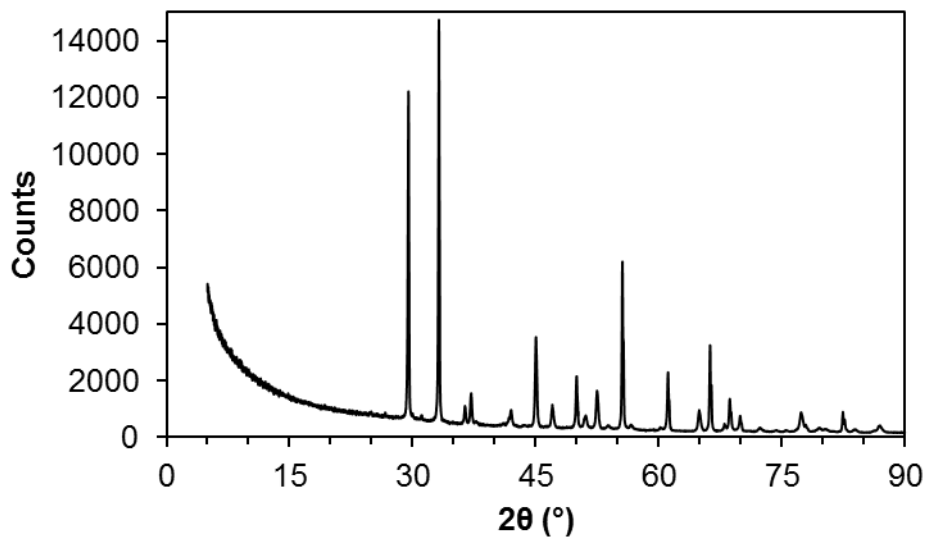
Figure B-5: XRD spectrum of the reaction residue of the 60 wt.% aluminium flake-based composition.
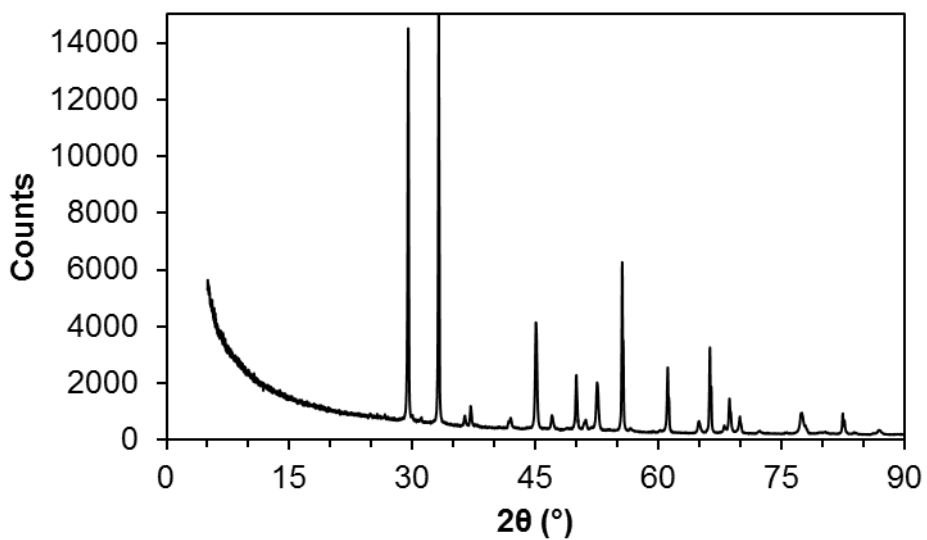
Figure B-6: XRD spectrum of the reaction residue of the 20 wt.% atomised aluminium-based composition.

81
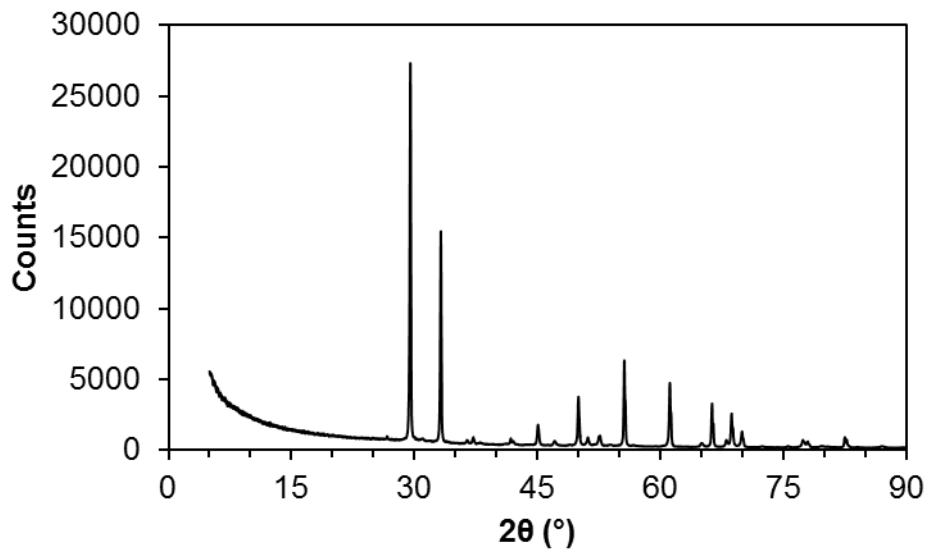
Figure B-7: XRD spectrum of the reaction residue of the 40 wt.% atomised aluminium-based composition.
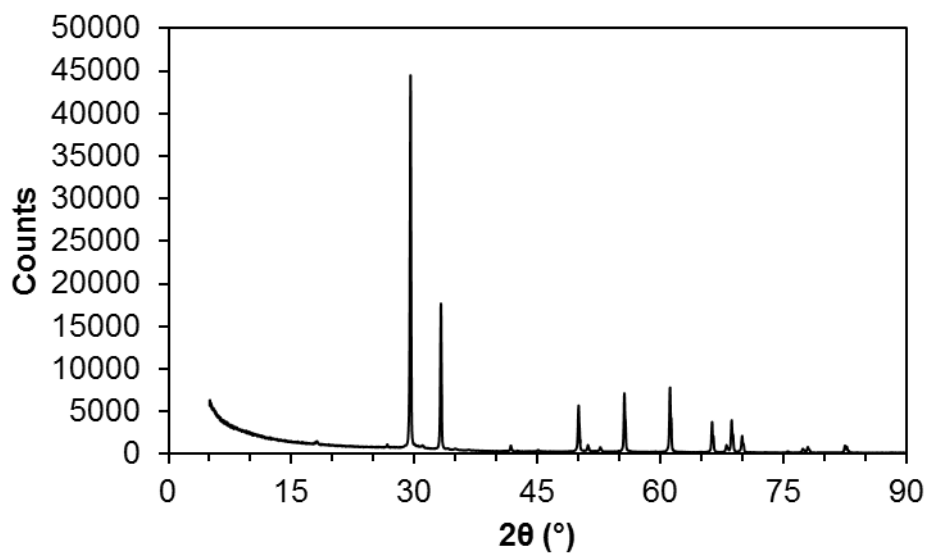
Figure B-8: XRD spectrum of the reaction residue of the 60 wt.% atomised aluminium-based composition.

82

Appendix C : FTIR spectrum of Viton B
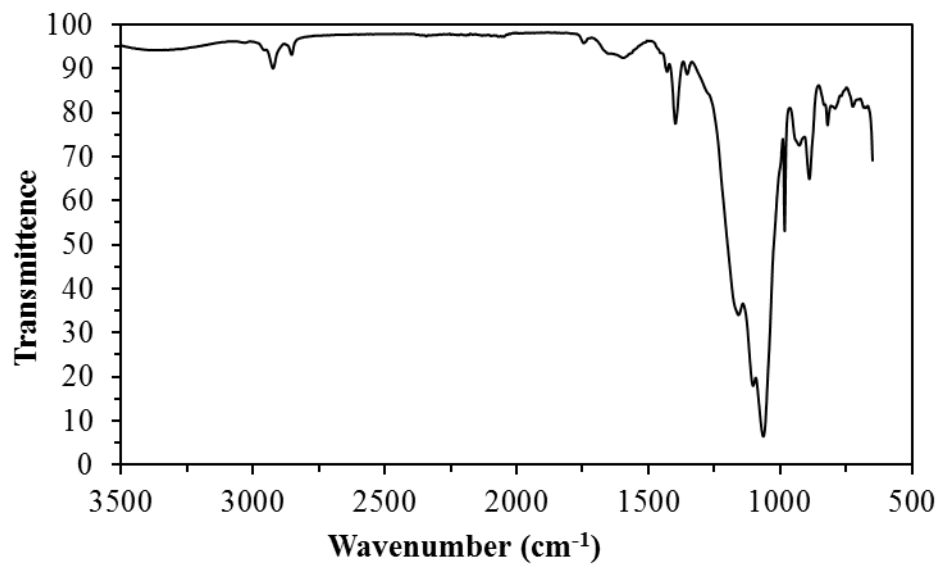
Figure C-1: FTIR spectrum of the Viton B used

83

Appendix D : SEM images
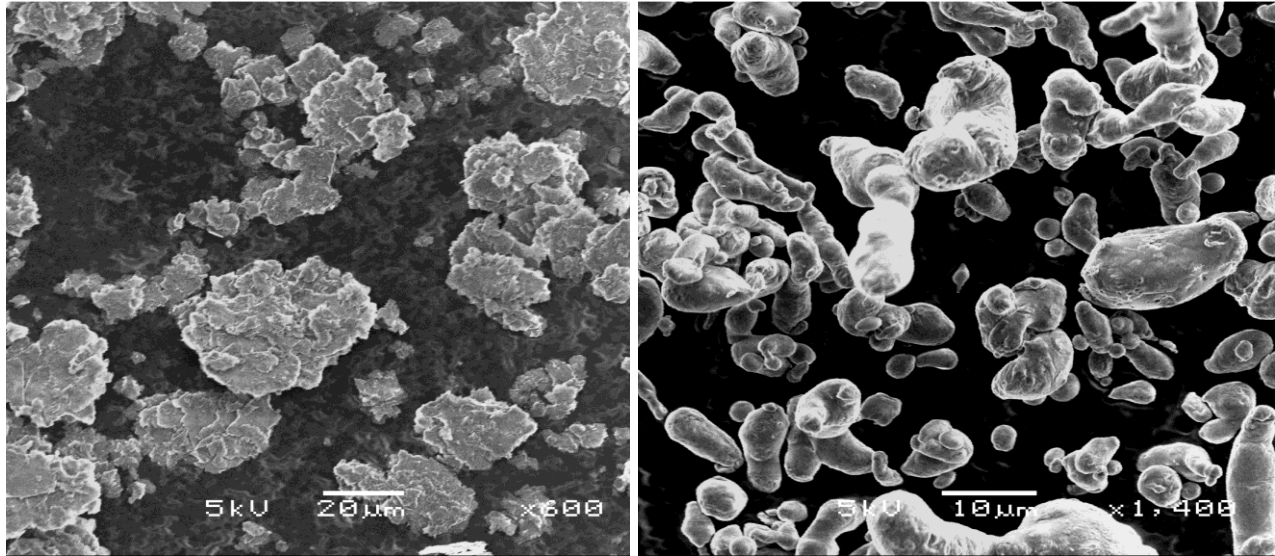
A)

B)
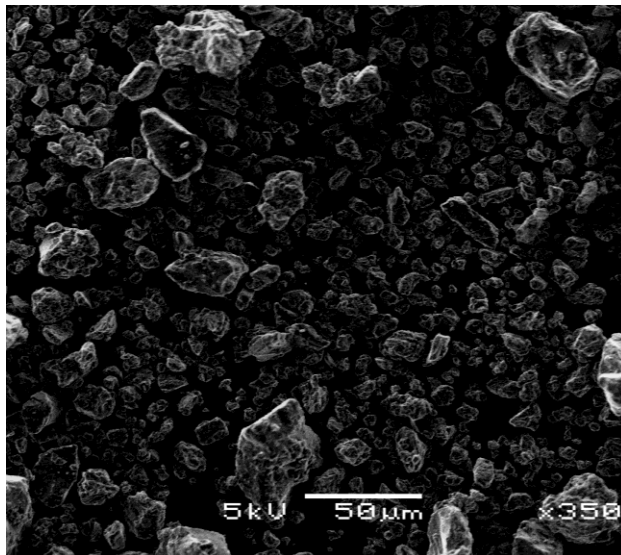
C)

Figure D-1: Scanning electron microscope images of the reducing agents used in pyrotechnic compositions. (A) Flake-like aluminium particles. (B) Atomised aluminium. (C) Magnalium particles.
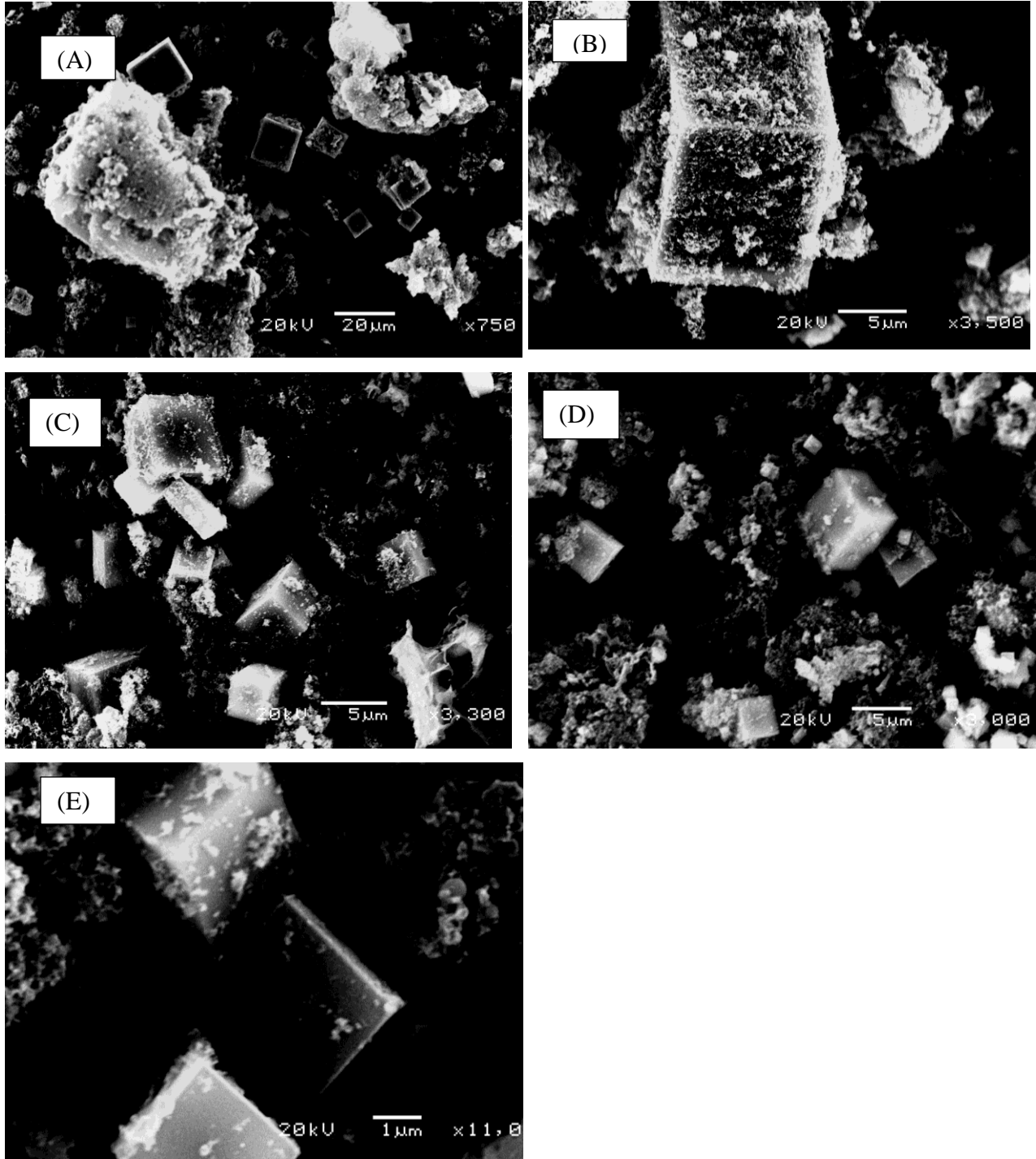
Figure D-2: SEM images of the reaction residue for the reaction between Viton B and flake like aluminium. (A) 20 wt.%. (B) 30 wt.%. (C) 40 wt.%. (D) 50 wt.%. (E) 60 wt.%.
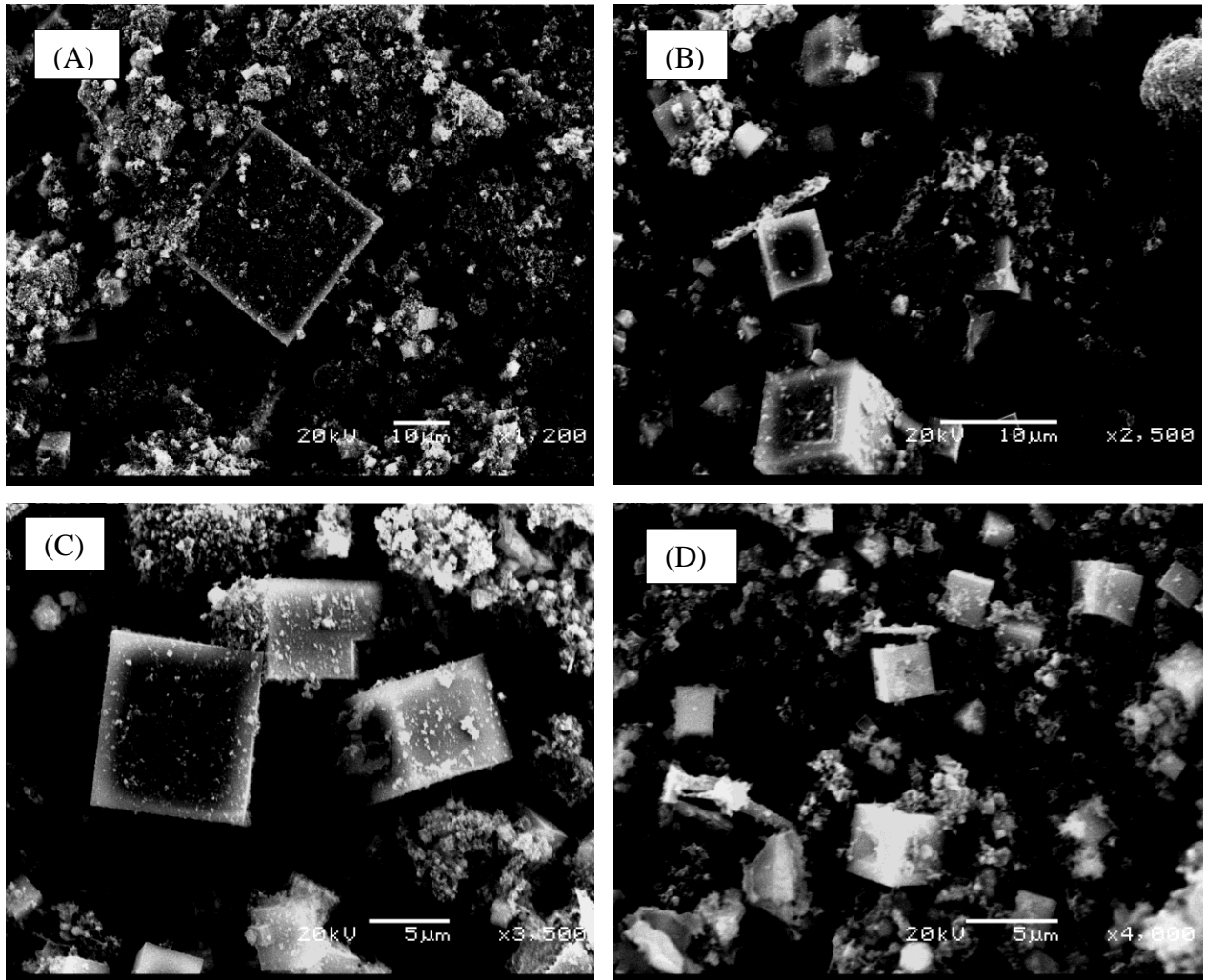
Figure D-3: Reaction residue of the reaction between Viton B and atomised aluminium. (A) 20 wt.%. (B) 30 wt.%. (C) 40 wt.%. (D) 50 wt.%.
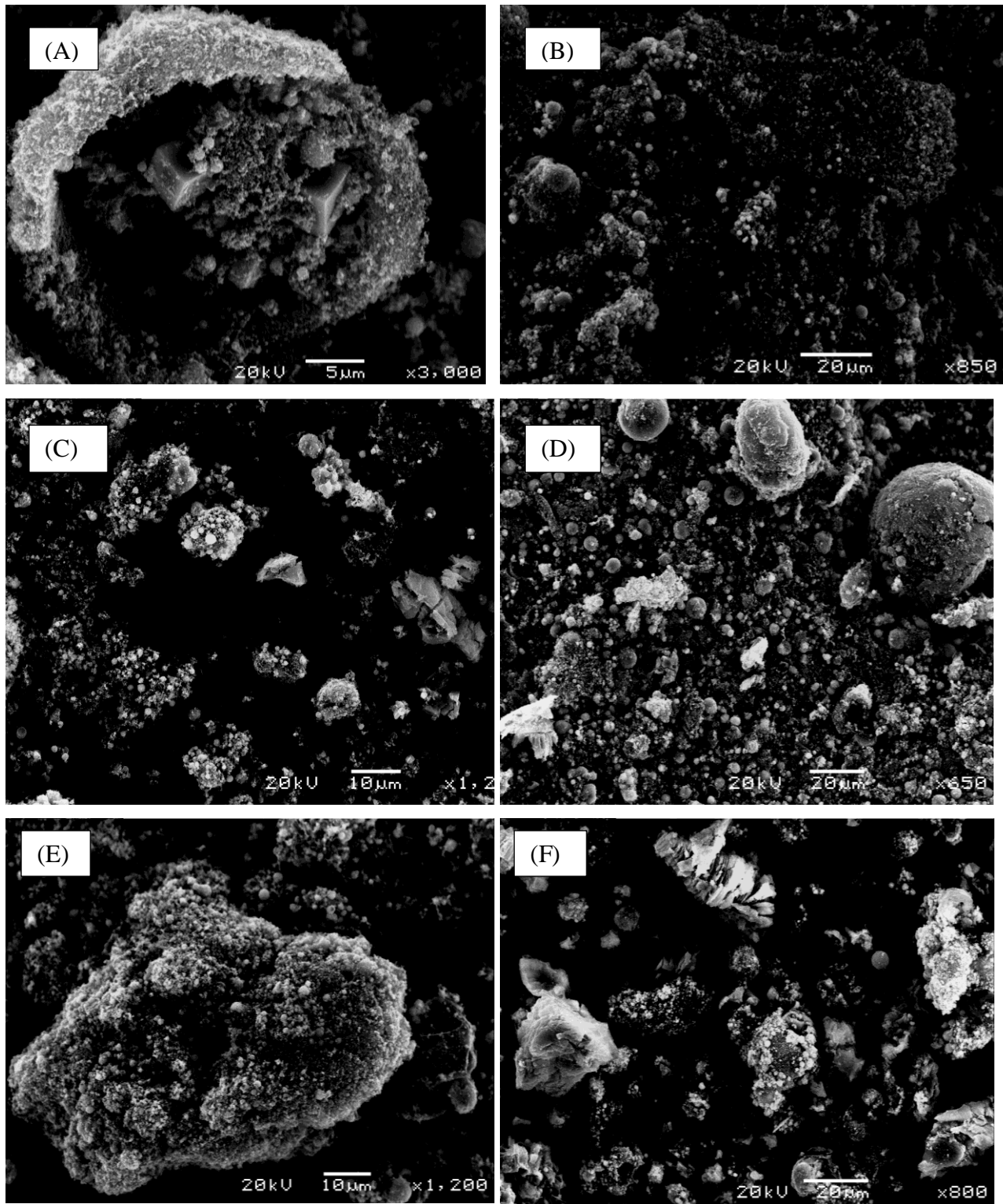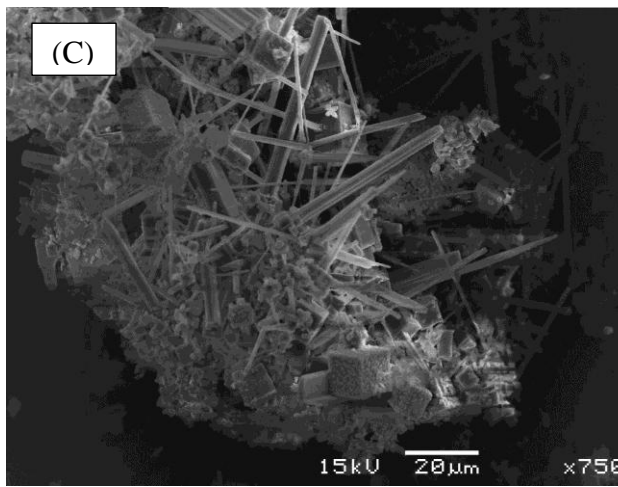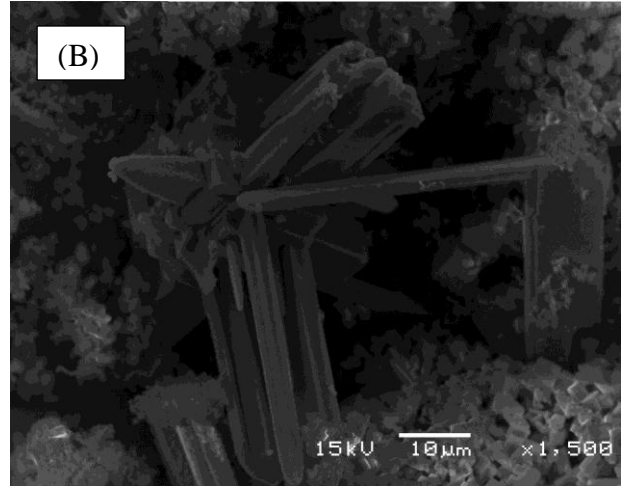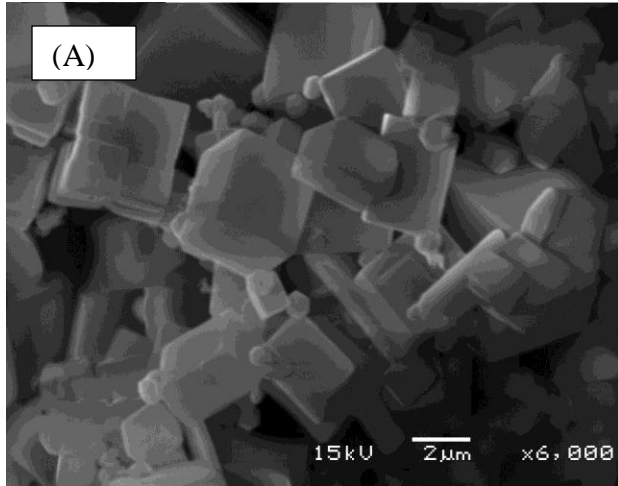
Figure D-4: SEM images of the reaction residue for the reaction between Viton B and magnalium. (A) 20 wt %. (B) 20 wt.%. (C) 30 wt.%. (D) 40 wt.%. (E) 50 wt.%. (F) 60 wt.%.
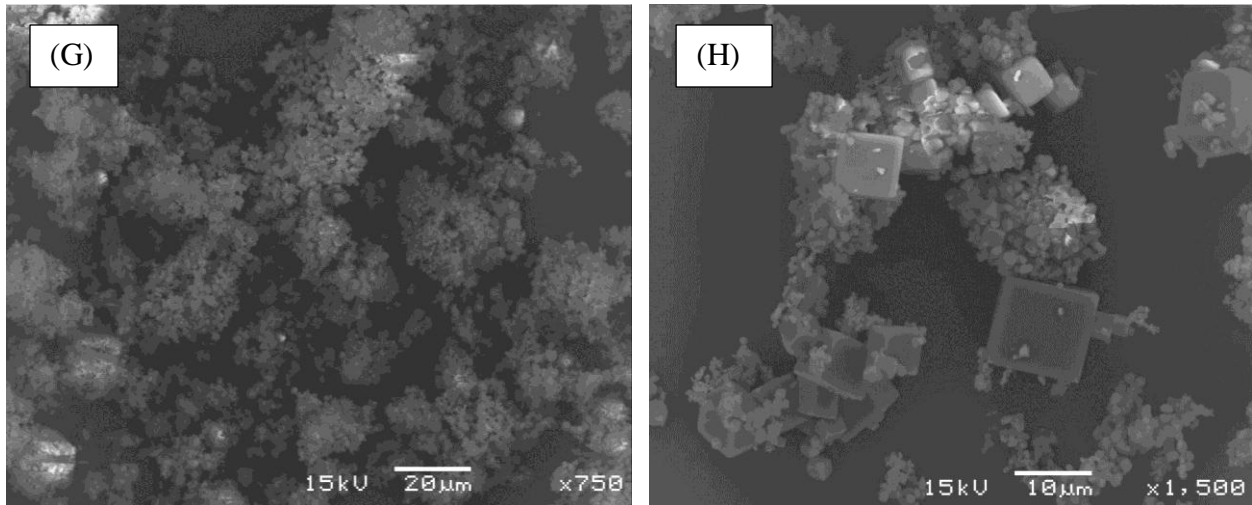
87
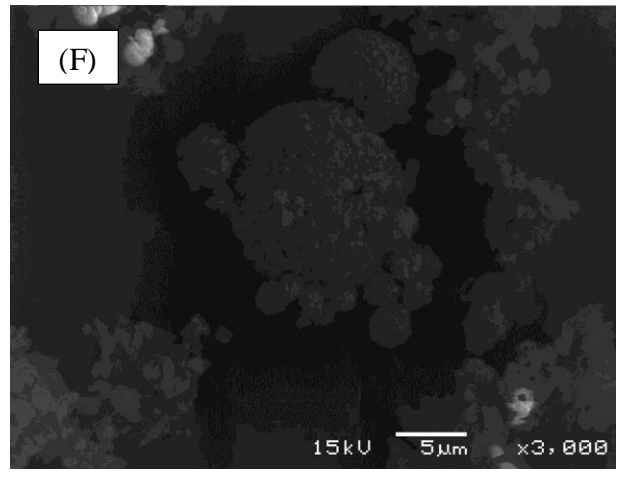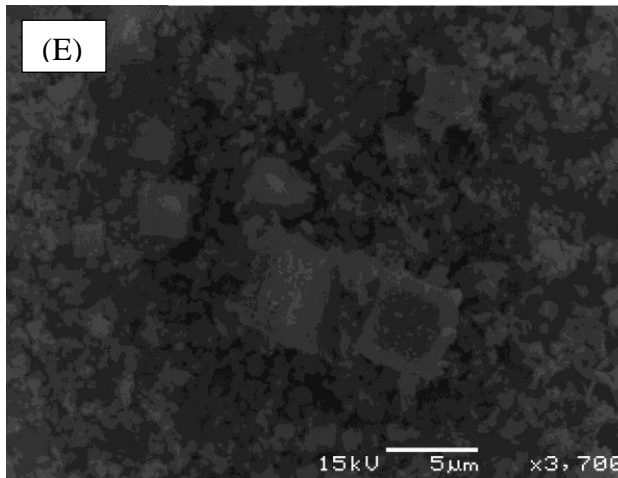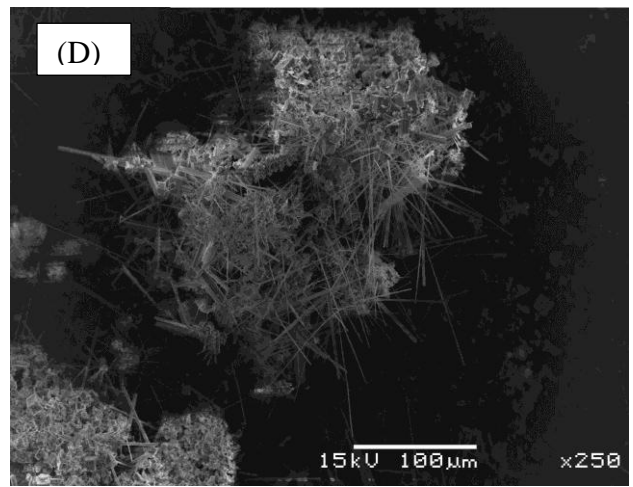
Figure D-5: Reaction residue heated to 900°C. (A) 20 wt.% flake like aluminium. (B) 20 wt.% flake like aluminium. (C) 30 wt.% flake like aluminium. (D) 30 wt.% flake like aluminium. (E) 50 wt.% flake like aluminium. (F) 20 wt.% magnalium. (G) 30 wt.% magnalium. (H) 20 wt.% atomised aluminium.